INCREASING SIGNAL TO NOISE RATIO AND MINIMISING MOTION ARTEFACTS IN BIOMEDICAL INSTRUMENTATION SYSTEMS

BY

SADDAM S. M. ZOUROB

OXFORD
BROOKES
UNIVERSITY

Ph.D. 2020

INCREASING SIGNAL TO NOISE RATIO AND MINIMISING MOTION ARTEFACTS IN BIOMEDICAL INSTRUMENTATION SYSTEMS

BY

Saddam S. M. Zourob

Faculty of Technology, Design & Environment Department of Mechanical Engineering & Mathematical Sciences

A thesis submitted in partial fulfilment of the requirements of Oxford Brookes University for the degree of Doctor of Philosophy

September 2020

OXFORD

BROOKES

UNIVERSITY

Acknowledgement

I would like to express my deepest appreciation to my director of research, Prof. Khaled Hayatleh, and my second supervisor, Dr Steve Barker, for giving me the opportunity to pursue and undertake this research. Their knowledge and insights helped me during the entire period of my research. They were always supportive and open for discussions that made me able to progress in my research. Special thanks go to Prof. John Lidgey and for his support and technical help throughout my research.

I would like to sincerely thank Dr Nabil Yassine, Ben Noble and Rajasekhar Nagulapalli for their consistent support and encouragement throughout my research. They were always happy to offer their valuable time to help me in progressing with my research.

My gratitude goes to my managers, supervisors and teammates at Sky UK, particularly my team leader, Russ Wood, and my department manager, Alex Barnett, for their support since the first day I started to work at Sky. They have happily offered me to have some time off work to work on my research, which massively helped me in reaching this final stage.

My greatest thanks go to my parents, Salahuddin and Nahla, who were always my limitless lovers and supporters throughout my entire life. They raised me and made me the man I am with their love and support. My deepest gratitude goes to my lovely wife, Razan, for her support, understanding and patience all the time. Special thanks to my uncle and auntie, Younus and Karima, who were my second parents that raised me and always supported me. Finally, a great thanks to my brothers and sisters who have always encouraged me with their best wishes.

Saddam Zourob
Oxford Brookes University
September 2020

Abstract

The research work described in this thesis was concerned with finding a novel method of minimising motion artefacts in biomedical instrumentation systems. The proposed solution, an Analog Frontend (AFE), was designed to detect any vertical (Y-Plane) or horizontal (X-Plane) movement of the electrode using two strain gauges, which were separated by 90° and fitted onto the electrode. The detected motion was fed back to the system for the removal of any motion artefact.

The research started by emphasising the importance of minimising motion artefacts from biomedical signals and explaining how important it is for a clinical misinterpretation of the results. Hence, various motion artefact minimisation techniques undertaken by other researchers in the field were reviewed. This study covered different sources of artefacts, including the 40kHz powerline interference (PLI), 50/60kHz common-mode noise, white noise, and motion artefacts.

The system was fully developed and tested and was firstly simulated using MATLAB Simulink tools to prove the effectiveness of the system before starting the implementation and build phase in the lab. The AFE system successfully produced a clean output signal, achieving an average correlation coefficient of 0.995. Also, the system output had a 98% SNR similarity with the clean source signal. Further, the system was then built and tested in the lab and successfully minimised the motion artefacts, achieving an average correlation coefficient of 0.974. Additionally, the final output had a 97.8% SNR similarity with the clean source signal. A novel test rig was developed to test the system with strain gauges. The system was able to remove the detected signal from the test rig and had an average correlation coefficient of 0.957. Lastly, the final output had a 94.2% SNR similarity with the clean source signal.

List of principal terms and abbreviations

3D Accelerometer	Is a device that measures 3-axis acceleration.
Amplifiers	An electrical device that is used to increase the amplitude of an electrical signal.
Artefacts	Minor blurring to significant distortion of the output signals, which may affect the interpretation of the medical interpretation (diagnosis).
Cadence	A System Design Enablement provider delivering tools and software to help in building circuits and simulating them.
Clear Signals	A signal without any kind of distortion or electric noise.
Common-Mode	A noise voltage that comes on both inputs of an opamp.
ECG (Electrocardiography)	A test that is used to detect and monitor the heart's electrical activity.
Filtering	Cleaning the unwanted noise from an electrical signal.
Instrumentation Amplifier (IA)	An amplifier that has been developed with input buffer amplifiers that are specifically used to reject common signals at the input and hence it is suitable for use in measurement and test equipment.

PLI	Powerline Interference or Electromagnetic Interference (EMI) is the power supply noise, and it appears at 50/60Hz.
Narrow bandwidth	Specific frequency range set from 5-20 kHz.
Noise	The electric noise that appears in the signal being read from a patient. This kind of noise will blur the true signal and make it inaccurate.
Opamp	(Operational amplifier) is a high-gain electronic voltage amplifier with a differential input and a single-ended output.
Active electrodes	Electric leads that are equipped with an amplifier and are attached to patients to simulate or record any potentials
Passive electrodes	Electric leads that are designed without the use of amplifiers and are attached to patients and suffer from artefacts.
Strain Gauge	A device for indicating the strain of a material or structure at the point of attachment.
ICA	Independent Component Analysis
Fast-ICA	An algorithm for linearly independent component analysis that has a high level of accuracy and computational complexity with datasets that are less than 2000 samples.

Kernel-ICA	An algorithm for linearly independent component analysis that has a high level of accuracy and computational complexity, especially with datasets that are more than 2000 samples.
JADE	Joint Approximate Diagonalization of Eigen-matrices is an ICA algorithm that aims to extract independent non-Gaussian sources from signal mixtures with Gaussian noise

List of figures and diagrams

List of tables

Table of Contents

CHAPTER 1

INTRODUCTION

1.1 Artefact Reduction in Medical Instrumentation

Nearly all medical equipment using passive electrodes attached to patients suffer from artefacts (Patterson and Yang, 2011) at the output source. These artefacts range from minor blurring to significant distortion of the output signal(s), which may affect the interpretation of the medical diagnosis. Artefacts may be caused by the movement of the electrodes relative to the patient, or by patient movement (Solis-Bustos and Silva-Martinez, 1999). However, there are many other causes of artefacts which need investigation. For example, a narrow bandwidth instrumentation amplifier (IA) could modify the output signal, which could be interpreted as an artefact. For this reason, it is important to identify how artefacts influence the output signal being measured. Artefacts can be viewed as unwanted noise on the desired signal (Patterson and Yang, 2011).

Biopotential signals are small amplitude waveforms that represent the activity of the nervous, muscular or glandular tissue (Yazıcıoğlu *et al.*, 2009). The need for having quality health care monitoring systems is increasing due to the importance of providing better health diagnostics of the biopotentials of the patients, such as an electrocardiogram (ECG), electromyogram (EMG), and electroencephalogram (EEG) (Hasan and Lee, 2015, Yazıcıoğlu *et al.*, 2009). Fig. 1-1 shows the characteristics of the amplitude and frequency of the biomedical signals: ECG, EEG, and EMG. Such small signals will be lost or distorted through the signal detection process, which will have a massive effect on the output signal interpretation. Therefore, the noise that is attached to the desired signal, such as the interference from the mains, common-mode signals, electrode movements, and any other source of distortion, must be rejected or filtered (Yazıcıoğlu *et al.*, 2009, Hasan and Lee, 2015).

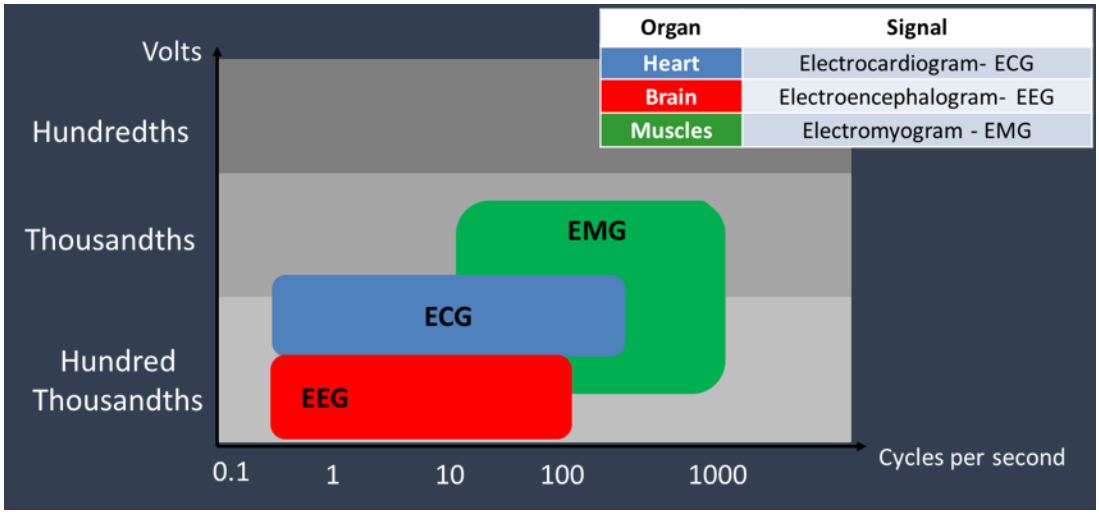

Fig. 1-1 Characteristics of the biopotential signals (Yazicioglu et al., 2008, p. 6)

The main focus and discussion of this research are on the artefacts related to ECG biopotentials. The research explores the various causes of ECG artefacts, the solutions provided to eliminate them, and introduces a novel technique to minimise these artefacts.

ECG artefact reduction is an ongoing topic for numerous research projects which offer various methods for the minimization of artefacts. The vast majority are based on the fact that the causes of such artefacts are due to noise/unwanted signals generated by the movement of the electrodes while they are attached to patients (Solis-Bustos and Silva-Martinez, 1999, Patterson and Yang, 2011). ECG signals can be obtained by using two electrodes and recording the potential difference between them (Neuman, 1998, Stork, 2017). The vast majority of the existing methods that are used to minimise motion artefacts are based upon filtering (Ma *et al.*, 2012), smoothing and averaging. Such approaches may be suitable (Ma *et al.*, 2009), but, of course, filtering also reduces the amplitude of the desired signal, which is undesirable.

Additionally, filtering may not be suitable for 'random' noise, where the frequency components can change with time. By its very nature, filtering always introduces some distortion of the optimal signal, which is undesirable as this could lead to a

misinterpretation of the results. Therefore, to avoid losing the weak and noisy biopotentials while undergoing amplification, the chosen amplifiers should have a stable gain, low noise, high common-mode-rejection-ratio (CMRR), and high input impedance (Hasan and Lee, 2015).

This research provides a new approach that will minimise artefacts due to the relative motion of the patient/electrode interface. The design of this approach includes a sensor to detect any vertical or horizontal movement of the electrode, which then feeds this information back to the system for the removal of any movement artefact. In this case, two strain gauges, separated by 90° are fitted onto the electrode to detect any X and Y plane movements with regards to the patient's chest. The output of these is then fed back into the novel Analog Frontend (AFE) for artefact removal.

Additionally, a novel test rig was developed to test the strain gauges using a loudspeaker with a plastic rod that was covered with a plastic sheet to represent the pseudo-skin. An electrode was placed on the plastic sheet, and the strain gauges were fitted onto the electrode and separated by 90° to allow the detection of movement of the sheet when it moved up and down. The test rig was able to detect the motion and fed it back to the AFE system, which cleaned the signal and produced a clean output signal.

1.2 Hypothesis and Research Questions

This research tests the following hypothesis:

> *Strain gauges can be used to detect relative body/electrode movement, which can then be eliminated from the detected signal.*

Answering the following research questions will help in testing the hypothesis:

1. How can strain gauges be used to capture relative body-electrode movement?
2. Can the movement captured in 1. above be removed using analog electronics techniques?
3. How can a test rig be developed to test 1. above?
4. How can the results be evaluated?

1.3 Research Aim and Objectives

The aim of this research was to answer the research questions and to develop a novel artefact removal system.

The objectives of the research were:

- Investigate and analyse different types of artefacts and research the current approaches in minimising these artefacts.
- Design an artefact removal system that works in the analog domain to get a more accurate, fast system that uses less power than a digital system would.
- Simulate the output using software techniques to prove the validity of the proposed design.
- Refine, build and test a working prototype using discrete components.
- Compare the results from the simulated and prototyped versions of the design. The design will then be optimised accordingly.
- Achieve an average correlation coefficient higher than 0.934.
- Increase the Signal-to-Noise Ratio (SNR) by more than 90% when compared to the SNR of the test signal.

1.4 Original Contribution

The original contribution of this research was to develop an Analog Frontend (AFE) system that removed any motion artefacts from biomedical signals. The system used two strain gauge sensors that were fitted onto the electrode at 90° to each other to detect the vertical and horizontal movements of the electrode. The proposed system was initially designed and tested using MATLAB Simulink. The simulation results of the system achieved an average correlation coefficient of 0.995 and improved the total harmonic distortion (THD) to become 99.8% like the THD of the test signal. Also, the system output had a 98% SNR similarity with the clean source signal. The system was also assembled and examined in the lab using generated noise signals. An average correlation coefficient of 0.974 was achieved during these tests and improved the THD to become 98.8% like the original test signal. Additionally, the final output had a 97.8% SNR similarity with the clean source signal.

To have a critical review of the results and examine the efficiency of the system, a novel test rig was built. The test rig used a loudspeaker covered with a plastic sheet, representing the pseudo skin, with a fitted plastic rod under the sheet. The strain gauges were fitted onto an electrode that was placed on the pseudo skin. The electrode was injected with the clean signal. The sheet moved up and down due to the rod movement, causing the strain gauges to strain. The AFE system received the detected signal from the strain gauges and removed the detected noise from the injected signal that was distorted due to the motion of the plastic rod. The system has achieved an average correlation coefficient of 0.957 and improved the THD to become 96.5% like the original test signal. In addition, the final output had a 94.2% SNR similarity with the clean source signal. Other motion artefact solutions such as (Berwal *et al.*, 2019) was able to produce an average correlation coefficient of 0.9337.

1.5 Structure of The Thesis

The thesis comprises nine chapters that explain the chosen procedures to achieve the research objectives. Following this chapter, the other chapters' compromise of:

Chapter 2 is a literature review of the current field of study and the different techniques used to minimise artefacts. In addition, a detailed investigation of the various causes of artefacts, such as the movement of the electrodes while they are attached to the patient, mains electrical noise, and electromagnetic interference, was presented. The information gathered from this will enable understanding of the extent and nature of the problem, which can then be used to develop the means to tackle it. This chapter includes a revision of the strain gauges design and usage in the medical instrumentations as well as the different types of amplifiers and electrodes that are widely used for biopotential capturing.

Chapter 3 is the product design specification which specifies the overall design of the system. Additionally, it explains the system requirements regarding the motion artefact reduction and the common-mode rejection ratio. It also includes the explanation of how the system would be tested using the various benchmarks such as MATLAB testing and strain gauges test rig.

Chapter 4 is the design method and system simulation, which explains the design of the Analog Frontend (AFE) system and its characteristics. In addition, it elaborates the system simulation in MATLAB and its results.

Chapter 5 explains the hardware implementation of the AFE system. This shows the experimental approach that was undertaken when evaluating the system performance and presents the final hardware implementation design of the system. In addition, it discusses the test results and analyses the experimental results.

Chapter 6 explores the research conclusions and discusses the outcomes of the research. In addition, the suggested future work, its advantages and limitations, were also discussed.

Chapter 7 includes the full reference list (in emphatical order) that were reviewed and used in this research.

Chapter 8 is the appendices. It included all supplementary material that is related to the previous chapters.

Chapter 9 is the published papers that were published by the author of this thesis during the research.

1.6 Summary

This chapter presented an introduction to the topic of this thesis and then continued to set out the hypothesis and research questions of the research. It then covered the aim and the objectives needed to achieve this aim. It also stated the original contribution of the approaches that will be followed to get to the final solution. Finally, the thesis structure was outlined.

The literature review is explored in the following chapter. It discusses modern approaches and technologies in this research area and provides a full critical evaluation of each of these technologies.

1.7 References

[1] BERWAL, D., V, C. R., DEWAN, S., J, C. V. & BAGHINI, M. S. 2019. Motion Artifact Removal in Ambulatory ECG Signal for Heart Rate Variability Analysis. *IEEE Sensors Journal,* 19**,** 12432-12442.

[2] HASAN, M. N. & LEE, K.-S. 2015. A wide linear output range biopotential amplifier for physiological measurement frontend. *IEEE Transactions on Instrumentation and Measurement,* 64**,** 120-131.

[3] MA, C. T., MAK, P. I., VAI, M. I., MAK, P. U., PUN, S. H., FENG, W. & MARTINS, R. P. A 90nm CMOS bio-potential signal readout front-end with improved powerline interference rejection. 2009 IEEE International Symposium on Circuits and Systems, 24-27 May 2009 2009. 665-668.

[4] MA, S., CHEN, C., ZHANG, Y. & REN, J. A low power programmable band-pass filter with novel pseudo-resistor for portable biopotential acquisition system. 2012 IEEE Asia Pacific Conference on Circuits and Systems, 2-5 Dec. 2012 2012. 232-235.

[5] NEUMAN, M. R. 1998. Biopotential amplifiers. *Medical instrumentation: application and design***,** 316-318.

[6] PATTERSON, J. A. & YANG, G.-Z. 2011. Ratiometric artifact reduction in low power reflective photoplethysmography. *IEEE transactions on biomedical circuits and systems,* 5**,** 330-338.

[7] SOLIS-BUSTOS, S. & SILVA-MARTINEZ, J. Design considerations for biomedical signal interfaces. Proceedings of the Third International Workshop on Design of Mixed-Mode Integrated Circuits and Applications (Cat. No.99EX303), 1999 1999. 187-191.

[8] STORK, M. Modeling and simulation of some biomedical signals. Measurement, 2017 11th International Conference on, 2017. IEEE, 221-224.

[9] YAZICIOGLU, R. F., VAN HOOF, C. & PUERS, R. 2008. *Biopotential readout circuits for portable acquisition systems*, Springer Science & Business Media.

[10] YAZıCıOĞLU, R. F., VAN HOOF, C. & PUERS, R. 2009. Introduction to Biopotential Acquisition. *Biopotential Readout Circuits for Portable Acquisition Systems.* Dordrecht: Springer Netherlands.

CHAPTER 2

LITERATURE REVIEW

2.1 Introduction

In this review, a definition of the causes of ECG signal artefacts and their importance and effect on heart activity diagnosis will be introduced. It will also explore signal noise reduction techniques and the latest findings in the field. The types of ECG measurement sensors will be discussed to draw a clear vision of the different usages of the different sensors. Additionally, a review of the main components used in the proposed solution would be discussed and explored. These components include strain gauges, medical instrumentation amplifiers, and the ECG electrodes. This includes the study of their use in medical equipment and the different types of strain gauges integrations with this equipment in the market. Studying the different types of components would direct the research in the right direction to choose the best-fit components within the research scope. Finally, each of these components would build towards the proposed solution and help in proving the concept of the proposed design.

2.2 Causes of Electrocardiograph (ECG) Artefacts

There were various pieces of research that introduce different solutions in the field of ECG artefact reduction. The ECG signal pattern consists of three main waves which are called: Q, R, and S. The combination of these graphical deflections seen on the ECG signal is called the QRS Complex (Jenkal *et al.*, 2015). It is common for artefacts to affect the ECG patterns, where it makes it difficult to read by the physician while studying the recorded signal and detecting any potential diseases or disorders. It is very important to know that any muscular activity or recorded motion activity other than the heart activity is considered as a noise that affects the recorded signal.

During the process of capturing the ECG signals, power supplies produce Electromagnetic Interference (EMI) at 50/60Hz, which is known as Powerline Interference (PLI). PLI partly occupies the same range of frequencies as the ECG signals which start from 0.5Hz to 100Hz (Shaik *et al.*, 2016, Belgurzi *et al.*, 2017). On the other hand, Baseline noise frequency is caused by artefacts that have a frequency below 5Hz, and it can be produced by many artefact sources such as breathing, muscle activity, and body motion (Imtiaz *et al.*, 2016, Shaik and Chakka, 2016, Singh *et al.*, 2015). Also, electromyography (EMG) is the noise introduced by the patient's movement, which causes muscular contractions that interferes with the detected ECG biopotentials. Such small signals that are commonly overlapping with the ECG signals must be eliminated. A lot of research has been done towards removing the detected PLI and Baseline noises which include filtering techniques (Romero *et al.*, 2012, Gautam *et al.*, 2008), wavelet transform (Garg *et al.*, 2011, Nagai *et al.*, 2017, Wei *et al.*, 2005, Haddad and Serdijn, 2009, Donghui, 2005, Mithun *et al.*, 2011), and adaptive techniques (Mneimneh *et al.*, 2006, Wu and Rangayyan, 2007). These have been proven to eliminate these kinds of artefacts, as reviewed by (Singh *et al.*, 2015).

Additionally, heart activity signals distortion can be caused by other types of artefacts such as common-mode interference (40kHz in switched-mode) in a power supply, patients movement and loose electrode connections (Singh *et al.*, 2015, Zhang *et al.*, 2016, Kishimoto *et al.*, 2007). In addition, the mostly noticed ECG artefacts are powerline interference, baseline wander and other muscles activities (Singh *et al.*, 2015, Shaik and Chakka, 2016). Therefore, these types of artefacts must be eliminated to have an improved noise-free ECG signal.

On the other hand, motion artefacts are one of the most common sources of ECG signal distortion. It can cause a random noise that would not be detected or minimised by any of the normal filtering, smoothing, or averaging techniques that are mostly used in removing the PLI and Baseline wandering artefacts. Methods used in dealing with motion artefacts varied from the use of Tri-Axis Accelerometers (Kishimoto *et al.*, 2007) to the use of Adaptive filtering (Zhang *et al.*, 2016) as well as using wavelet transform based techniques (Mithun *et al.*, 2011). However, each of these methods has advantages and disadvantages that would only give the correct results in very specific conditions (e.g. a solution that would not work unless the patient is sleeping) and would not be used outside these boundaries.

(Kishimoto *et al.*, 2007) used a 3D Accelerometer to measure the relative body movement while capturing the ECG signals. They were able to reduce the amount of noise to a good amount. However, it was only targeting the patients while they were asleep, which is different than what the research presented in this thesis considers, and it does not capture the movement of the patient/electrode interference. A new kind of adaptive filtering was used by (Zhang *et al.*, 2016) to reduce motion artefacts in ambulatory ECG signals. Their proposal involves using two separate Adaptive Filters (AFs) to accommodate the poor diagnosis caused by the non-stationary property of the ambulatory ECG. While their proposed method showed good results, it was based around adding more filtering stages in the motion artefact reduction process, which this

research aimed to avoid. Having more filters in the artefact reduction process would make the process prone to other types of distortion, caused by the filters, which is not desirable. Other methods used by (Nagai *et al.*, 2017) involve using the Stationary Wavelet Transform (SWT) to extract the ECG signal 'QRS complex' based on the energy of a heartbeat signal. This method focuses on using the non-contact electrodes and ignores the use of the gel electrodes in most of the biomedical systems, which is different than what the research presented in this thesis considers.

EMG noises are usually considered as part of the motion artefacts that are affecting the small ranges of the ECG segments that are lying between the S and T waves. These segments are called the ST Segments (Hampton, 2008). (Mithun *et al.*, 2011) introduced an improved thresholding function using both soft and hard thresholding types. This method showed a significant cut down of the EMG artefacts. However, the use of hard thresholding would cause a signal loss, especially when it comes to random motion artefacts that have different ranges (Priya *et al.*, 2016). In addition, soft thresholding could over smooth the noise signal, which would make it looks like a genuine ECG harmonics (Priya *et al.*, 2016).

2.3 Artefacts Minimisation Techniques

2.3.1 Statistical Approach

The extraction of the characteristics of signals generated by the different types of signal sources is one of the important processes in the signal processing techniques. These characteristics contain the status of the captured human system, which would then be studied and interpreted to reflect the current system state. Statistical signal processing is one of the important approaches that rely on the collection of the signal characteristics to formulate an appropriate image of the system behaviour which would provide the required useful interpretation of the human body status (Kannan and Kundu, 2016). It is part of the statistical analysis approach that is widely used in different types of applications that vary from one research area to another. For example, it is used in seismology (earthquakes and seismic waves study) to differentiate between nuclear explosions happening underground and natural seismic activity (Kannan and Kundu, 2016). Voice recognition is another application of the statistical signal processing that is used to recognise the speech waveform characteristics of the person speaking (Dumitru and Gavat, 2003) and it is also widely used by financial institutions around the world (Steland, 2012).

Signal processing researchers used different statistical tools such as Fourier analysis, nonlinear regression, time series analysis, etc. One of the main challenges to statistically process signals is to develop fast and efficient techniques to analyse the large datasets, especially in the existence of today's powerful computers (Kannan and Kundu, 2016). There are many different models, each of which has different estimation techniques, that are widely researched and studied in the field of statistical signal processing. Independent Component Analysis (ICA) and Principal Component Analysis (PCA) are the most used statistical techniques for biomedical signal processing and ECG signal error detection (Kong *et al.*, 2008).

ICA is a higher-order data-mining technique that is used to extract the independent components (ICs) from the dataset in a study without the need for prior knowledge about the sources of these datasets (Kasturiwale, 2012, Kong *et al.*, 2008, Rutledge and Jouan-Rimbaud Bouveresse, 2013). This specific model has two assumptions that should be satisfied in the datasets in order to work properly. The first assumption is the independence of the sources of the data, and the second is that the independent components mixing ratio are different from the mixing ratio of each data source. ICA has different types of algorithms that can be used in the extraction process. Some of these algorithms, such as Fast-ICA, Kernel-ICA and JADE, were used in Kasturiwale (2012) to improve the signal to noise ratio (SNR) of an ECG and an electroencephalogram (EEG) signals. Despite that, the author is concluding different levels of success in enhancing the SNR levels. The applied algorithms were able to minimise the motion artefact from the tested ECG and EEG dataset. However, the algorithms had a high computational complexity, and the performance of each of them was not perfect.

In order to reduce motion artefacts and prevent signal distortion and attenuation, (Yoon *et al.*, 2013) introduced an automatic noise detection and removal ICA technique that considers the independency between the ECG signal components and the motion artefacts. The used workflow employs several decision rules to analyse the signal of three ECG electrodes. The analysis decides the noisiness and Gaussianity of the signal and, consequently, predicts if the motion artefacts and ECG signal need to be separated and reconstructed without distortion (Yoon *et al.*, 2013). The proposed technique shares the same limitations as the other ICA techniques in that they are restricted to Gaussian random variables. However, they propose the decision rules that would help in skipping the limitation. This method has many drawbacks that make it unsuitable for many ECG reduction applications. The method is based on short-term segmented datasets (5 seconds) which make it a non-real-time analysis technique. Although the proposed algorithm would supposedly lessen the processing time by skipping the unnecessary

processing of the Gaussian signals, it is still an expensive process to store and analyse due to its complex computational rules and steps.

In theory, using ICA for noise reduction showed very promising results. However, the optimality and robustness of these results are not clearly shown. Many researchers used ICA for motion reduction. Nevertheless, there are drawbacks related to the ICA assumptions that affect the accuracy of such a method. For instance, the body movement affects the independency of the motion artefacts and ECG electrical activity which makes them not exactly independent (Yoon *et al.*, 2013). Additionally, motion artefacts are normally random noises, non-Gaussian variables, that interfere with the ECG signal and using ICA, which follows the Gaussian property, will cause distortion and eliminate meaningful information from the signal.

The other common statistical approach is Principal Component Analysis (PCA) that is used to detect abnormalities in informational data in the pre-processing and classification steps of data preparation. It is commonly used in applications due to its approach that uses analytical solutions from linear algebra to reveal the simple underlying structures of the complex data, as well as extracting the principal component that has the maximum data variance to find the spatial directions of the data set (Kasturiwale and Ingole, 2012). The measured variance is independent of any parameters, which makes PCA work regardless of the way the data was recorded. This independency gives PCA the feature of plug-and-play and obtaining the results straight after. However, the same feature makes PCA unable to completely separate artefacts from an ECG signal as it mainly works on dimension reduction. In addition, ignoring the source of the data would result in losing the beneficial data of ECG signals (Deshpande and Rajankar, 2013).

In summary, statistical approaches were extensively explored and employed by researchers in order to eliminate motion artefacts. They were very useful in the case of extracting the required information from the datasets. However, statistical approaches

are computationally expensive, time-consuming, and they are used to process the datasets after collecting the data from the subjects which would lead to an extensive data loss. As a result, pre-processing the data is the popular approach using different filtering techniques which makes the noise reduction process less time consuming and less computational power will be used.

2.3.2 Adaptive approach

The most used technique for motion artefact reduction is adaptive filtering, and it is used to minimise the artefacts from the biopotentials due to its simple computations (Alkhidir et al., 2015, Lanata et al., 2015). The adaptive approach uses a reference signal to adjust the filtering of the biomedical signals. The performance of this approach would rely on the level of relationship between the reference signal and the signal in question. As human behaviour is unpredictable, the use of adaptive filtering techniques helps to overcome this random state situation (Chandrakar and Kowar, 2012). In ECG artefact reduction, a number of researchers used a sensor to detect the motion artefacts signal as a reference signal (Alkhidir et al., 2015, Tong et al., 2002) which would have a close relationship with the ECG noise source.

(Tong *et al.*, 2002) designed and fabricated two motion sensors. The first is a two-axis anisotropic magnetoresistive (AMR) sensor which is a surface-mount sensor that is designed for low field magnetic sensing (Honeywell, 2019). The second is a developed three-axis accelerometer (ACC) sensor. Both motion sensors output signals were used as the reference signal. They compared the noise reduction results using each type of reference signal. As a result, they collected three different types of movements, which were: pushing on the electrode, pushing on the skin and finally pulling the lead wire of the electrode. They collected the data from eight human subjects. Using the ACC sensor gave a better result in comparison to the AMR sensor which could be a result of the

nature of the 3D accelerometer where it provides a 3-axis measurement of the motion rather than 2-axes as provided by the AMR (Tong *et al.*, 2002).

Similarly, (Liu, 2011) used 3D accelerometers to detect the 3-axis motion of the human body and used it as a referencefor the adaptive filter to reduce the ECG motion artefacts in their ECG recorder. The captured 3D motion is converted into the digital domain and then transferred along with the captured ECG signal via a Bluetooth module to the remote recorder, as shown in Fig. 2-1.

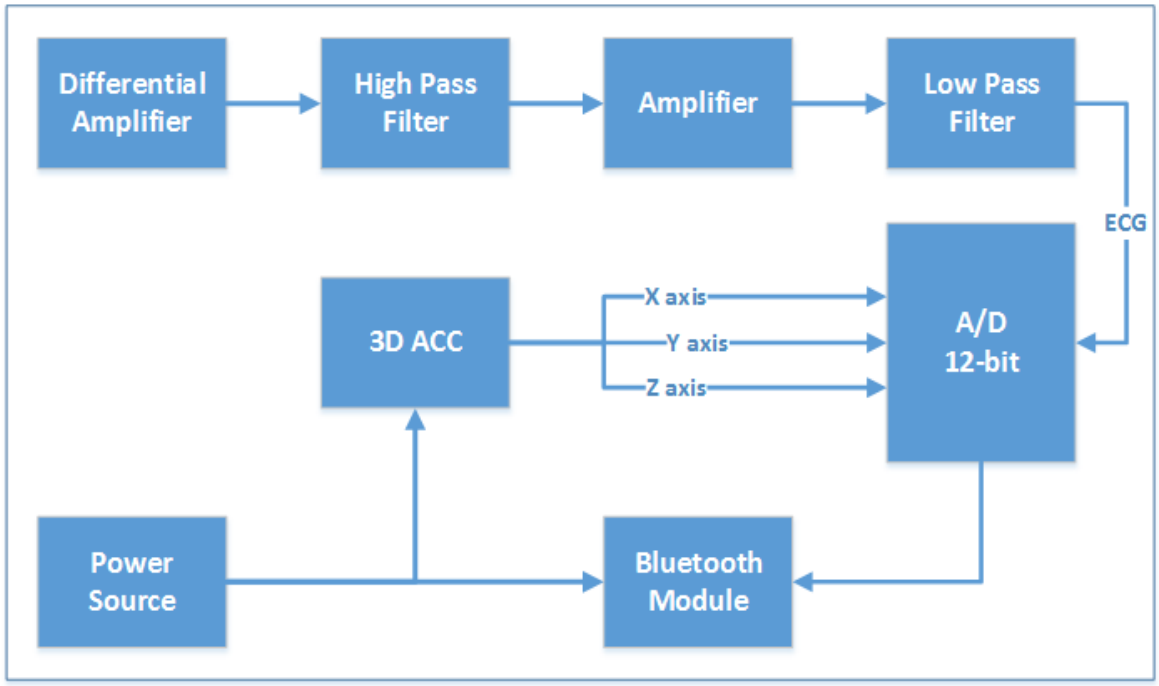

Fig. 2-1 Block diagram for the portable ECG recording system, (Liu, 2011).

The system captures the ECG signal in the analog domain using a differential amplifier and then filters it using a high pass filter and a low pass filter. The signal is captured in the analog domain, which is then converted to the digital domain and transmitted to the remote ECG recorder. The issue with the (Liu, 2011) solution is that the method of filtering the signal uses multiple filters and A/D converters before starting the process of motion artefact detection in the digital domain. By their very nature, filters introduce distortion to the desired signal as well as the unexpected packets drop while transferring the data segments to the remote destination. Nevertheless, the 3-axis accelerometers

method showed good results for (Tong *et al.*, 2002) and (Liu, 2011). However, they are not always suitable, especially for a non-contact electrode structure, where attaching an electrode to the human body is not acceptable (Nagai *et al.*, 2017).

(Alkhidir et al., 2015) used two additional electrodes that were placed near the ECG electrodes to capture the reference signal and compared the results with the statistical results of the independent component analysis (ICA). Fig. 2-2 shows the configuration of the additional electrodes and the detection of the ECG signal and the reference signal.

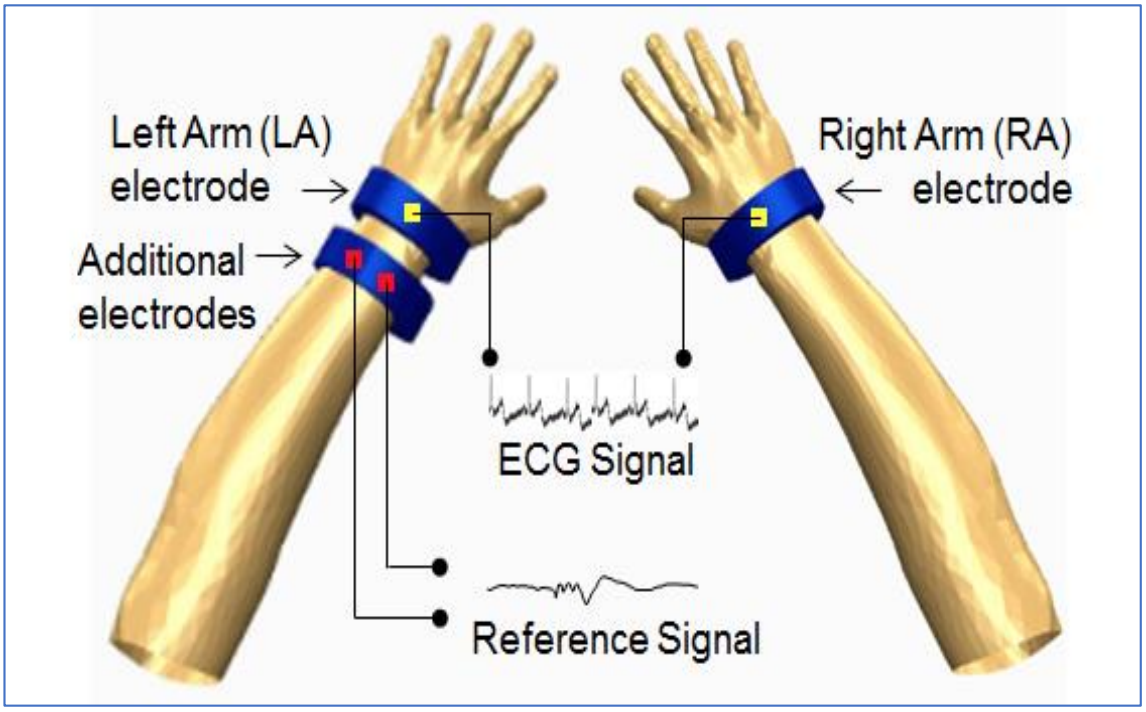

Fig. 2-2 Electrode configuration for measurement of the ECG signal and the reference signal (Alkhidir et al., 2015, p. 3808).

The use of the additional electrodes would help in detecting the artefacts without the need for any extra sensors that would require further development of the system. In addition, they claim to have improved performance over the ICA results. However, comparing the statistical results of the ICA with the results of their adaptive method is unfair as the improved performance is likely to happen due to the difference in both methods' nature. The results should be compared with a different approach that used a different adaptive approach to reduce the artefacts, such as the one used by (Tong *et*

al., 2002). In addition, their approach placed the extra two electrodes on the left hand which was not isolating the motion produced by the right hand, and they suggested placing additional reference electrodes on the right hand to overcome this issue. Increasing the number of electrodes might help in minimising the detected noise, but it also would increase the noise sources that need processing. As a result, this increase in the electrodes count would compromise the patient's comfort, which they were trying to avoid. In addition, both (Alkhidir *et al.*, 2015) and (Tong *et al.*, 2002) were relying on the use of the Least Mean Square (LMS) algorithm as an adaptive noise canceller. The LMS algorithm is an iterative adaptive signal processing technique that minimizes the Mean Square Error (MSE) between the primary signal and the reference signal (Thakor and Zhu, 1991). However, LMS and Normalised LMS require high computational power which makes it difficult to be implemented in clinical applications (Chandrakar and Kowar, 2012).

On the other hand, Chandrakar & Kowar utilized a Recursive Least Square (RLS) algorithm, which requires large computational power as well as the LMS and NLMS. They introduced an algorithm that is faster than the conventional RLS algorithm by incorporating the algorithm with the knowledge of the room impulse response. The algorithm was tested against four different types of artefacts which are: PLI, baseline wandering, muscle artefacts, and electrode motion artefacts. SNR results of the introduced algorithm show a better ratio when compared to the use of the conventional RLS algorithm. However, the method is still computationally expensive and is not suitable to get real-time ECG motion artefacts reduction results.

Adaptive Fourier Decomposition (AFD) was used by Wang *et al.* to denoise the ECG electrode motion artefacts and the muscle contractions. AFD represents the total summation of the mono energy components that are sequentially extracted from high-energy and low-energy modes to ensure the completeness of the original signal (Wang *et al.*, 2014). They used the estimated-SNR-based judgement along with AFD to detect

the electrode motion and muscle contraction noises and filter them out. In addition, they introduced rules to help in choosing and adjusting the decomposition level, which would help in getting the optimal results. The simulation results showed that AFD performs better than the other denoising methods, that were compared to the results. Fig. 2-3 shows the ECG signal and its filtering using the proposed technique.

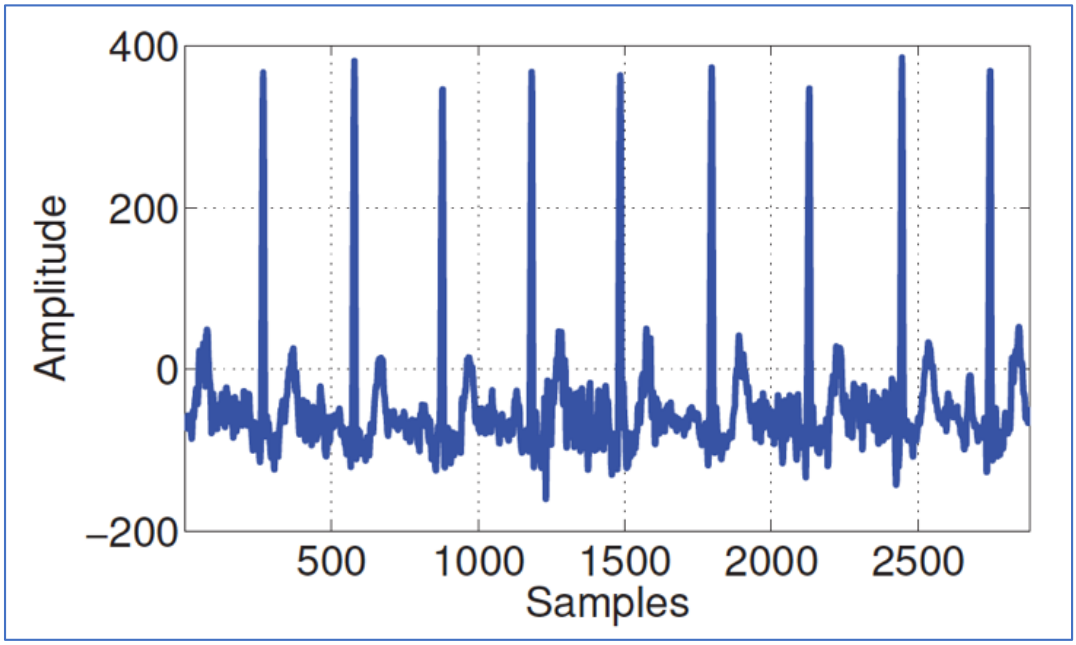

(a)

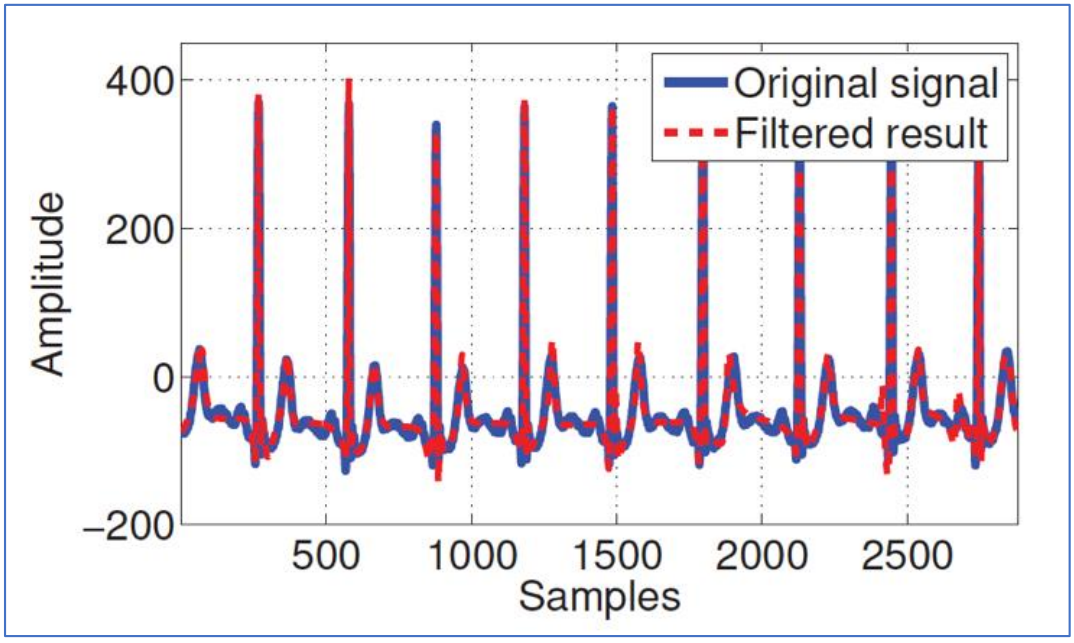

(b)

Fig. 2-3 (a) ECG Signal with real noise. (b) Reconstructed ECG signal after filtering (Wang et al., 2014, p. 1459).

The AFD method provided a good result when accompanied by the estimated-SNR-based judgement. However, finding the appropriate decomposition level to filter the artefacts and retain the original ECG signal is still problematic. Nevertheless, the provided guidelines showed the limitations of the usage of this method. For example, the proposed AFD method would not work if the SNR of the signal is smaller than 0 dB where the energy of the noise is larger than the original signal. The reason why AFD would not work when the noise is larger than the original signal is that it is based on energy decompositions which means that the reconstructed summation of the mono energy components will be constructed from noise.

2.4 Types of ECG Measurement Electrodes

ECG electrodes are the sensors which detect the heart activity and transduce the bioelectric activity into an electrical current which helps in measuring and recording the heart electrical activity in a recorder machine. The detected ECG signal can indicate the state of the heart in real-time by capturing inconsistent heart activity which, in turn, would highlight a highly life-threatening condition that can be treated in its early stages. There are different types of electrodes whereby each of them is suitable in its different applications and context. Some of these electrodes are suitable for wireless signal sensing; while others are for wearable medical applications. Each type of application also includes different types of electrodes, as in the dry electrodes. A detailed comparison that was done by (Fiedler *et al.*, 2014) to compare titanium pin electrodes, polyurethane multi-pin electrodes, and gold multi-pin electrodes that are mainly used in the routine application for electroencephalography (EEG; the brain activity).

Biopotential electrodes can be classified into two ideal designs depending on the use of a net current between the electrode surface and the electrolyte. Polarizable electrodes are one of the ideal designs of electrodes where the electrode does not use net current between the electrode surface and the electrolyte: which are called dry electrodes (Albulbul, 2016, Schmidt *et al.*, 2004). In addition, polarizable electrodes are reusable due to their resistance to corrosion (Martinsen and Grimnes, 2011). On the other hand, non-polarizable electrodes are wet electrodes that use electrolysation between the electrode and the skin to facilitate the bioelectrical activity detection process.

Wearable sensors are usually used in the remote health monitoring systems, and there are different types of electrodes that can be used in such an ambulatory environment. Such systems are designed to conduct the signal detection process at home, which requires well-designed electrodes that would last for longer periods and require less human effort, especially when a non-specialist is capturing the signal. Ambulatory

systems are long-term health monitoring systems which make the non-invasive (do not require biofluids), non-instructive sensors crucial elements in the construction of such systems (Majumder *et al.*, 2017). The use of non-invasive electrodes in wearable health applications has a high dependency on the electrode-skin impedance. Avoiding the high electrode-skin impedance will enhance the performance of the non-invasive electrodes as well as achieving a higher bioelectrical signal quality, better amplitude, and higher signal to noise ratio (SNR) (Albulbul, 2016). Having a high electrode-skin impedance would work as a barrier that prevents the biopotentials from being detected by causing a mismatch between the electrode and the skin (Martinsen and Grimnes, 2011, Albulbul, 2016). Such a gap would lower the common-mode rejection ratio and introduce more powerline artefacts (Webster, 2009). Therefore, the selected type of electrode that is used in the portable applications would help in forming the characteristics of the ambulatory medical applications.

Silver/Silver chloride (Ag/AgCl) reference electrodes, as shown in Fig. 2-4, are one of the most commonly used wet non-polarized electrodes that are used for recording many bioelectrical activities such as ECG, EMG, and EEG.

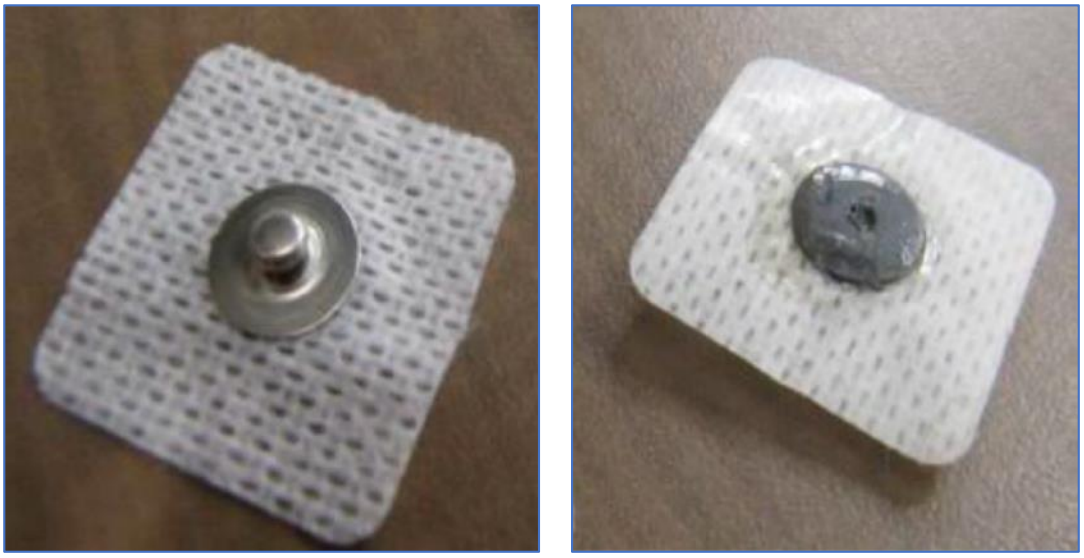

(a) (b)

Fig. 2-4 (a) Ag/AgCl electrode (snap side). (b) Ag/AgCl electrode (skin side) (Albulbul, 2016, p. 4).

It has a low noise level in addition to a lower electrode-skin impedance which allows the biopotential electrical activity to be easily detected. Such characteristics nominate the Ag/AgCl to be used in ambulatory applications. However, these electrodes have a limited wear time depending on the use of the electrolytes (gels) as well as them requiring a well-trained medical technician (Fiedler et al., 2014, Albulbul, 2016).

Stainless steel electrodes, shown in Fig. 2-5, are another type of polarizable electrodes that are commonly used in wireless applications to monitor the biological signals. However, they generate a high electrode-skin impedance that is higher than all other types of electrodes as reviewed by (Ragheb and Geddes, 1991).

(a) (b)

Fig. 2-5 (a) Stainless steel electrode (snap side). (b) Stainless steel electrode (skin side) (Albulbul, 2016, p. 5).

Dry orbital electrodes, shown in Fig. 2-6, are made to last longer on the body, and they do not require any electrolysation which eliminates the need for skin preparation prior to the signal recording process (Schmidt et al., 2004).

(a) (b)

Fig. 2-6 (a) Orbital electrode (snap side). (b) Orbital electrode (skin side) (Albulbul, 2016, p. 5).

Orbital electrode design includes pins (spikes) that enable it to penetrate a deeper layer of the skin and facilitate the detection of the bioelectrical activities (Schmidt *et al.*, 2004, Albulbul, 2016) as shown in Fig. 2-7. This design of orbital electrodes gives it stronger connectivity to the skin than the Ag/AgCl electrodes.

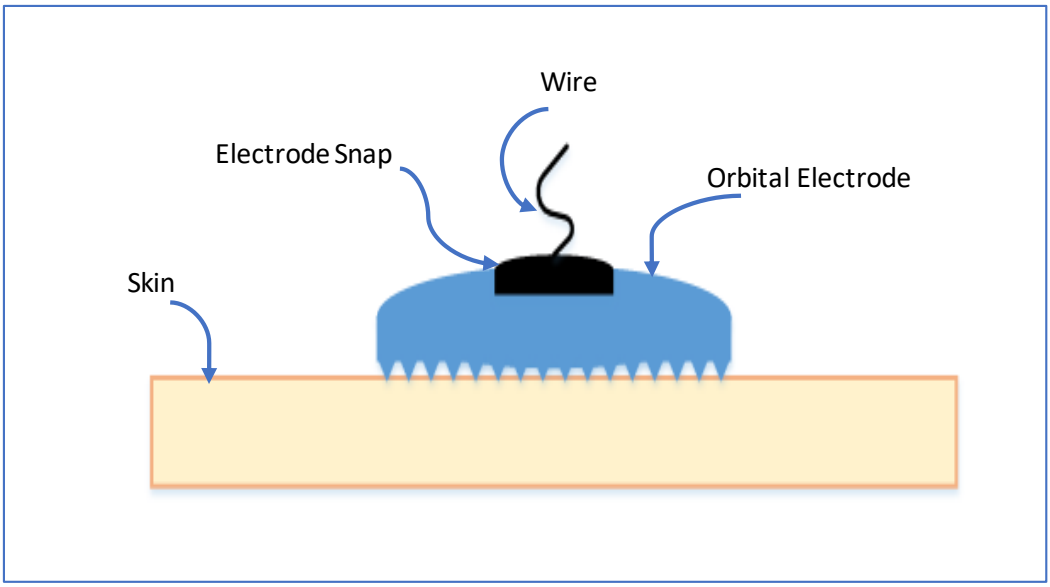

Fig. 2-7 Orbital Electrode penetration into skin surface(Albulbul, 2016)

2.5 Strain Gauges

Motion artefacts are one of the most difficult noises introduced into ECG signals which requires us to develop better techniques to eliminate these artefacts due to its effect on the correct interpretation of an ECG biopotential. Researchers explored and introduced various solutions that varied between the different approaches such as statistical, adaptive, and a pre-distortion approach. As mentioned earlier, adaptive noise reduction techniques were the most commonly used methods that included the use of different components such as additional electrodes, motion sensors, two-axis anisotropic magnetoresistive (AMR) sensors, a developed 3-axis accelerometer (ACC) sensors, LMS, RLS, and AFD. Motion noises can be considered as small and precise mechanical strains which make the use of strain gauges one of the possible life-savers in the noise reduction process. In addition, it has a very small change in resistance which would not be measurable by the normal direct measurement tools such as an ohmmeter. Therefore, the precise determination that is applicable when using strain gauges helps in putting through a solid determination of the change in resistance. Strain gauges have an infinite range of measurement possibilities as it could measure a 1/10,000 micro-strain and are capable of detecting a vibration of 1dB that is happening within a 10-foot room (Chevalier, 2011, Ştefănescu, 2011). Fig. 2-8 shows a typical strain gauge design and the idea behind strain detection.

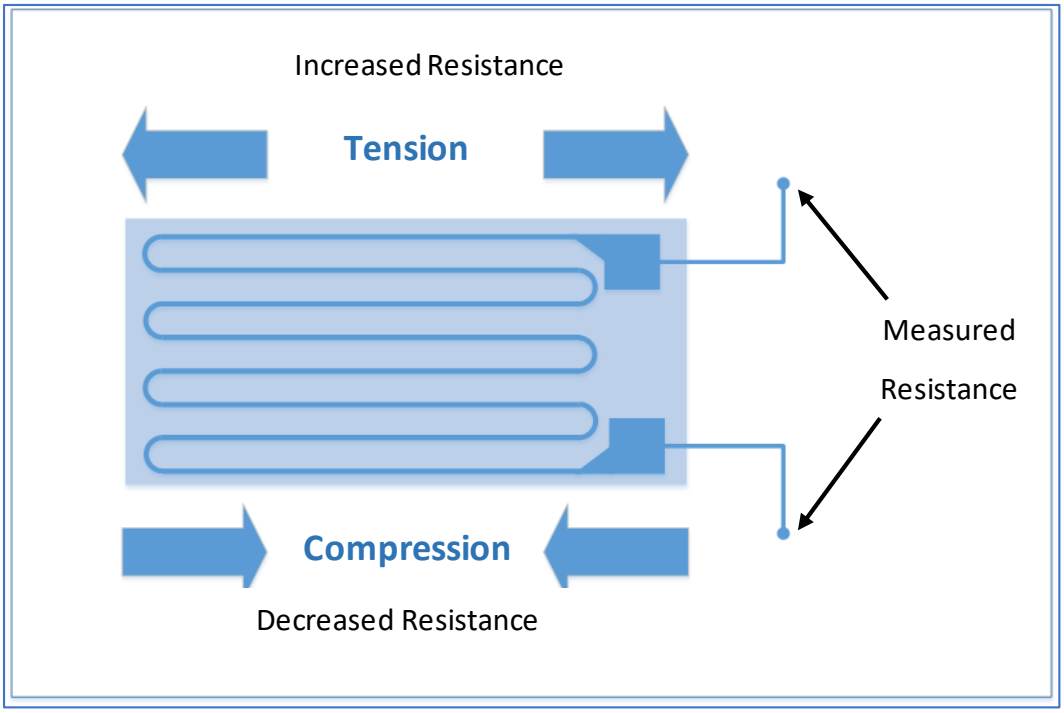

Fig. 2-8 Typical Strain Gauge Design

Many strain sensors types can be used in medical applications. For example, the most commercially low-cost strain gauges are the metallic strain gauges (Liu and Choi, 2009). However, their large size makes them less compatible with implanted medical devices that are naturally small, as well as the need for long-term embedded solutions. Alternatively, elastomeric materials offer much more flexible strain sensors that are more compatible with biomedical applications. In addition, the sensors fabrication capability is more efficient when using sensors made from elastomeric materials (Liu and Choi, 2009).

HBM is one of the industrial businesses that use strain gauges in their design, development and manufacture of medical equipment. They build custom strain gauges that would be used in critical high-precision robotic surgeries and some other non-critical applications such as patient scale weight distribution (Chevalier, 2011). For example, a CT scan is a Non-Invasive Medical Imaging and Diagnostic Equipment which requires a precise patient weight distribution as well as repeated table positioning in order to perform highly accurate imaging functions. HBM incorporated multi-axis strain gauges to

ensure a smooth and consistent movement of the table during the weight distribution adjustment process. One other example is the development of Insulin Pump Fluid Flow Monitoring systems; these utilise the strain gauge technology to monitor and control the output of the pump.

The typical design approach in incorporating the strain gauges is to create a Wheatstone bridge circuit, as shown in Fig. 2-9. A strain gauge would be wired into the Wheatstone balanced bridge that would convert the mechanical movement into a change in resistance. The change in resistance that is detected by the strain gauge in case of a strain will affect the bridge symmetry and makes it unbalanced. In this case, the bridge output voltage will change from zero or null to some translated voltage that is caused by the new bridge state.

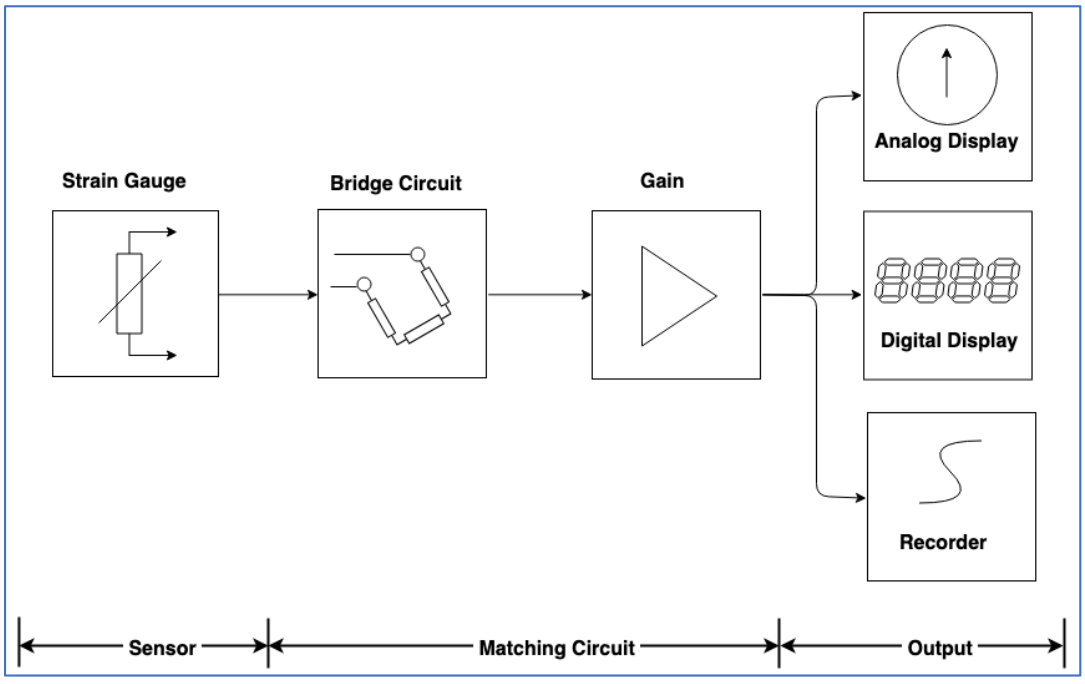

Fig. 2-9 A typical Wheatstone bridge circuit design

Two-Axis strain gauges were part of (Lee *et al.*, 2010) research to detect the motion artefacts of the human body while recording the ECG bioactivity. The introduced design incorporates the ECG electrode with a strain gauge and a G-sensor (3-Axis Accelerometer) where all the detected signals are amplified and filtered and then

processed by a microcontroller (MCU) as shown in Fig. 2-10. The G-sensor detects the human activity inertia signal such as walking. They adhered the strain gauge on the body of the sensing module, which makes it reusable and would accurately detect the skin stretches signals (Lee *et al.*, 2010). Similar to the explained approach earlier, the strain gauge is incorporated with a Wheatstone bridge and the change in resistance is detected and the voltage output will be produced when the bridge is unbalanced.

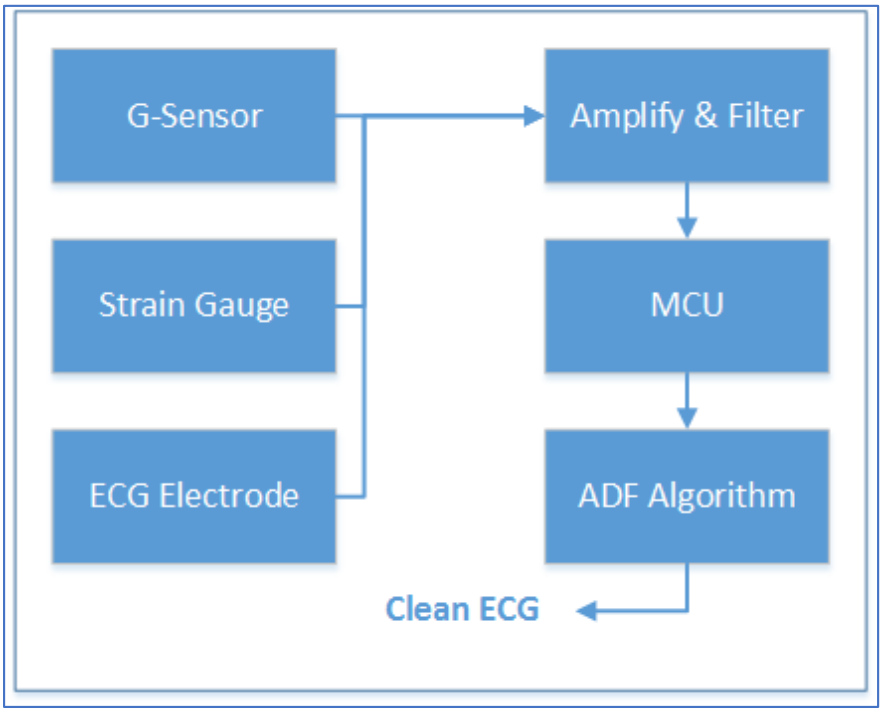

Fig. 2-10 System Block Diagram of an Adaptive Reduction of ECG Artefacts (Lee et al., 2010)

In this adaptive filtering research, authors are correlating between the detected ECG signal and the accelerometer signal, and between the ECG signal and the G-sensor signal, respectively. This would provide the two reference signals (master and slave) for the master-slave multiple noise reduction adaptive filtering process; where the higher signal should be the master signal as the higher coefficient means better noise cancellation within the adaptive filter (Lee *et al.*, 2010). The NLMS adaptive algorithm uses the reference signal from the accelerometer and the G-sensor to eliminate the motion artefacts and adjusts the Finite Impulse Response (FIR) filter accordingly. The solution shows good experimental results and the SNR was improved. However, using

LMS and Normalised LMS still requires a high computational power as was discussed earlier. Thus, it is difficult to use the NLMS in the clinical applications that need a large number of taps in the adaptive filters (Chandrakar and Kowar, 2012).

Monitoring human body movement, respiration, and heart activity during sleep is one of the topics that employed the use of strain gauges. Many researchers and industrial entities are providing various commercial solutions that are suitable for hospital use, such as EarlySense, or home use, such as Beddit. These solutions provide statistical data about the quality of the human sleeping pattern by tracking the data collected from ECG signals, respiration rates, and stress levels. The purpose of such solutions is to monitor the sleep pattern without disturbing the patient while sleeping, which makes it more difficult to detect and track the required signals without direct attachment to the human body. Hence, these solutions were able to track the relatively large signal changes such as respiration and body movement during sleep. However, they were unable to provide accurate ECG signals due to its small range. To solve the problem, additional analysis and adaptive filtering process had to be done externally (Kwak *et al.*, 2018), which this research tries to avoid.

Strain gauges were widely used in different industrial solutions and biomedical applications. It was used for torque control of robotic platforms (Djermanova *et al.*, 2015, Kashiri *et al.*, 2017), respiration signal estimation (Busono, 2014, Kwak *et al.*, 2018, Chevalier, 2011, Bowman, 1992), bone fracture treatment (Liu and Choi, 2009), Non-Invasive Medical Imaging and Diagnostic Equipment and Weight Distribution Applications (Chevalier, 2011), among many other solutions. However, there was no use for strain gauges in ECG artefact reduction, which influenced this research.

In this research, two strain gauges were used to detect the X-plane and Y-plane movements and strains which then can be subtracted from the original obtained ECG signal to produce a cleaner output signal, when compared to the input signal.

2.6 Biomedical/Biopotential Amplifiers

The human body consists of many biological systems where each system has its own characteristics and physiological phenomena. These systems include the nervous system, muscular system, cardiovascular system and many other systems. The physiological processes within the different human body subsystems express themselves as a bioelectrical signal that represents their nature and activity. Any defection to the norm and nature of this activity is dealt with as an abnormal activity of the human body physiological processes, which would be interpreted in its own context and its danger would be specified accordingly. Most of the accompanying bioelectrical signals of the body subsystems are small coefficients which increase the need for signal amplification in order to be able to apply additional signal processing such as filtering, smoothing, averaging and noise cancellation. ECG, EEG and EMG signals are the heart electrocardiogram, brain electroencephalogram, and muscles electromyogram subsystems signals, respectively. Fig. 2-11 shows the frequencies of these physiological processes' ranges from 0.5Hz to 1000Hz with a small amplitude voltage that is ranging from 10^{-6} V to almost 1V. This explains the need for biomedical amplifiers to increase the amplitude of the captured small potentials and make them compatible with medical devices, such as displays and recorders.

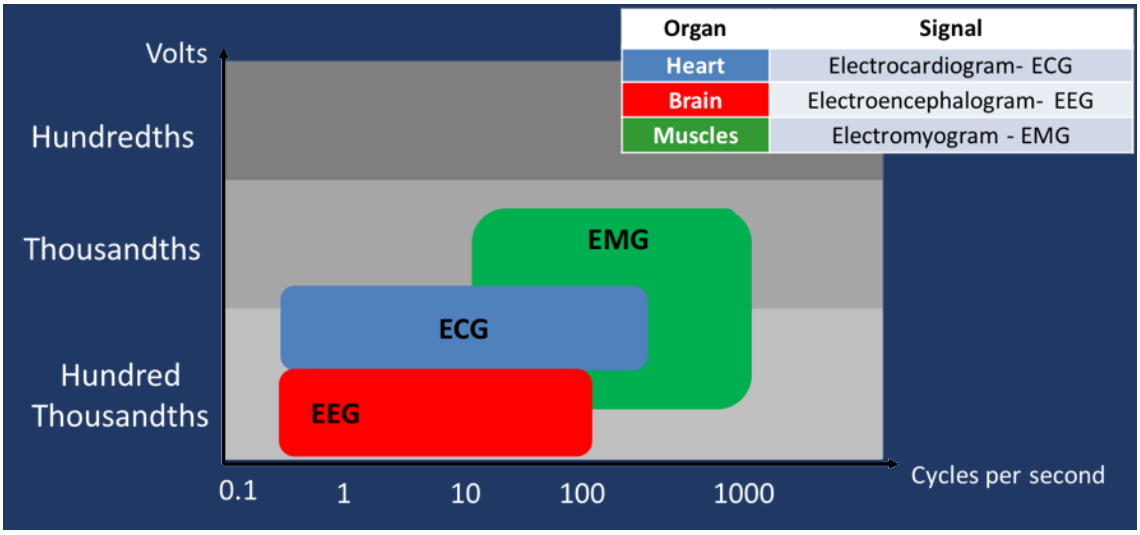

Fig. 2-11 Electrical characteristics of common bio-potential signals (Yazicioglu et al., 2008)

As discussed earlier, the obtained biopotentials could include the desired signal, the undesired noise, powerline interference signals, and the motion artefacts. Therefore, biomedical amplifiers must amplify the physiologic signals and reject any noises attached to the desired signal. The typical biomedical amplifiers process voltage. However, some amplifiers process currents and its frequency response start from 0.05Hz up to 100kHz (Sathiyabama *et al.*, 2015).

Designing a biopotential amplifier has to satisfy some basic requirements that would guarantee the quality of the measured signal and reject the large portion of the artefacts. These requirements include preventing the amplifier from influencing the physiological process by any means and the best possible separation of the desired signal and other noise interferences has to be provided by the amplifier. In addition, the amplifier has to protect the patient against any potential micro-shocks that can happen due to the input electric currents (Neuman, 1998), a protection for the amplifier itself against the high input voltages has to be considered, and the amplifiers must have high input impedance (Nagel, 2000).

When excessive electric loading is present at the biomedical electrodes, a distortion of the signal will occur. Therefore, increasing the amplifier input impedance will provide the minimal signal loading, which, consequently, will minimise the loading effect. Recent biopotential amplifiers use an input impedance of at least 10 MΩ, whereas the output impedance must be small to provide minimal distortion with respect to the load impedance (Neuman, 1998). The schematic shown in Fig. 2-12 illustrates the main stages of biopotential signal amplification. Biopotential signals are obtained using bipolar electrodes that are often symmetrically located on the patient's skin with respect to the ground. Therefore, differential amplifiers are considered as the most appropriate amplifiers for biomedical applications. The preamplifier part is the critical part of the amplifier that could eliminate or minimise most of the undesired interfering signals. Current technology offers preamplifiers that exhibit about five times the voltage noise

density compared to bipolar transistors such as Field-effect transistor (FET) preamplifiers (Nagel, 2000).

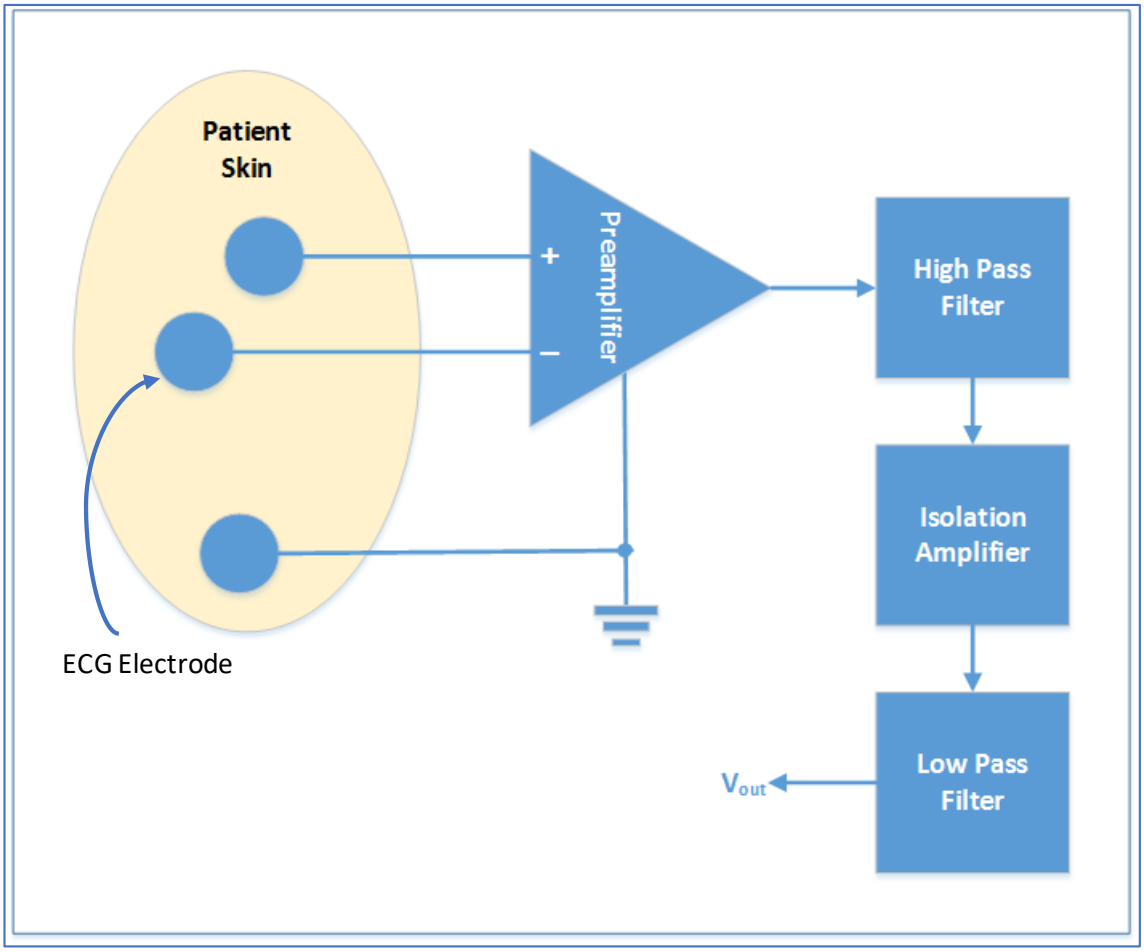

Fig. 2-12 Schematic design of the main stages of a biopotential amplifier (Nagel, 2000)

The frequency of the bioelectrical signals is as low as 0.5Hz and can go up to 1000Hz, and the voltage varies from 10^{-6} V to almost 1V. With this said, the requirement of limiting the biomedical amplifiers bandwidth is important, so it only amplifies the portion of the frequencies that represents a potential bioelectrical activity, which explains the use of the high-pass and low-pass filters in the schematic design in Fig. 2-12. These filters must have a high order sharp-cutting linear phase to avoid bio-signal distortion and attenuation such as the Active Bessel filters. These are known for their smooth transfer function (Nagel, 2000), which results in having a high signal-to-noise ratio. To achieve the safety requirements in the design of the biomedical amplifier: such as avoiding electrical

hazards, and preventing ground loops, the isolation amplifier stage is used as a galvanic decoupling layer. In analog applications, the isolation amplifiers can transfer the signal through the isolation barrier using a transformer, optical or capacitive couplers.

Differential amplifiers are designed to reject the line frequency interference (common-mode signal) and provide the desired differential signal that appears as a voltage between the positive and negative interfaces of the amplifier. The higher the common-mode signal rejection ratio, the better the biopotential amplifier design.

Instrumentation Amplifiers (IAs) are very important analog signal processing circuits that could have differential-inputs and differential outputs or differential-inputs and a single output (Spinelli et al., 2004, Van and Van De Plassche, 1975, Franco, 1989). Most IA circuits typically perform at low frequency with a typical CMRR > 100dB and their performance declines in higher frequencies. Designing Instrumentation Amplifiers circuits to achieve high CMRR is still challenging in the biomedical applications field that essentially requires a typical CMRR that is bigger than 100dB, a minimum power supply voltage that is less than 5V, and a minimum output current of 1mA (Dool and Huijsing, 1993, Stout and Kaufman, 1976). To achieve a better CMRR and provide optimum signal quality that is suitable for further signal processing, the amplifier has to have a high gain, of order 1000 or greater. Moreover, the design of the amplifier has to be adapted to the specific bioelectrical activity to be measured by choosing the appropriate bandwidth and gain factors based on the ranges of the amplitude and bandwidth as explained in Fig. 2-11.

2.7 Summary

This chapter reviewed the previous work towards artefact reduction, which forms the foundation of this research. It covered the original sources of artefacts, including powerline interference, common-mode interference, and motion artefacts. Additionally, the review included the various approaches involved in solving the motion artefact, such as the statistical and adaptive approaches. The review outlined the different challenges within these approaches. In addition, the different types of biopotential electrodes were explored, showing the relationship between the motion artefacts and the types of electrodes and how the different types were used to minimise this type of artefacts. For example, the orbital electrode design included pins that enabled it to penetrate a deeper layer of the skin and facilitate the detection of the bioelectrical activities. Finally, a review of the strain gauges as sensors and how they could be used in artefact reduction, along with the use of the biomedical amplifiers, was discussed.

2.8 References

[1] ALBULBUL, A. 2016. Evaluating major electrode types for idle biological signal measurements for modern medical technology. *Bioengineering,* 3**,** 20.

[2] ALKHIDIR, T., SLUZEK, A. & YAPICI, M. K. Simple method for adaptive filtering of motion artifacts in E-textile wearable ECG sensors. Engineering in Medicine and Biology Society (EMBC), 2015 37th Annual International Conference of the IEEE, 2015. IEEE, 3807-3810.

[3] BELGURZI, S., ELSHAFIEY, I. & NOUH, A. Artifacts removal from ECG signal using an ANFIS technique. Cybernetics and Computational Intelligence (CyberneticsCom), 2017 IEEE International Conference on, 2017. IEEE, 147-152.

[4] BOWMAN, B. R. 1992. Strain gauge for medical applications. Google Patents.

[5] BUSONO, P. Algorithm for respiration estimation from 12-lead ECG machine. Information, Communication Technology and System (ICTS), 2014 International Conference on, 2014. IEEE, 43-46.

[6] CHANDRAKAR, C. & KOWAR, M. 2012. Denoising ECG signals using adaptive filter algorithm. *International Journal of Soft Computing and Engineering (IJSCE),* 2**,** 120-123.

[7] CHEVALIER, R. 2011. Understanding the Benefits of Strain Gauge Technology in OEM Medical Devices and Equipment. *Electronic Component News* [Online], 2018. Available: https://www.hbm.com/en/3517/understanding-the-benefits-of-strain-gauge-technology-in-oem-medical-devices-and-equipment/#:~:text=The%20relatively%20low%2Dcost%20design,and%20minimally%20invasive%20device%20designs.

[8] DESHPANDE, S. & RAJANKAR, S. 2013. Removing Artifacts from the ECG By using Independent component analysis. *International Journal for Research in Science & Advanced Technologies,* 5**,** 182-184.

[9] DJERMANOVA, N. J., MARINOV, M. B. & GANEV, B. T. 2015. Alternating Current-Driven Strain-gage Bridge Amplifier System for Brushless Motors Torque Measurement. *ANNUAL JOURNAL OF ELECTRONICS*, 159-162.

[10] DONGHUI, Z. Wavelet Approach for ECG Baseline Wander Correction and Noise Reduction. 2005 IEEE Engineering in Medicine and Biology 27th Annual Conference, 2005 2005. 1212-1215.

[11] DOOL, B. J. V. D. & HUIJSING, J. K. 1993. Indirect current feedback instrumentation amplifier with a common-mode input range that includes the negative roll. *IEEE Journal of Solid-State Circuits,* 28, 743-749.

[12] DUMITRU, C. & GAVAT, I. Voice-dial by statistical recognition of continuous speech. Signals, Circuits and Systems, 2003. SCS 2003. International Symposium on, 2003. IEEE, 157-160.

[13] FIEDLER, P., HAUEISEN, J., JANNEK, D., GRIEBEL, S., ZENTNER, L., VAZ, F. & FONSECA, C. 2014. Comparison of three types of dry electrodes for electroencephalography. *Acta Imeko,* 3, 33-37.

[14] FRANCO, S. 1989. Current-feedback amplifiers benefit high-speed designs. *EDN,* 34, 161.

[15] GARG, G., GUPTA, S., SINGH, V., GUPTA, J. R. P. & MITTAL, A. P. Identification of optimal wavelet-based algorithm for removal of power line interferences in ECG signals. India International Conference on Power Electronics 2010 (IICPE2010), 28-30 Jan. 2011 2011. 1-5.

[16] GAUTAM, A., LEE, Y. D. & CHUNG, W. Y. ECG Signal De-noising with Signal Averaging and Filtering Algorithm. 2008 Third International Conference on Convergence and Hybrid Information Technology, 11-13 Nov. 2008 2008. 409-415.

[17] HADDAD, S. A. P. & SERDIJN, W. A. 2009. *Ultra low-power biomedical signal processing: an analog wavelet filter approach for pacemakers*, Springer Science & Business Media.

[18] HAMPTON, J. 2008. The ECG made easy, Churchill Livingstone. Elsevier.

[19] HONEYWELL 2019. 1- and 2-Axis Magnetic Sensors. *In:* INC, H. I. (ed.). Honeywell.com.

[20] IMTIAZ, S. A., MARDELL, J., SAREMI–YARAHMADI, S. & RODRIGUEZ–VILLEGAS, E. 2016. ECG artefact identification and removal in mHealth systems for continuous patient monitoring. *Healthcare technology letters,* 3**,** 171-176.

[21] JENKAL, W., LATIF, R., TOUMANARI, A. & CHARRI, O. E. B. Efficient method Of QRS complex extraction using a multilevel algorithm and an adaptive thresholding technique. 2015 Third World Conference on Complex Systems (WCCS), 23-25 Nov. 2015 2015. 1-5.

[22] KANNAN, N. & KUNDU, D. 2016. Statistical Signal Processing. *Wiley StatsRef: Statistics Reference Online*.

[23] KASHIRI, N., MALZAHN, J. & TSAGARAKIS, N. G. 2017. On the Sensor Design of Torque Controlled Actuators: A Comparison Study of Strain Gauge and Encoder-Based Principles. *IEEE Robotics and Automation Letters,* 2**,** 1186-1194.

[24] KASTURIWALE, H. P. 2012. Analysis & Interpretation of Biomedical Signals using component extraction techniques. *Analysis,* 7**,** 8.

[25] KASTURIWALE, H. P. & INGOLE, P. 2012. Component extraction of complex biomedical signals and performance analysis. *Int. J. Comput. Sci. Inf. Technol,* 3**,** 3544-3547.

[26] KISHIMOTO, Y., KUTSUNA, Y. & OGURI, K. Detecting motion artifact ECG noise during sleeping by means of a tri-axis accelerometer. Engineering in Medicine and Biology Society, 2007. EMBS 2007. 29th Annual International Conference of the IEEE, 2007. IEEE, 2669-2672.

[27] KONG, W., VANDERBURG, C. R., GUNSHIN, H., ROGERS, J. T. & HUANG, X. 2008. A review of independent component analysis application to microarray gene expression data. *BioTechniques,* 45**,** 501-520.

[28] KWAK, Y. H., KIM, J. & KIM, K. 2018. Sleep monitoring sensor using flexible metal strain gauge. *Japanese Journal of Applied Physics,* 57**,** 05GD03.

[29] LANATA, A., GUIDI, A., BARAGLI, P., VALENZA, G. & SCILINGO, E. P. 2015. A Novel Algorithm for Movement Artifact Removal in ECG Signals Acquired from Wearable Systems Applied to Horses. *PloS one,* 10**,** e0140783.

[30] LEE, W.-C., YANG, Y.-S. O., KE, T.-C., WEI, C.-S. & LEE, H.-C. Adaptive reduction of motion artifact in a portable ECG system. Sensors, 2010 IEEE, 2010. IEEE, 704-707.

[31] LIU, C.-X. & CHOI, J.-W. An embedded PDMS nanocomposite strain sensor toward biomedical applications. Engineering in Medicine and Biology Society, 2009. EMBC 2009. Annual International Conference of the IEEE, 2009. IEEE, 6391-6394.

[32] LIU, S.-H. 2011. Motion artifact reduction in electrocardiogram using adaptive filter. *J. Med. Biol. Eng,* 31**,** 67-72.

[33] MAJUMDER, S., MONDAL, T. & DEEN, M. J. 2017. Wearable sensors for remote health monitoring. *Sensors,* 17**,** 130.

[34] MARTINSEN, O. G. & GRIMNES, S. 2011. *Bioimpedance and bioelectricity basics*, Academic press.

[35] MITHUN, P., PANDEY, P. C., SEBASTIAN, T., MISHRA, P. & PANDEY, V. K. A wavelet based technique for suppression of EMG noise and motion artifact in ambulatory ECG. 2011 Annual International Conference of the IEEE Engineering in Medicine and Biology Society, Aug. 30 2011-Sept. 3 2011 2011. 7087-7090.

[36] MNEIMNEH, M. A., YAZ, E. E., JOHNSON, M. T. & POVINELLI, R. J. An adaptive kalman filter for removing baseline wandering in ECG signals. 2006 Computers in Cardiology, 17-20 Sept. 2006 2006. 253-256.

[37] NAGAI, S., ANZAI, D. & WANG, J. Motion artifact removal for wearable ECG using stationary wavelet multi-resolution analysis. Electromagnetic Compatibility (EMC-Beijing), 2017 IEEE 5th International Symposium on, 2017. IEEE, 1-5.

[38] NAGEL, J. H. 2000. Biopotential amplifiers. *Bronzino JD: Biomedical engineering hand book, 2nd edition, Springer-Verlag New York*, 70.1-70.14.

[39] NEUMAN, M. R. 1998. Biopotential amplifiers. *Medical instrumentation: application and design*, 316-318.

[40] PRIYA, K. D., RAO, G. S. & RAO, P. S. V. S. 2016. Comparative Analysis of Wavelet Thresholding Techniques with Wavelet-wiener Filter on ECG Signal. *Procedia Computer Science,* 87, 178-183.

[41] RAGHEB, T. & GEDDES, L. 1991. The polarization impedance of common electrode metals operated at low current density. *Annals of biomedical engineering,* 19, 151-163.

[42] ROMERO, I., GENG, D. & BERSET, T. Adaptive filtering in ECG denoising: A comparative study. 2012 Computing in Cardiology, 9-12 Sept. 2012 2012. 45-48.

[43] RUTLEDGE, D. N. & JOUAN-RIMBAUD BOUVERESSE, D. 2013. Independent Components Analysis with the JADE algorithm. *TrAC Trends in Analytical Chemistry,* 50, 22-32.

[44] SATHIYABAMA, G., VINUDEVI, G., R, A. & INDHUPRIYA, P. 2015. A Survey on Instrumentation Amplifiers used for Biomedical Application. *International Journal of Advanced Research in Electrical, Electronics and Instrumentation Engineering,* 4, 1224-1231.

[45] SCHMIDT, R. N., LISY, F. J., SKEBE, G. G. & PRINCE, T. S. 2004. Dry physiological recording electrode. Google Patents.

[46] SHAIK, B. S. & CHAKKA, V. K. Joint reduction of baseline wander, PLI and its harmonics in ECG signal using Ramanujan Periodic Transform. India Conference (INDICON), 2016 IEEE Annual, 2016. IEEE, 1-5.

[47] SHAIK, B. S., CHAKKA, V. K., GOLI, S. & REDDY, A. S. Removal of narrowband interference (PLI in ECG signal) using Ramanujan periodic transform (RPT). Signal Processing and Communication (ICSC), 2016 International Conference on, 2016. IEEE, 233-237.

[48] SINGH, B., SINGH, P. & BUDHIRAJA, S. Various Approaches to Minimise Noises in ECG Signal: A Survey. 2015 Fifth International Conference on Advanced Computing & Communication Technologies, 21-22 Feb. 2015 2015. 131-137.

[49] SPINELLI, E. M., MARTÍNEZ, N., MAYOSKY, M. A. & PALLÀS-ARENY, R. 2004. A novel fully differential biopotential amplifier with DC suppression. *IEEE transactions on biomedical engineering,* 51**,** 1444-1448.

[50] ŞTEFĂNESCU, D. M. Strain gauges and Wheatstone bridges — Basic instrumentation and new applications for electrical measurement of non-electrical quantities. Eighth International Multi-Conference on Systems, Signals & Devices, 22-25 March 2011 2011. 1-5.

[51] STELAND, A. 2012. *Financial Statistics and Mathematical Finance: Methods, Models and Applications*.

[52] STOUT, D. F. & KAUFMAN, M. 1976. Handbook of operational amplifier circuit design.

[53] THAKOR, N. V. & ZHU, Y.-S. 1991. Applications of adaptive filtering to ECG analysis: noise cancellation and arrhythmia detection. *IEEE transactions on biomedical engineering,* 38**,** 785-794.

[54] TONG, D., BARTELS, K. & HONEYAGER, K. Adaptive reduction of motion artifact in the electrocardiogram. Engineering in Medicine and Biology, 2002. 24th Annual Conference and the Annual Fall Meeting of the Biomedical Engineering Society EMBS/BMES Conference, 2002. Proceedings of the Second Joint, 2002. IEEE, 1403-1404.

[55] VAN, D. E. & VAN DE PLASSCHE, R. J. 1975. A WIDE-BAND MONOLITHIC INSTRUMENTATION AMPLIFIER.

[56] WANG, Z., WONG, C. M., DA CRUZ, J. N., WAN, F., MAK, P.-I., MAK, P. U. & VAI, M. I. Muscle and electrode motion artifacts reduction in ECG using adaptive Fourier decomposition. Systems, Man and Cybernetics (SMC), 2014 IEEE International Conference on, 2014. IEEE, 1456-1461.

[57] WEBSTER, J. 2009. *Medical instrumentation: application and design*, John Wiley & Sons.

[58] WEI, Z., XU, W., LINLIN, G. & ZHUO, Z. Noise Reduction in ECG Signal Based on Adaptive Wavelet Transform. 2005 IEEE Engineering in Medicine and Biology 27th Annual Conference, 17-18 Jan. 2006 2005. 2699-2702.

[59] WU, Y. & RANGAYYAN, R. M. An Algorithm for Evaluating the Performance of Adaptive Filters for the Removal of Artifacts in ECG Signals. 2007 Canadian Conference on Electrical and Computer Engineering, 22-26 April 2007 2007. 864-867.

[60] YAZICIOGLU, R. F., VAN HOOF, C. & PUERS, R. 2008. *Biopotential readout circuits for portable acquisition systems*, Springer Science & Business Media.

[61] YOON, H., KIM, H., KWON, S. & PARK, K. An automated motion artifact removal algorithm in electrocardiogram based on independent component analysis. Proceedings of the 5th International Conference on eHealth, Telemedicine, and Social Medicine (eTELEMED'2013), 2013. 15-20.

[62] ZHANG, H., ZHANG, S., JIN, Q., LIU, X., LI, Q., YANG, J. & ZHAO, J. Motion artifact suppression in ambulatory ECG with feed forward combined adaptive filter. Computing in Cardiology Conference (CinC), 2016, 2016. IEEE, 1-4.

CHAPTER 3

PRODUCT DESIGN SPECIFICATIONS

3.1 Introduction

This chapter elaborates on the design process, refinement and building of the complete novel AFE that were the core of the ECG motion artefact reduction system. It starts by exploring the initial design of the AFE system that was published in 2018 and explains how the initial design was built and how it formed the core kernel of the system. It also explores the final system design requirements and how the motion artefacts and common-mode noise signals were expected to be handled and processed in the system. Additionally, the different test approaches that were taken to test the final system outputs were discussed. These approaches included the simulation of the system in MATLAB first and then comparing the results with the laboratory results. In addition, the novel test rig that was built to test the strain gauges detection of motion artefacts is explained. Also, the components that were used in minimising the common-mode noise were discussed. Finally, the harmonic distortion spectrum analysis is introduced, and the meaning of each of the spectrum parts and their use in measuring the harmonic distortion is clarified.

3.2 Overall Product Design Specifications

The system design included electrode fitted sensors. The sensors detect any vertical or horizontal movement of the electrode and then feed this information back to the system for the removal of any movement artefact. In this case, two strain gauges, separated by 90° were fitted onto the electrode to detect any X and Y plane movements, with regards to the patient's chest. The output of these was then fed back into the novel AFE for artefact removal, as shown in Fig. 3-1.

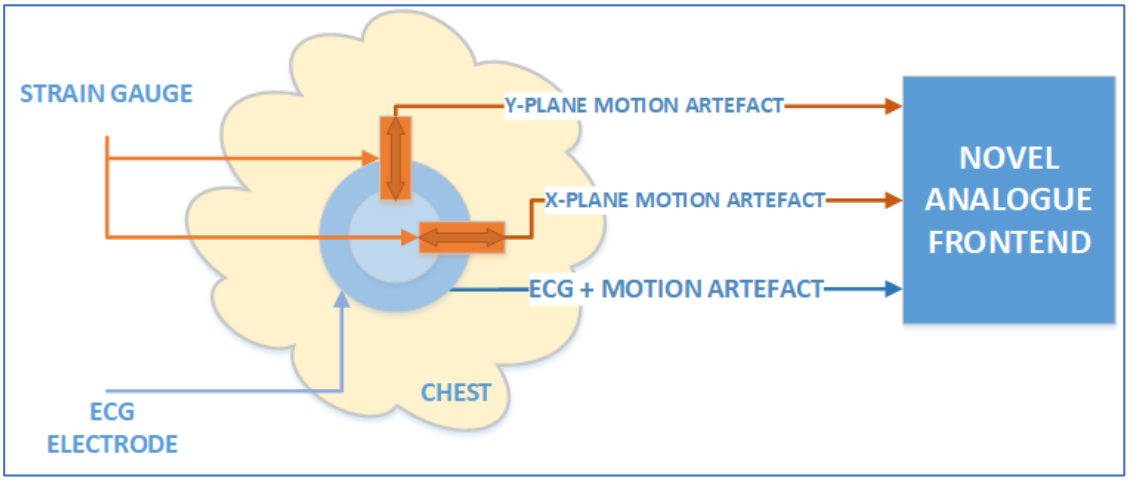

Fig. 3-1 System High-Level Design

The electrode captures the desired heartbeat (ECG signal) together with any movement artefacts and sends the resultant signal to the AFE. The AFE worked in the analog domain, which enabled faster signal processing and consumes less power than processing in the digital domain.

The initial AFE system design, shown in Fig. 3-2, included the removal of common-mode noise first and then the removal of any motion artefacts using the detected X-Plane and Y-Plane strain gauges signals as a reference. *Inp* and *Inn* (Fig. 3-2) were the external input signals which were made up of differential signals and common-mode noise. The Frontend needed to amplify the differential component and reject the common-mode noise. A conventional instrumentation amplifier would be appropriate to deal with the common-mode signals, as they were limited by the common-mode rejection ratio

(CMRR) of the amplifier. The presented AFE had two buffers (components 1,2 in Fig. 3-2) to increase the input impedance. A subtracting amplifier (component 4 in Fig. 3-2) was used to amplify the differential signal, and the output of this block (node X in Fig. 3-2), should have had a very little common-mode noise. To amplify the common-mode signal, the external input *Inn* was inverted by a high-speed opamp, which should not have introduced a phase shift, to prevent severe mode conversion errors. The output of this amplifier (node Y in Fig. 3-2) had an amplified common-mode signal due to the previous input signal inversion. A scaled subtraction of X and Y generated a 'clean' signal at node Z, but this voltage also had some electrode movement information. The detected motion artefact (nodes W and M) was then subtracted from node Z and then node N.

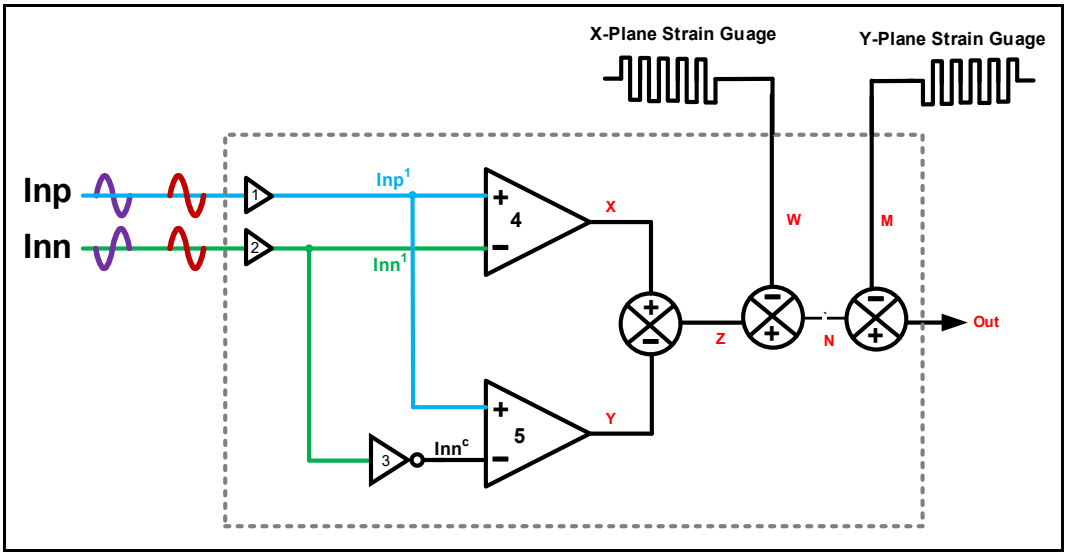

Fig. 3-2 AFE Initial System Design

The initial design showed that the preliminary results were promising to the problem of relative patient/electrode movement artefacts and common-mode signal interference and the work was published in the OXCAS2017 conference. The full published paper text was added to Chapter 9 of this thesis.

In the next stages, the AFE system design was improved, and an updated design was implemented. This improved design will be explained in the coming sections.

3.3 System Requirements

3.3.1 Motion Artefact Detection and Minimisation

To detect the body movement and deduct it from the distorted ECG signal, two strain gauges were fitted at 90° onto the electrodes to be able to detect the 2-dimensional motion artefacts. These strain gauges are a general-purpose gauge made by Micro-Measurements (Micro-Measurements, 2016). They have a nominal resistance of 350 Ω and a gauge factor of 2.02.

The reason why the strain gauges were fitted at 90° is to detect the X and Y Plane movements. Detected motion from the strain gauges was then added together, producing a combined motion artefact (*MA*), and fed into a differential amplifier to deduct the relative motion artefacts from the noisy ECG signal (*ECG+MA+CM*). Fig. 3-3 shows the strain gauge design and how they are fitted onto the electrodes. The output signals from this stage are two differential ECG signals (*Inp* and *Inn*) from two electrodes that connect to the next stage of common-mode reduction.

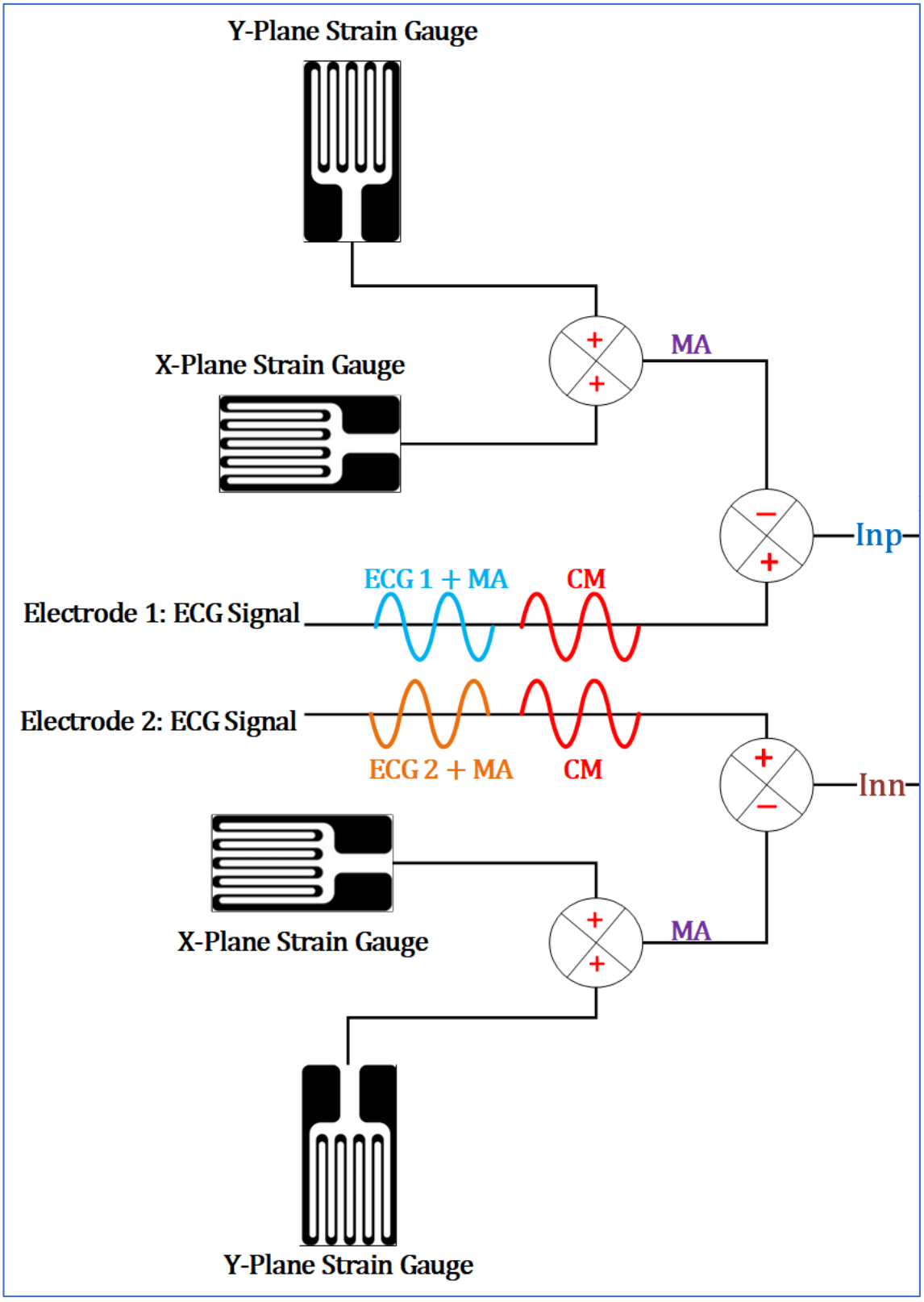

Fig. 3-3 Strain Gauges design arrangements

3.3.2 Common-mode Rejection Ratio

In order to achieve a high CMRR, two instrumentation amplifiers were used. Both amplifiers were isolated, using a shield, to minimise any extra common-mode signals. As shown in Fig. 3-4, the input signal includes the desired differential ECG signal as well as the undesired CM signal. Each IA eliminates the attached CM noise and amplifies the differential signal. Additionally, each IA has a gain of 2. The final output from both IAs is then fed to a summing amplifier to add the resultant signal and produce the final clean signal, which was eight times the original signal.

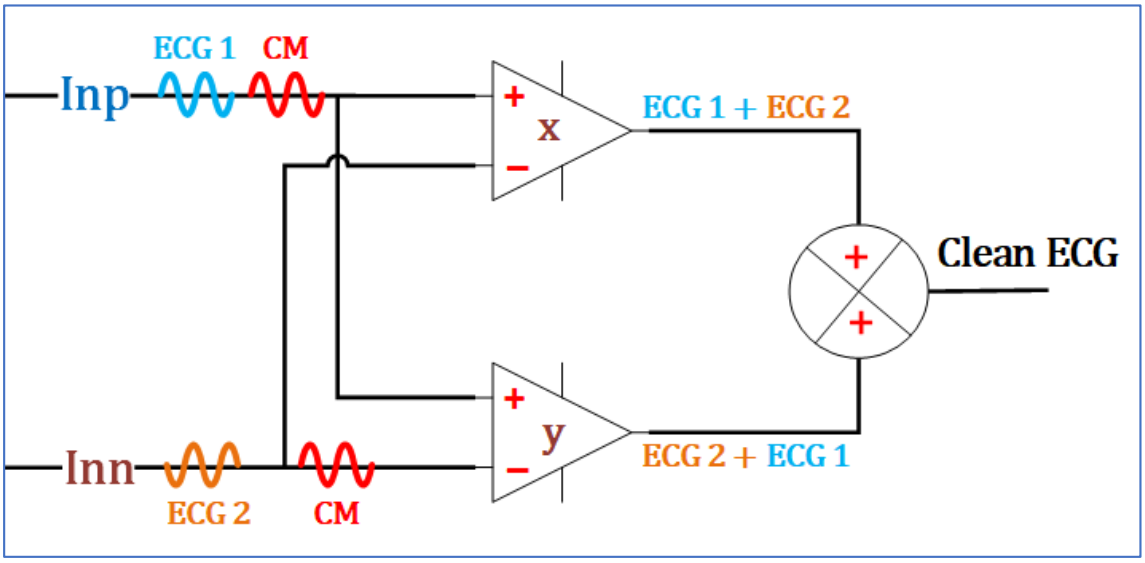

Fig. 3-4 Design of Common-mode Processing Stage

3.4 Benchmarks

In this section, the test approaches and simulation solutions were elaborated. To achieve the best possible results, the system was first simulated using MATLAB Simulink. The test results demonstrated a promising solution, that was capable of removing motion artefacts from biomedical signals and were discussed further in chapter 4. Also, the system was built using discrete components in the lab and tested, as discussed in chapter 5.

3.4.1 Strain Gauges Testing

Testing the strain gauges in the lab was challenging and needed a more robust method due to the strain gauges lack of sensitivity. Hence, varying the resistance of the strain gauges was not helpful and gave unrealistic results. In reality, testing the strain gauges required straining and flexing of the gauges. The test idea that was implemented was to use a loudspeaker that had an attached paper cone which moved vertically. The speaker is connected to a flexible plastic sheet which represented the skin and was connected with a plastic rod that was very stiff and not flexible. As the rod moved up and down, the pseudo-skin was moving vertically as well. The strain gauges were then attached to this sheet, and the produced strain was detected.

A heartbeat signal (sinewave) was fed into the speaker to simulate how the chest moves with the heartbeat. This method provided the ability to simulate the different types of patient movement. For this instance, movement artefacts can be made up to simulate a patient wriggling around.

3.4.2 Common-mode Rejection Ratio Testing

Two methods were used to overcome the common-mode noise interference with the desired ECG biopotentials. The first method was using the LM324N opamp, which consisted of four independent, high-gain, internally frequency compensated operational amplifiers. This was to save space while building the system blocks. The LM324N quad-

opamp was used in combination with the required resistances to create the circuit prototype. This test provided an excellent reduction of the common-mode signal from the source ECG signal. The second method was using the AD623 IAs to apply the same level of common-mode reduction as achieved in the first method. This method showed a cleaner output and an improved build of the system as it had fewer components. Additionally, it showed that the system design was resilient, and the changes to the type or build of the IA improved the results.

3.4.3 Harmonic Distortion Spectrum Analysis

In order to measure the level of minimisation that the AFE system applied to the distorted signal, the harmonic distortion spectrum was computed. In MATLAB, the THD block used the root mean square (RMS) value of several harmonics of the signal, divided by the fundamental signal, to calculate the total harmonic distortion (THD) value (Kester, 2009, Bishop, 2001).

The other factor that was calculated to measure the accuracy of the system was the signal-to-noise ratio (SNR). SNR was obtained by dividing the fundamental signal amplitude by the noise signal amplitude. (Kester, 2009, Bishop, 2001). The higher the SNR; the better.

Both THD and SNR were used as a reference in examining the final output signal when compared to the original signal. This helped show how the THD was degrading and the SNR was improving when processing the distorted signal with the AFE system.

3.4.4 Correlation Coefficients

In order to compare the similarity between the original and final output signal, the correlation coefficients were calculated in each of the testing stages. The resultant value was then compared with other research results to prove the advantage of using the AFE in minimising motion artefacts over the other methods.

The latest correlation coefficient result achieved by (Berwal *et al.*, 2019) showed an average of 0.9337. The AFE system had three different tests, where each of them showed a different average correlation coefficient. The MATLAB simulation had an average of 0.995. The lab tests without the test rig showed an average of 0.974, whereas the test rig test showed an average of 0.957.

3.5 Summary

In this chapter, the different design specifications of the AFE system were elaborated and explained. The aims of the system design were to explain how the system was built and what kind of results were expected to be gained. As discussed in the sections of this chapter, the design included the use of discrete components to physically build the system up. Also, a novel idea of using the loudspeaker and a plastic sheet to simulate the skin and measure the strain of the strain gauges. This method simulated the random motion artefacts by having different levels of sounds that caused the sheet to vibrate. The results showed a clean ECG signal that was successfully cleared of the two biggest noise sources, which were the motion artefacts and the common-mode signal.

3.6 References

[1] BERWAL, D., V, C. R., DEWAN, S., J, C. V. & BAGHINI, M. S. 2019. Motion Artifact Removal in Ambulatory ECG Signal for Heart Rate Variability Analysis. *IEEE Sensors Journal,* 19**,** 12432-12442.

[2] BISHOP, O. 2001. Understand Electronics. *In:* BISHOP, O. (ed.) *Understand Electronics (Second Edition).* Oxford: Newnes.

[3] KESTER, W. 2009. Understand SINAD, ENOB, SNR, THD, THD + N, and SFDR so You Don't Get Lost in the Noise Floor.

[4] MICRO-MEASUREMENTS. 2016. *Precision Strain Gages and Sensors Databook* [Online]. docs.micro-measurements.com: Micro-Measurements.com. Available: https://docs.micro-measurements.com/?id=4079 [Accessed 02/05/2020].

CHAPTER 4

DESIGN METHOD & SIMULATION

4.1 Introduction

The primary purpose of this investigation is to minimise the artefacts due to the relative motion of the patient/electrode interface. However, this depends on the removal of several types of artefacts, all of which can be considered unwanted noise on the desired signal (Patterson and Yang, 2011). Hence, it could lead to a clinical misinterpretation of the results. The process to minimise the artefact from the noisy biopotentials will be done using sensors to detect any vertical or horizontal movement of the electrode, and then feeding this information back to the system for the removal of any artefacts it causes. These artefacts may be caused by the movement of the electrodes relative to the patient (Solis-Bustos and Silva-Martinez, 1999). In this case, two strain gauges are fitted onto the electrode to detect any horizontal and vertical movement in the plane of the patient's chest (Aktakka *et al.*, 2017). The output of which is fed back into an Analog Frontend (AFE) for artefact removal, as it was shown in Fig. 3-1.

The advantage of using the strain gauges is that it can be fitted onto the ECG electrode. The electrode captures the heartbeat (ECG signal) together with any movement artefacts and sends the resultant signal to the AFE. The AFE works in the Analog domain, which enables faster signal processing, and consumes less power than processing in the digital domain.

4.2 Analog Frontend (AFE)

Fig. 4-1 shows the proposed design of the AFE, which will amplify the heartbeat signals - while rejecting common-mode artefacts such as those due to electrode motion or 50/60Hz power supply noise. The system receives six different inputs that can be classified according to their source. Note; a single electrode provides three sources. Two of these sources are the X-Plane, and Y-Plane strain gauge detected motions of the electrode, whereas the third signal is the captured ECG signal. The motion that is captured by both strain gauges is added together as a first step to make up a single source of noise which needs to be removed from the ECG signal of that electrode. Once the motion artefact is removed from the signals of both electrodes, two resultant signals (*Inp* and *Inn*) are produced for the next stage of processing, which is common-mode signal processing. As it can be seen from Fig. 4-1, *Inp* and *Inn* are the final outputs of the motion artefact processing stage, which means that they are clean from any detected motion artefact and only include differential signals and common-mode (CM) noise. CM noise could have the 40KHz switched-mode power supply electromagnetic interference and other such signals from the mains supply and other nearby electronic equipment. The frontend needs to amplify the differential component and reject the common-mode noise.

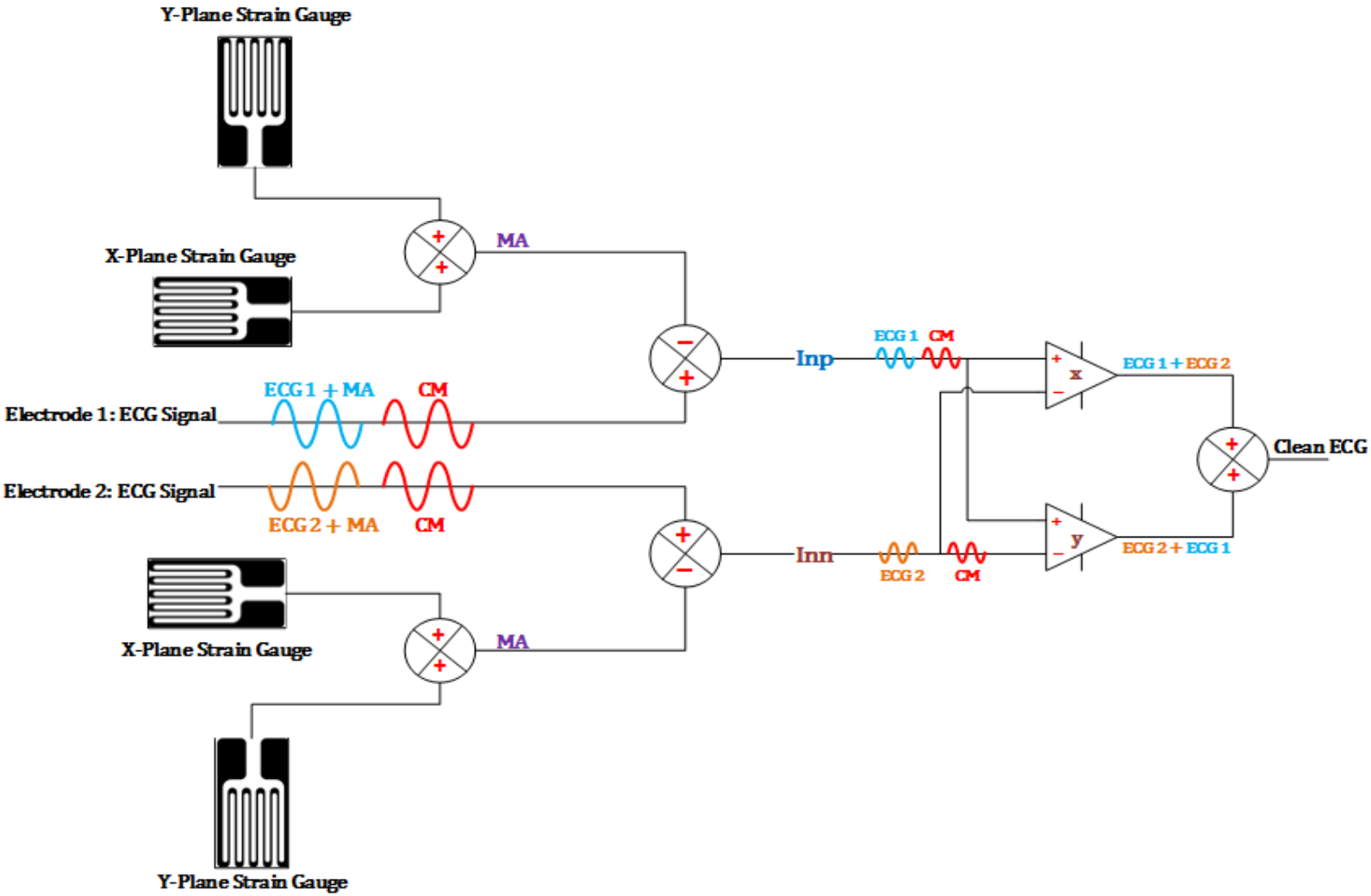

Fig. 4-1 Analog Frontend block diagram.

A conventional instrumentation amplifier is the most appropriate component to deal with the common-mode signals, as they will be limited by the common-mode rejection ratio (CMRR) of the amplifier (Nagel, 2000, Neuman, 1998). A typical IA will have 80-90dB CMRR at DC, but due to opamp implementation imperfections, the CMRR will degrade with frequency (Sathiyabama et al., 2015, Solis-Bustos and Silva-Martinez, 1999). However, at the very low frequencies employed in an ECG system, this imperfection is not an issue.

The CM signal will then be minimised using the unique design that was proposed in section 3.3.2, using a circuit that consists of two instrumentation amplifiers (IAs) (labelled x and y) as shown in Fig. 3-4 and the full system design in Fig. 4-1. IA-X and IA-Y are subtracting amplifiers that are used to amplify the differential signal, and the output of this block, should have a very little common-mode noise. The output from each IA is then fed to a summing amplifier that would produce the total ECG signal that is a (theoretically) CM-free ECG signal.

4.3 Proposed System Design

In this section, the overall system design is discussed. Fig. 4-2 shows the system design block diagram produced using Simulink, where each block represents functionality that needs testing and a performance measurement. The overall system consists of a number of smaller subsystems that can be tested individually, and its operational parameters can be measured separately too. Each of these blocks was designed and built using MATLAB Simulink tools which provide the ability to simulate the electric circuit in the system level. Each block will be explained in-depth in the next section.

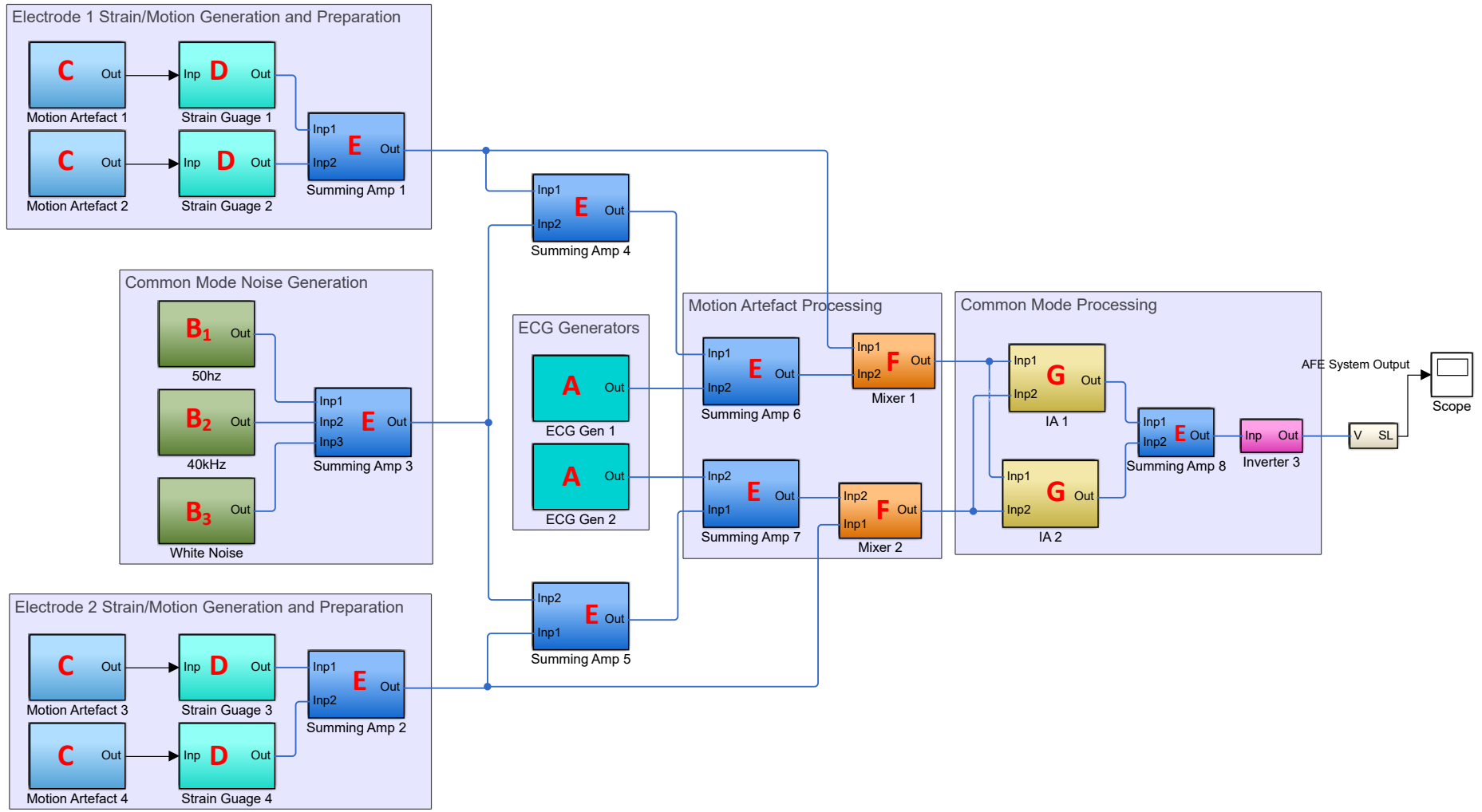

Fig. 4-2 Proposed System-Level Design

4.4 Sub-Systems of System-Level Design

4.4.1 ECG Signal Generator

Due to the need for (ideally) total precision in biomedical systems, the signals used in testing should be as realistic as possible, to ensure that they represent, as close as possible, 'real-life' physiological signals. To achieve this, a sinewave generator was used to produce a signal that represented an ECG signal, both in terms of frequency and amplitude. A sinewave was used to represent an ECG signal, as it is very easy to detect noise and distortion on a sinewave. While, it would be extremely difficult to do so with a more complex signal, even when using both time and frequency domain analysis. The block 'A' from Fig. 4-2 symbolises the signal generators, where each one generates a sinewave signal that represents the ECG signal that would be captured by each electrode. Fig. 4-3 shows the configuration of the sinewave voltage signal generator, with a scope that would measure the produced signal. The generator produces a signal with a voltage amplitude of 1V with a frequency of 1Hz in order to closely represent the parameter of an ECG signal.

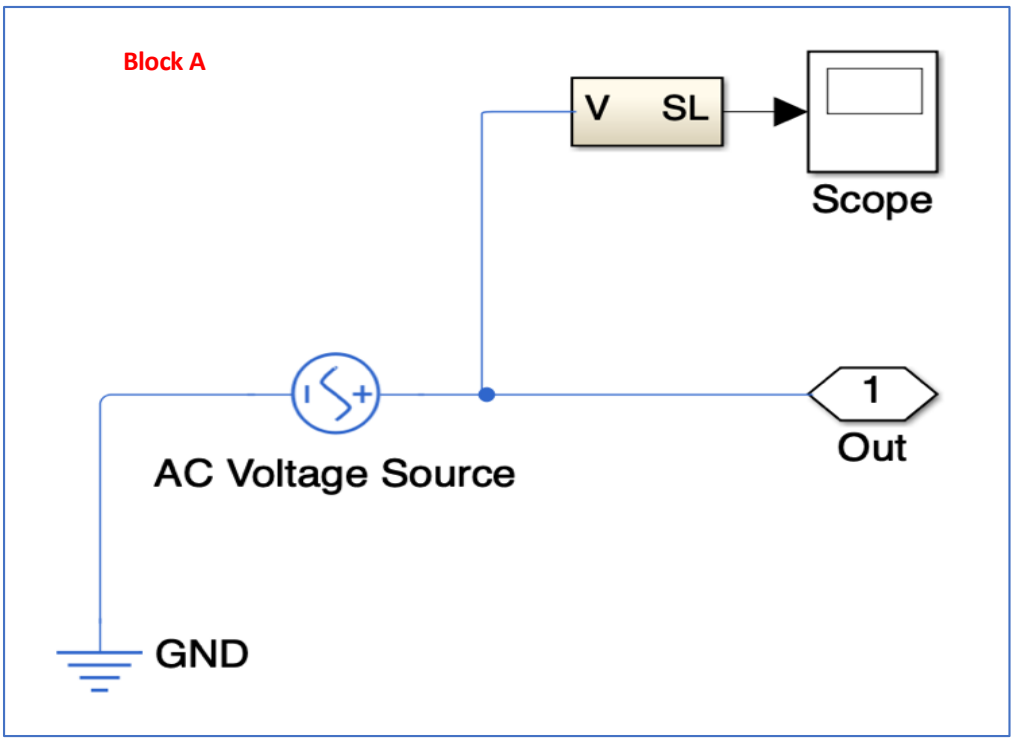

Fig. 4-3 MATLAB Sinewave generator configuration.

The generated signals from the A blocks are then fed to a series of summing amplifiers to combine the biopotential representations with the generated motion artefacts and common-mode noise sources to produce a signal for simulation purposes.

4.4.2 Common-Mode Noise Generators

There are three types of common-mode signals that any electrical signal could have during the signal capturing process. These are power supply harmonics (50Hz), common-mode interference (40kHz) and White noise. Power supply harmonics and common-mode interference noise signals can be represented with a sinewave signal that has an amplitude of 50mV. Similar to the ECG (sinewave) generation, an AC voltage generator is used with the required config to produce both common-mode noise signals. Blocks B_1 and B_2 in Fig. 4-2 represent the generators for the power supply harmonics noise and the PLI noise. Fig. 4-4 shows the circuit used in MATLAB Simulink to generate the signals.

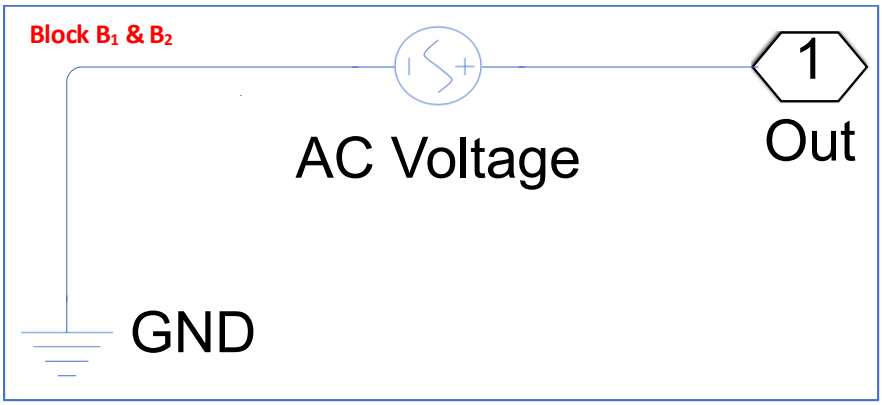

Fig. 4-4 Common-mode Signal AC Voltage Generator

On the other hand, the white noise signal is generated using a band-limited white noise generator which generates random numbers. To convert the generated random numbers into a normal squared wave signal, a Simulink-PS converter and a controlled voltage source are used. The S-PS component converts the numbers into a physical voltage signal which is then converted into a square wave signal using the controlled voltage source. The output of the controlled voltage source is V=Vs where Vs is the numerical value presented at the physical port. Block B_3 in Fig. 4-2 represents the white noise generator and Fig. 4-5 shows the configuration used to generate the white noise in MATLAB.

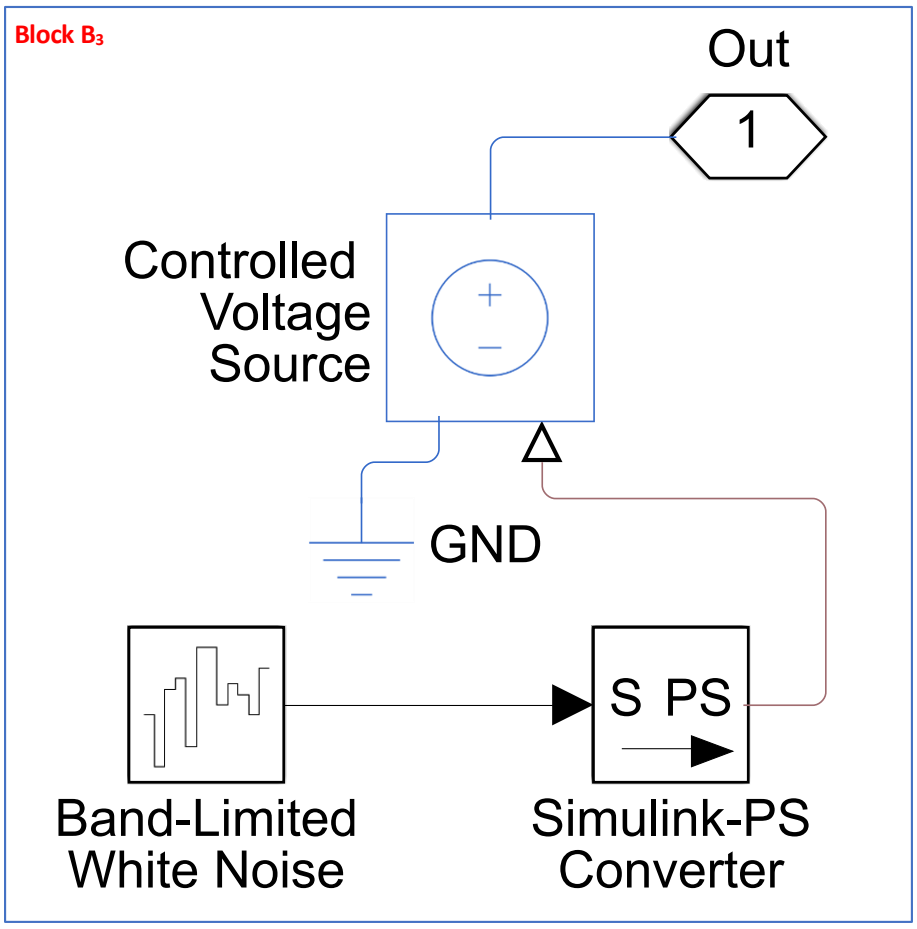

Fig. 4-5 White Noise Signal Generator

4.4.3 Motion Artefact Generator

Motion artefacts can vary from very small amplitude signals to signals even higher in amplitude than the ECG biopotentials. To simulate such signals, a random number generator, which outputs a normally (Gaussian) distributed random signal, was used. An additional component (Simulink-PS) was required to convert the unitless Simulink input signal to the physical signal that is required to cause the strain on the strain gauges. The resultant random strain/motion is then applied to the strain gauges sensor. Blocks with the Label 'C' in Fig. 4-2 represent the MA generators and Fig. 4-6 shows the configurations used in the MATLAB simulation.

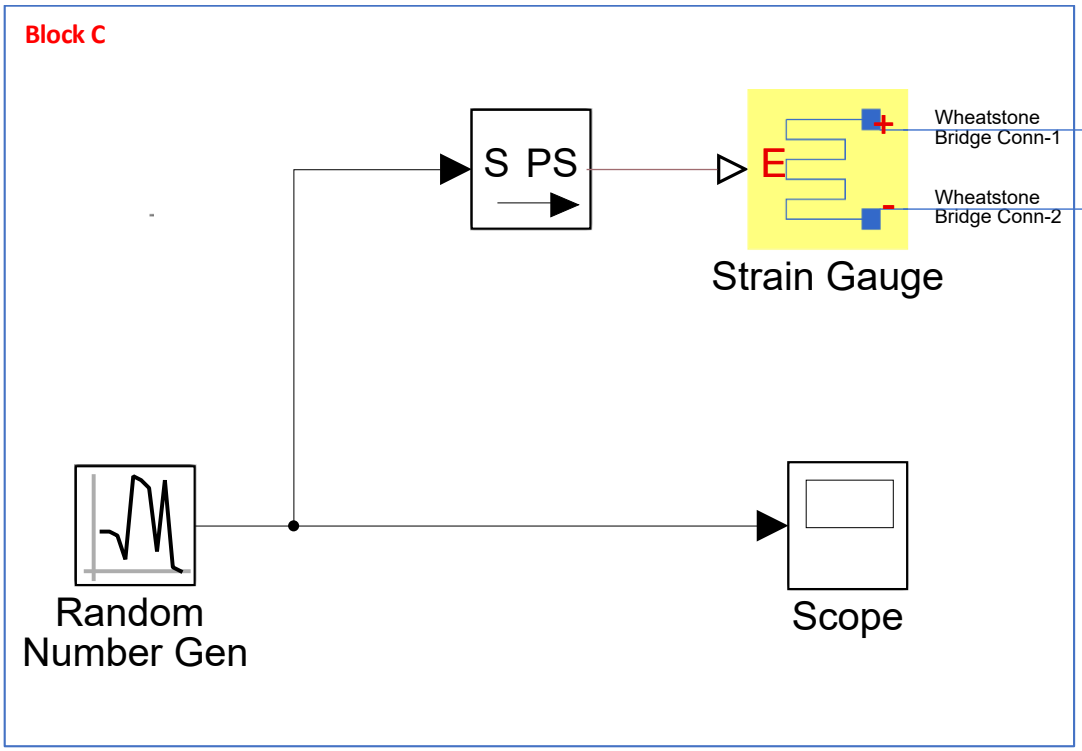

Fig. 4-6 Motion Artefact Generation

4.4.4 Strain Gauges

Strain gauges are resistors, whose resistance alters when they are flexed (Ştefănescu, 2011). Thus, to detect a directional signal, strain gauges are needed both in the X and Y Planes. Therefore, two strain gauges are used for each electrode, and they are labelled with the letter 'D' as shown in Fig. 4-2. The X and Y motion artefacts from the strain gauges are combined to produce a unified strain/artefact signal that is then combined with the common-mode noise and the simulated ECG signal from the AC voltage generator. Additionally, the signal is also supplied to the differential amplifier that would be subtracting this signal from the simulated ECG biopotentials to test the performance of the system and to remove the motion artefacts from the desired biopotential signals.

The classical configuration of the strain gauge is done by associating it with a Wheatstone bridge, as shown in Fig. 4-7. The bridge circuit mechanism is that it only produces a voltage whenever it becomes unbalanced, which is the time the generated

strain/motion is detected. The strain gauge Wheatstone bridge circuit equation is elaborated in Eq. 4-1.

$$V_{out} = V_{in}\left[\frac{R_4}{R_3+R_4} - \frac{R_2}{R_1+R_2}\right] \quad \text{Eq. 4-1}$$

R_1, R_2, R_3 and R_4 represent the four sides of the Wheatstone bridge, and the initial balance condition (Ştefănescu, 2011) of the bridge can be summarised in Eq. 4-2.

$$R_1 \cdot R_4 = R_2 \cdot R_3 \quad \text{Eq. 4-2}$$

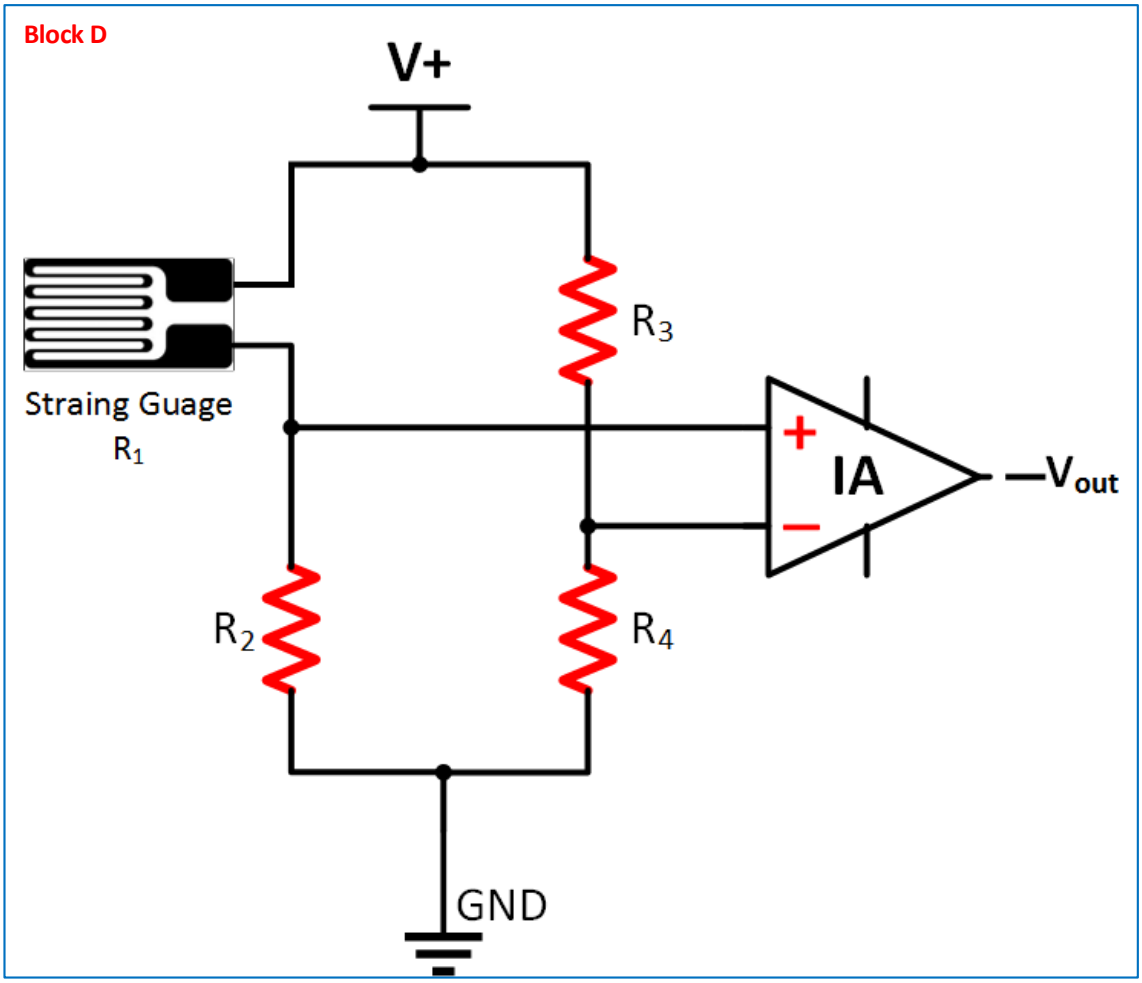

Fig. 4-7 Strain Gauge Circuit configuration

4.4.5 Summing Amplifiers

The different stages of the simulation include various amounts of generated signals which need to be added together at some point to reach the real-life scenario. Therefore,

a summing amplifier is used for this purpose. It is used to add both the X-Plane and the Y-Plane motion artefact of each electrode. Also, it is used to add the various common-mode noise signals to produce a single common-mode source. It is then used to add the resultant common-mode noise to the resultant combined motion artefact signal to produce a single final source of the noise. An additional summing amplifier is also used to add the combined noise signal to the generated ECG signal. This produces a noisy ECG signal that is ready for simulation. Out of the four usages of the summing amplifier, there is only one use that is part of the final system design. This step is the addition of the X and Y Plane motion artefact. However, the other usages of this circuit can be classified as part of the simulation stage only. Fig. 4-8 shows the summing amplifier circuit, which was labelled as Block E in Fig. 4-2.

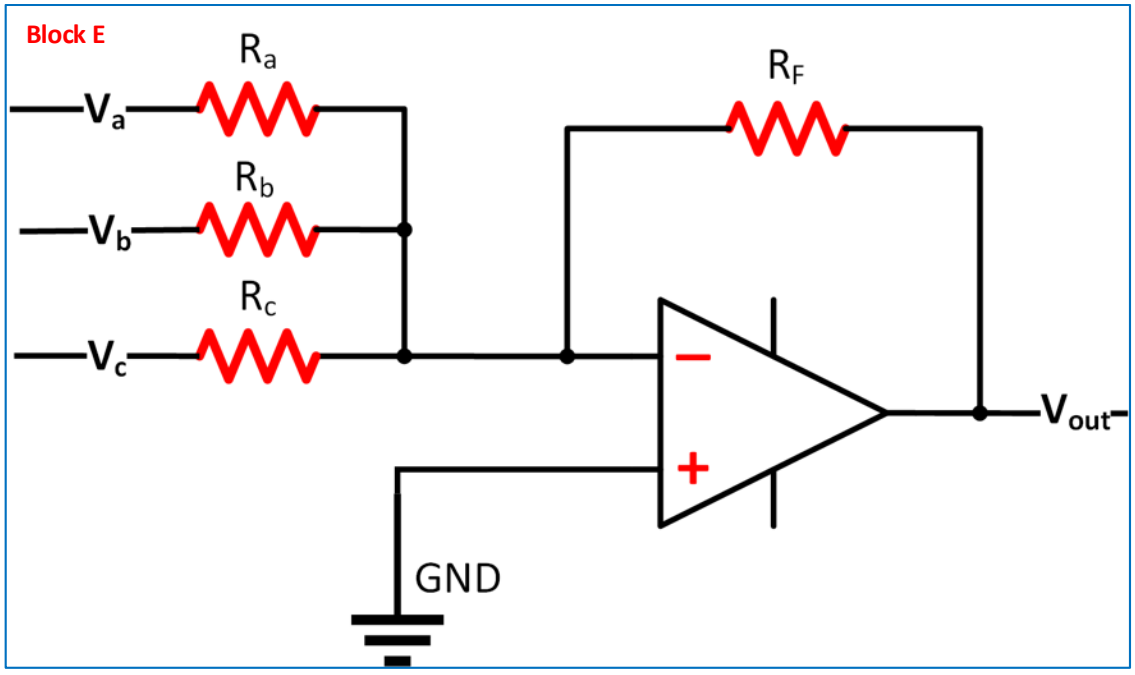

Fig. 4-8 Summing Amplifier

When $R_a = R_b = R_c$, the equation for the summing amplifier is elaborated in Eq. 4-3.

$$-V_{out} = \frac{R_F}{R_{in}}[V_a + V_b + V_c + \ldots etc] \qquad \text{Eq. 4-3}$$

4.4.6 Differential Amplifiers

The novel Analog Frontend (AFE) uses differential amplifiers to remove the motion artefacts from the ECG biopotentials. Each electrode captures the distorted signal, which consists of the desired ECG signal and the noise signal. The electrode output is connected to one of the inputs of the AFE system, which connects this input signal to the first differential amplifier (Block F) as shown in Fig. 4-2. This mixer takes the combined X-Plane and Y-Plane motion artefact signal as a second input. Having the second input as the noise source means that the mixer knows what the shape and form of the motion artefacts that need to be subtracted. The expected/ideal output signal from this stage is a clean ECG signal that does not have any motion artefacts. The produced signal would still, however, contain common-mode interference signals that will be minimised in the following stage. Fig. 4-9 shows the mixer circuit and its inputs and outputs.

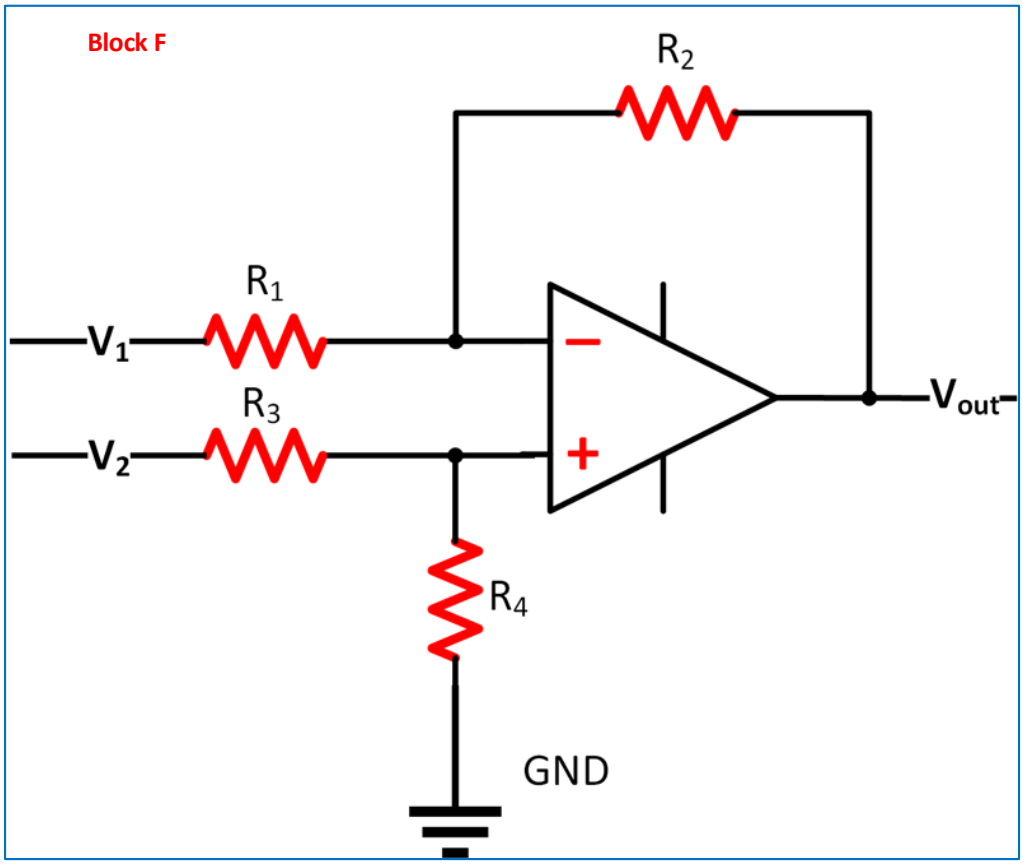

Fig. 4-9 Differential amplifier

The equation for the differential amplifier is elaborated in Eq. 4-4.

If $R_1 = R_3$ and $R_2 = R_4$ then

$$V_{out} = \frac{R_2}{R_1}(V_1 - V_2) \quad \text{Eq. 4-4}$$

4.4.7 Instrumentation Amplifiers

The nature of instrumentation amplifiers (IAs) enables them to respond to differential signals and reject common-mode signals and hence, have a very high common-mode rejection ratio (CMRR). ECG signals, on the other hand, are differential input signals that are processed using the different components within the AFE system, and they might contain common-mode signals due to the surrounding medical equipment. IAs are extensively used in medical applications to amplify small signals that are normally noisy, such as a heartbeat and any other biomedical signals from the muscles and nerves (Dool and Huijsing, 1993).

IAs play an important role after cleaning the ECG signal from any motion artefacts. This role can be concluded by cleaning the resultant signal from the previous stage from common-mode (CM) artefacts that might have been captured from sources. For example, the electrical mains supply, switched-mode power supplies and another nearby electrical/electronic equipment. These CM signals are comparatively small signals that need amplification in order to remove them using differential amplifiers. Blocks with the label 'G' in Fig. 4-2 represent the IAs and Fig. 4-10 shows the instrumentation amplifier (IA) circuit that was used to amplify the signals whilst keeping any resultant distortion to a minimum.

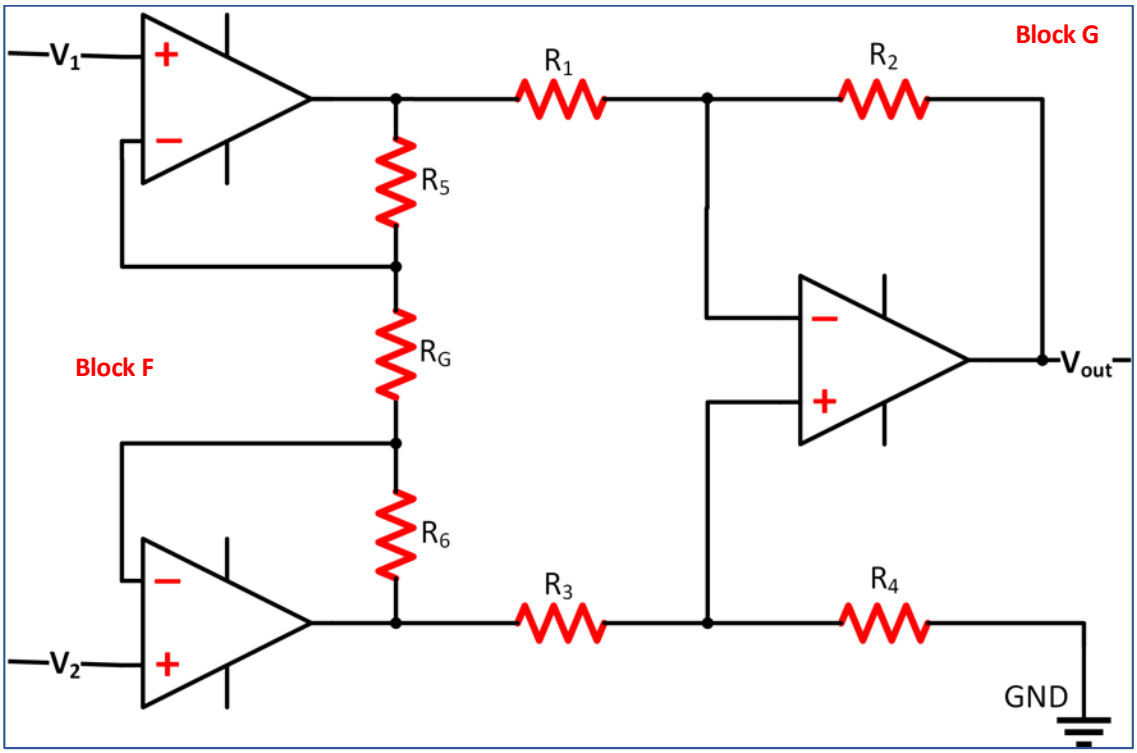

Fig. 4-10 Instrumentation Amplifier.

The equation for the instrumentation amplifier is elaborated in Eq. 4-5.

$$V_{out} = (V_2 - V_1)\left(1 + \frac{R_5+R_6}{R_G}\right) \qquad \text{Eq. 4-5}$$

4.5 System Simulation in MATLAB

The system was simulated in MATLAB Simulink to test the ability of the system to achieve the main goal of this research. This stage consists of two important steps that construct the basis for the system simulation. The first stage works out the generation and preparation of the three different sources of signals that are required to be tested. The three sources are the ECG signals, Motion Artefacts (MA), and Common-mode (CM) signal. The common-mode signal itself consists of the different types of noise which are the 50Hz mains noise, 40KHz Powerline noise, and the white noise.

The second stage, on the other hand, is the testing of the system and validating the concept of the design according to the input signals.

4.5.1 Test Signal Generation Stage

1. Heartbeat Signal Generation

To facilitate the test process and see clearer results, the normal heartbeat biopotentials signal was replaced by a sinewave signal. Therefore, a voltage generator was used to generate the required signal. As the two inputs of the system are differential ECG signals, one of the heartbeat generators output was inverted, which matches the way the ECG signals are captured in hospitals using the ECG machines. The generated signal has a 1V amplitude and a frequency of 1Hz. Fig. 4-11 shows the produced signals from the generators.

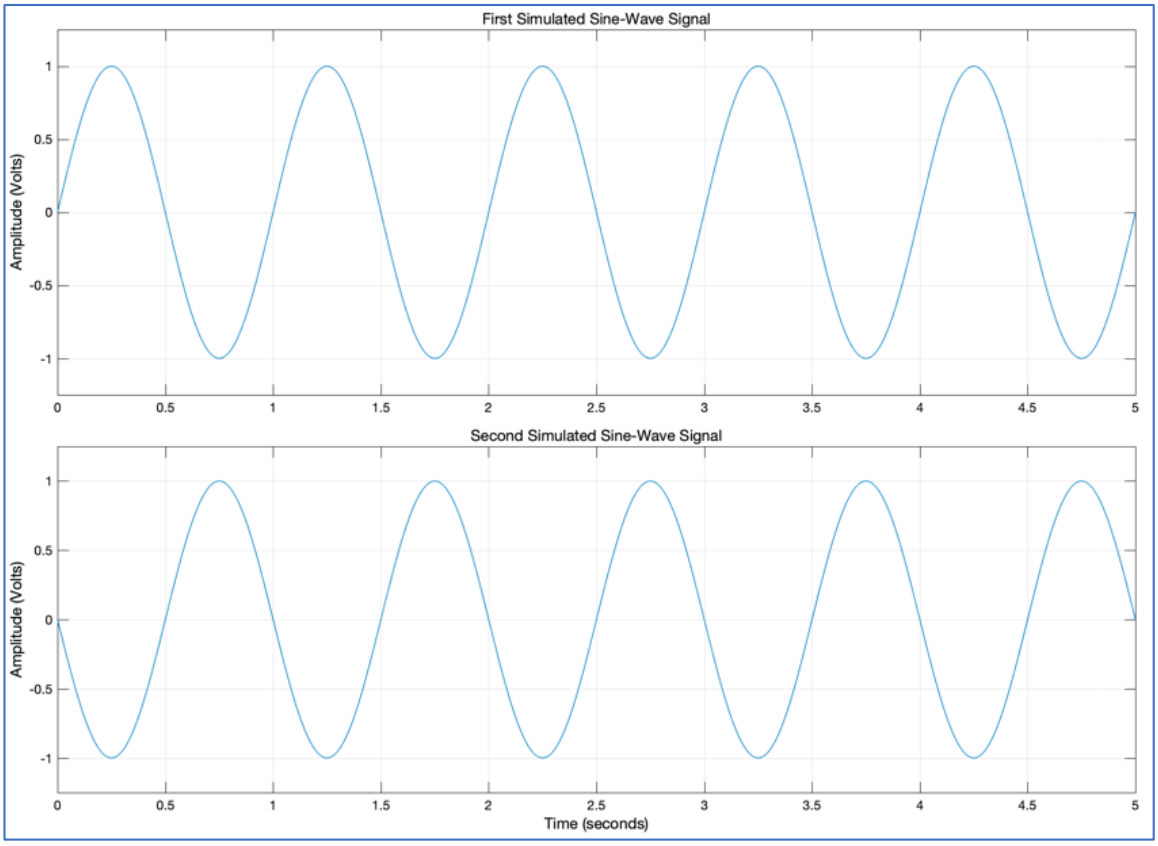

Fig. 4-11 Generated Sinewave Signals

As ECG signals are quite high (*circa* 1V) in amplitude, the simulated motion artefact signals need to be comparatively small to be realistic.

2. Noise Signals Generation

- **Motion Artefact Signal Generation**

In order to represent 'noise' as accurately as possible, the signals were derived from pulse generators that are configured to generate square wave signals. Fig. 4-12 shows a sample of the generated strain/motion artefact signal from the strain signal generators. Table 4-1 shows the different parameters that were used for the noise generators to ensure the detection process functionality over a range of noise figures.

Table 4-1 Motion Artefact Generators Configurations

Motion Artefact	Variance	Sampling Time
Electrode 1 X-Plane	0.1	0.01
Electrode 1 Y-Plane	0.3	0.02
Electrode 2 X-Plane	0.5	0.07
Electrode 2 Y-Plane	0.1	0.01

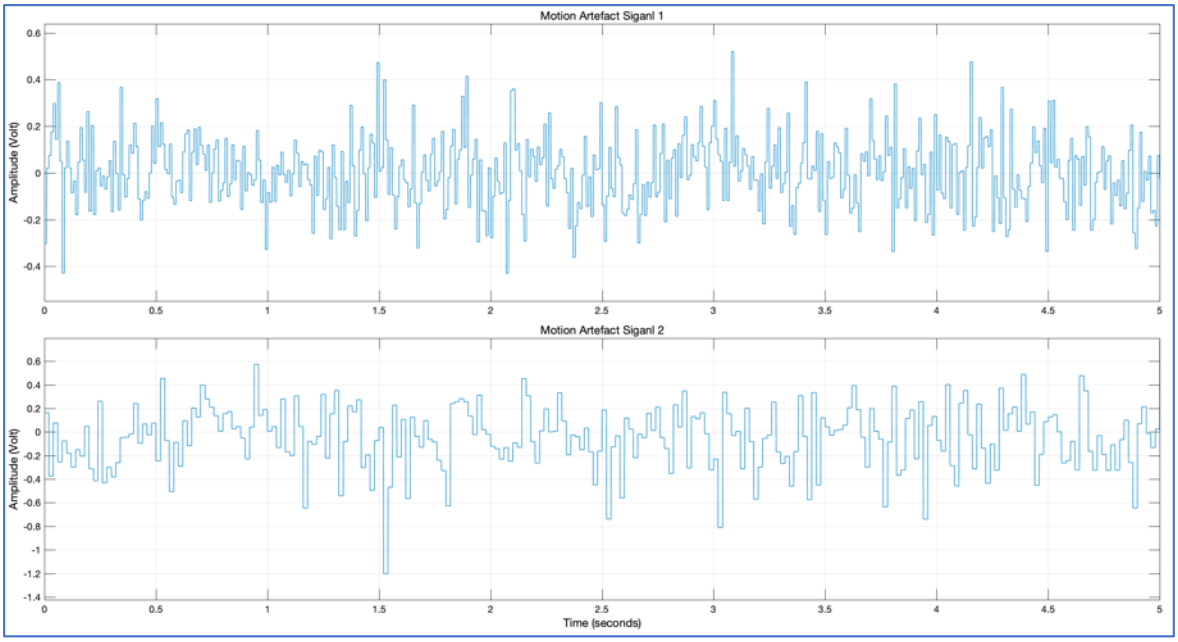

Fig. 4-12 Combined Square Wave Signals (represents Strain/Motion)

The detected X-Plane and Y-Plane signals from the strain gauges were combined, as explained earlier to produce one motion signal that can be removed from the electrode signal. To combine the two strain gauge signals, a summing amplifier was used, which was explained previously in Fig. 4-8.

The resultant motion artefact signals are then combined with the generated common-mode signals and then with the simulated ECG signal in order to enable the subtraction of the motion artefacts at a later stage.

- **Common-Mode Signal Generation**

The common-mode signal can include signals from different sources such as the 50Hz Mains noise, 40KHz Powerline noise, and the white noise. Table 4-2 shows the configurations used to produce the common-mode signals.

Table 4-2 Common-Mode Signals Configurations

	Amplitude	Phase Shift	Frequency
Power Supply Noise	50mV	0	50Hz
Power Line Noise	50mv	0	40KHz

- **Power Supply Harmonic (50Hz) Noise**

It is a well-known fact that power supply noises are a common source of distraction for most of the electrical, biomedical systems due to the amount of power that exists in the medical equipment rooms (Shaik and Chakka, 2016, Shaik *et al.*, 2016). More importantly, its frequency is much higher than the ECG signal, which would cause a misinterpretation of the biopotentials (Shaik and Chakka, 2016). Power supplies produce Electromagnetic Interference (EMI) at 50/60Hz, which is known as powerline interference (PLI). PLI relies upon the same range of the ECG signals frequency, which starts from 0.5Hz to 100Hz (Shaik *et al.*, 2016, Belgurzi *et al.*, 2017). Therefore, simulating and considering this type of noise in the simulation stage is essential to the ECG signal processing stage that includes motion artefact and common-mode noise minimisation.

The power supply harmonics were generated in MATLAB using an AC Voltage Source that produces a sinewave with an amplitude of 50mV and a frequency of 50Hz. Fig. 4-13 shows the resultant power supply noise.

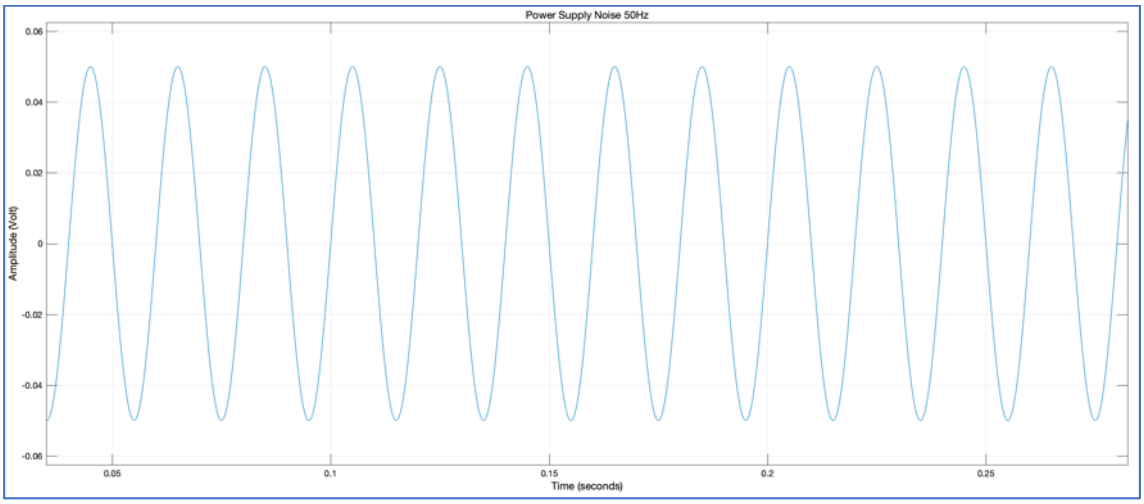

Fig. 4-13 Power Supply 50Hz Harmonics

- **Power Line Interference (40KHz) Noise**

Similar to power supply noises, power line noises have a high potential to interfere with the different types of biomedical signals.

As discussed earlier in the review of literature, heart activity signals could get distorted by noise signals that are caused by different types of artefacts. One such noise signal is the switched-mode 40kHz noise that can be delivered by the surrounding power supplies (Singh et al., 2015, Zhang et al., 2016, Kishimoto et al., 2007). This type of noise can be seen along with many other types of noises such as baseline wander and other muscles activities (Singh et al., 2015, Shaik and Chakka, 2016). Thus, such types of artefacts have to be taken into account in any simulation stages of this project to help in having a better, noise-free, well-presented ECG signal.

The power supply harmonics were generated in MATLAB using an AC Voltage Source that produces a sinewave with an amplitude of 50mV and a frequency of 40kHz. Fig. 4-14 shows the resultant power supply noise.

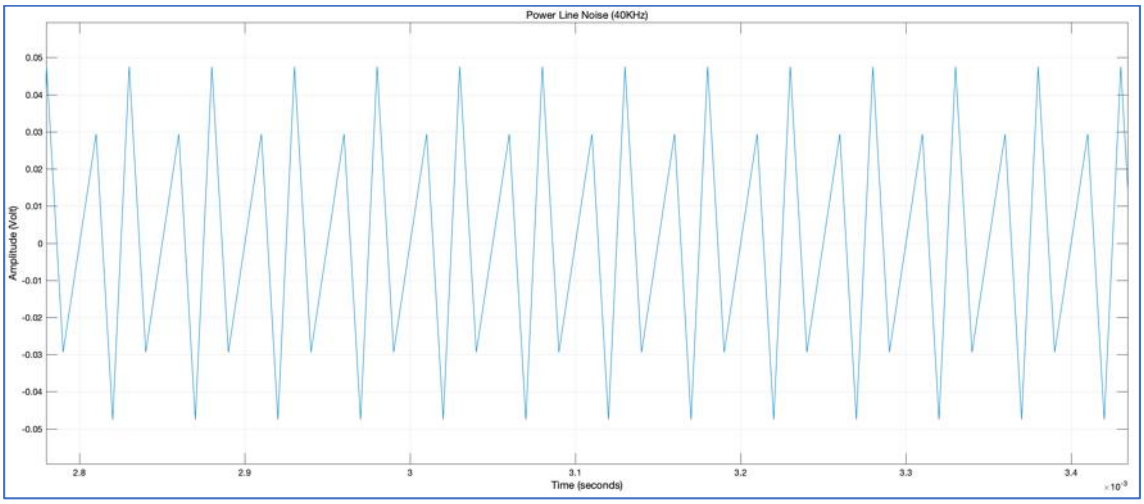

Fig. 4-14 Power Line interference (40KHz) Noise

- **White Noise Generation**

To generate a white noise signal, a Band-Limited White Noise block was used in Simulink. This component produces random numbers that are suitable for use in white noise simulation. The configured noise power (the height of the signal) that was used is 10^{-9} V and the sampling time was 10^{-5} seconds. The resultant generated white noise signal can be seen in Fig. 4-15.

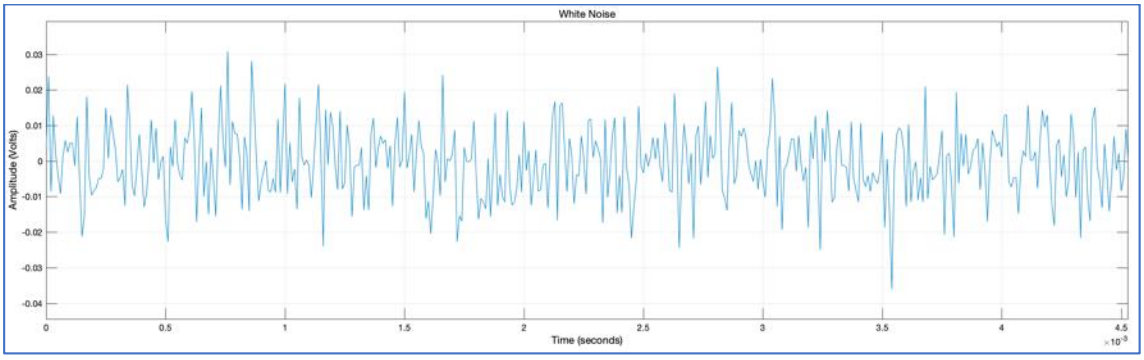

Fig. 4-15 Generated White Noise

- **Combined Common-mode noise:**

After generating the various types of common-mode noise, a summing amplifier is responsible for adding them together to represent a single common-mode signal. Fig. 4-16 shows the resultant combined common-mode signal. This signal is then fed to

another summing amplifier that adds the generated Motion Artefact noise and the common-mode signal to make them ready to be combined with the simulated ECG Signals.

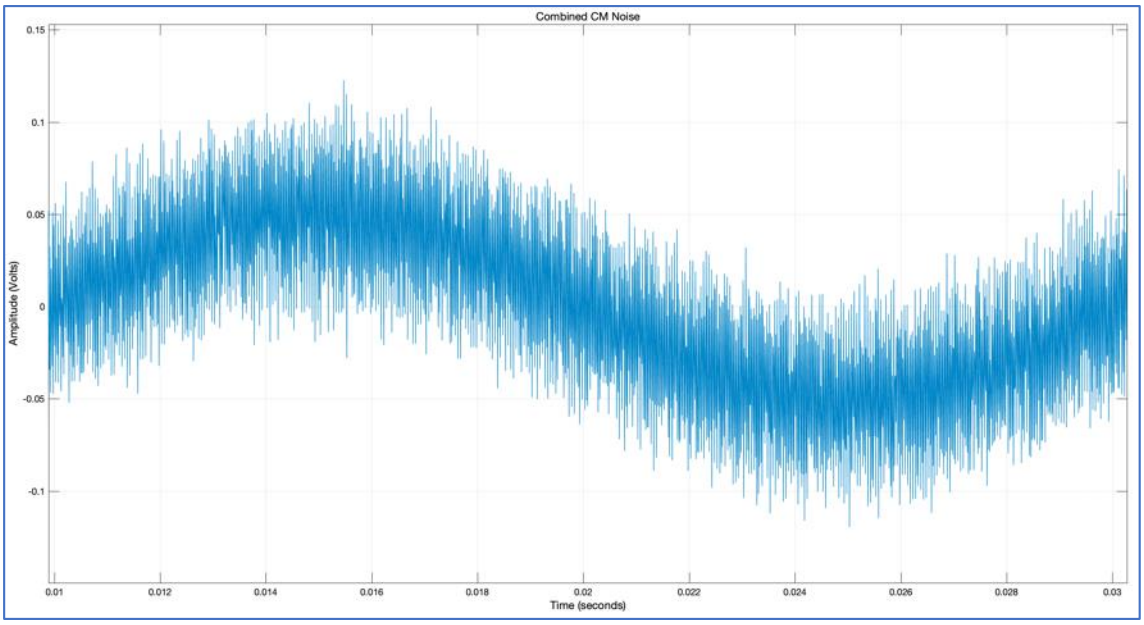

Fig. 4-16 Combined Common-mode noise

4.5.2 Signal Generation Final Output (Noisy ECG)

The generated noise from the motion artefact generators and the common-mode signal generation stages are then combined together to represent one combined noise signal. The resultant combined noise is then prepared to be added to the generated differential ECG signals. The addition of the different types of noises was done in stages according to which signals were generated or by how they came together. Fig. 4-17 shows the resultant simulated ECG signals after adding the various types of generated noise.

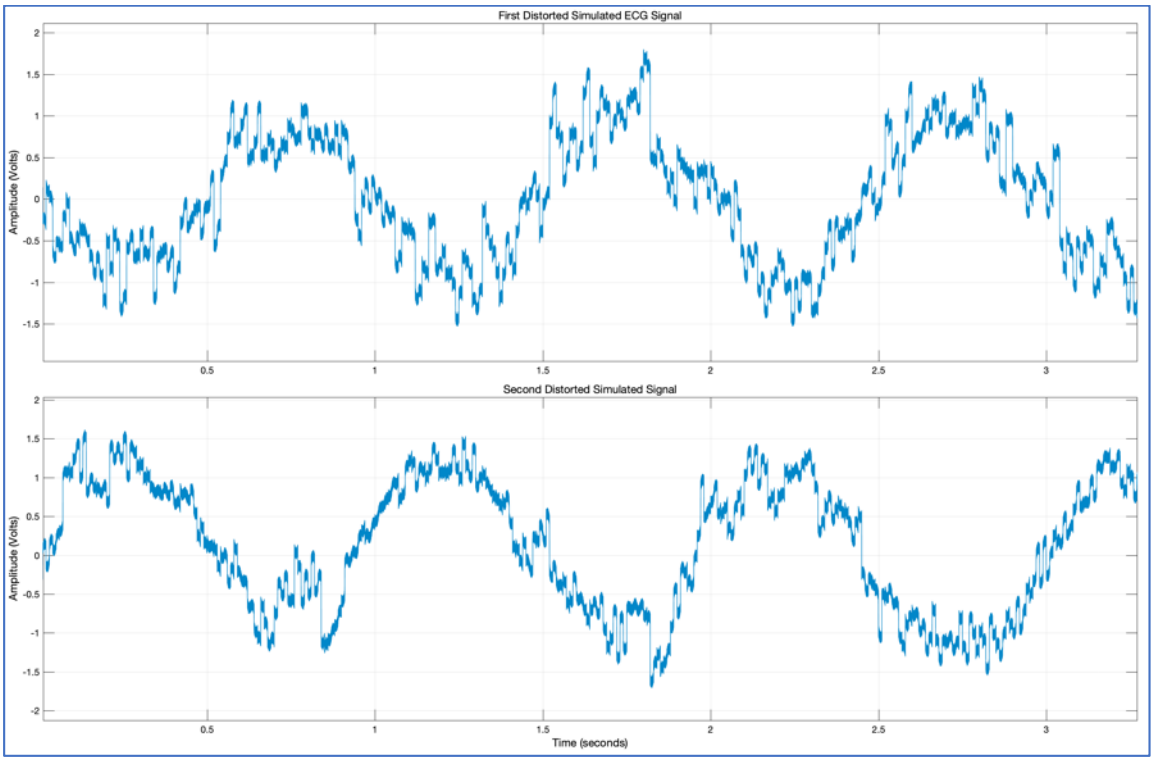

Fig. 4-17 Resultant Distorted Simulated ECG Signal (A differential signal with motion and common-mode noise)

4.5.3 Signal Processing and Simulation Results

Motion Artefact Minimisation

Fig. 4-18 and Fig. 4-19 show the resultant signals from the combination of the noise signals and the simulated ECG signals. As can be seen, the first and second simulated signals compared to the distorted signals are shown in the figure. Additionally, the combined signal acquired more of a positive DC bias, and also, the waveshape became distorted.

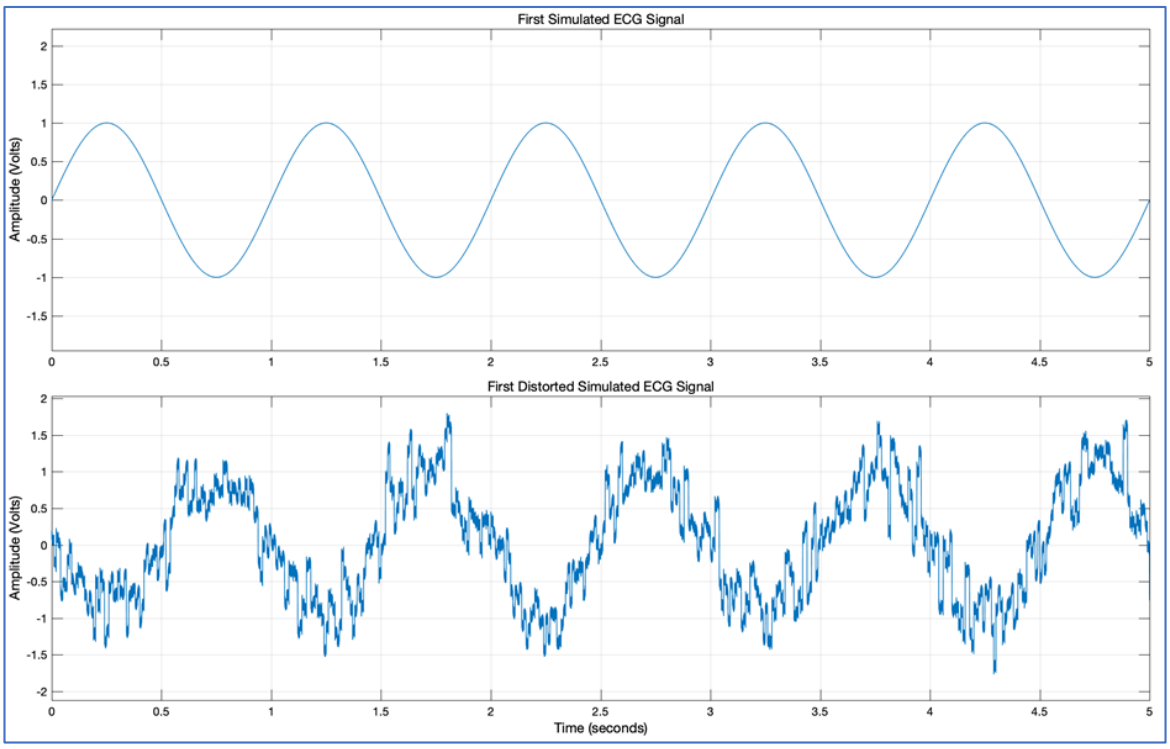

Fig. 4-18 First Original Sinewave Signal (top) and Distorted Sinewave Signal (bottom)

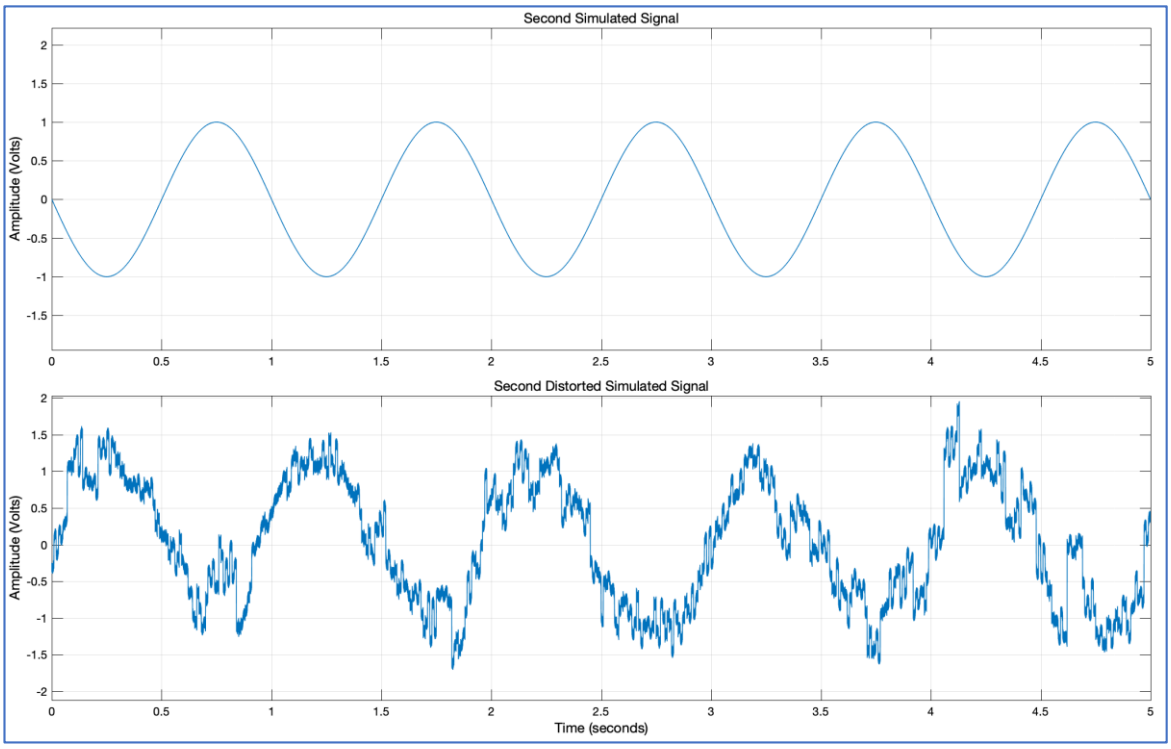

Fig. 4-19 Second Original Sinewave Signal (top) and Distorted Sinewave Signal (bottom)

After preparing the distorted signals, the combined distorted ECG signal and the generated combined strain signals of each electrode were then fed into a differential

amplifier to remove the motion artefacts from the motion artefact/ECG signal of each electrode.

Fig. 4-20 shows the harmonic distortion spectrum of the original sinewave signal compared to the distorted sinewave signal. The spectrum of the source signal looked clean and smooth, whereas the combined noisy signal spectrum showed lots of additional noise and extra harmonics that did not exist in the source signal.

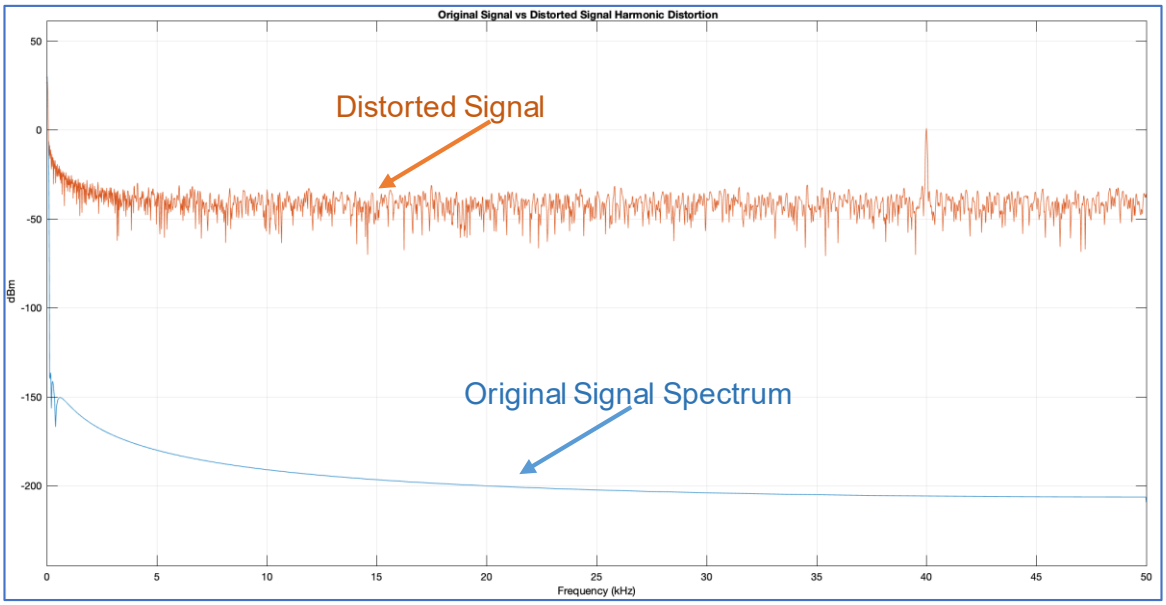

Fig. 4-20 Distortion Harmonics of Original Sinewave Signal and Distorted Sinewave Signal

Table 4-3 shows the harmonic distortion spectrum measurements of the original clean signal compared to the distorted signal (clean signal plus added noise). The THD of the clean signal increased from 29.68% to 76.21% in the new distorted signal. The percentage of this increase was 157%, which illustrates the amount of noise that was added to the source signal. Also, SNR of the original signal was 0.52 dB and then became -2.98 dB in the distorted signal with a decrease of 3.50 dB.

Table 4-3 Harmonic Distortion Spectrum measures of original signal and Distorted Signal

	Clean Source Signal	Combined Noisy Signal	Decrease
THD	29.68%	76.23%	157% (increased)
SNR	0.52 dB	-2.98 dB	3.50 dB (decreased)

As shown in Fig. 4-21, the output of the subtraction process showed the simulated ECG signal, including the common-mode signal. This made the signal ready for its next stage that worked on minimising the common-mode signal.

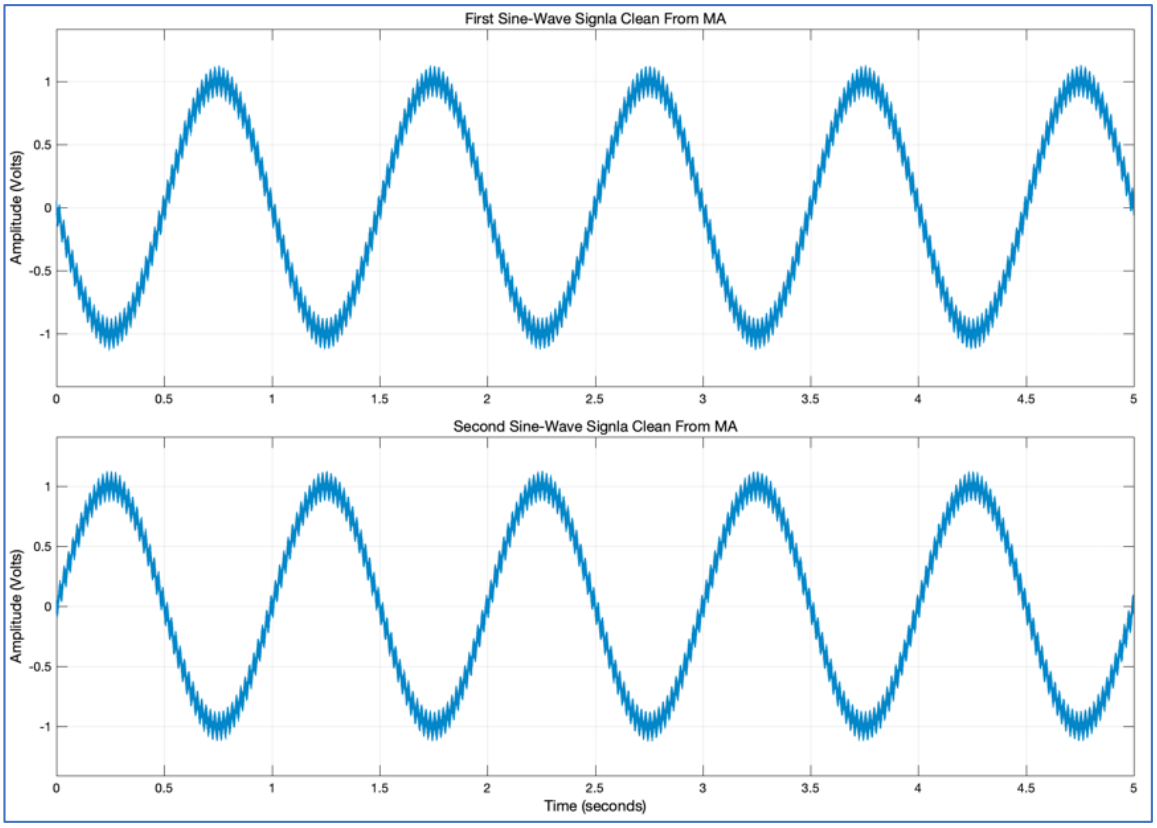

Fig. 4-21 Simulated Sinewave Signals After Motion Artefact Processing

Common-mode Signal Processing

The final part of the simulation is designed to produce an enhanced common-mode rejection ratio using two instrumentation amplifiers (IAs), an inverter and a mixer as shown in Fig. 4-2. of the Analog Frontend (AFE). Both IAs were fed with the two differential

ECG signals outputted from the mixers of the previous stage. In the MATLAB simulation, a single IA was perfectly capable of minimising the common-mode noise and produced a nice and clean output. However, the proposed approach in this research was to use two IAs, which left the system with a much better output as the two IAs produced a fully cleaned output. The output of the two IAs was then fed to a summing amplifier, as seen in Fig. 4-22. Fig. 4-23 shows the output from IA-1 and IA-2, where each IA produced a clean sinewave output that was four times the originally generated sinewave amplitude due to the amplification of the signal.

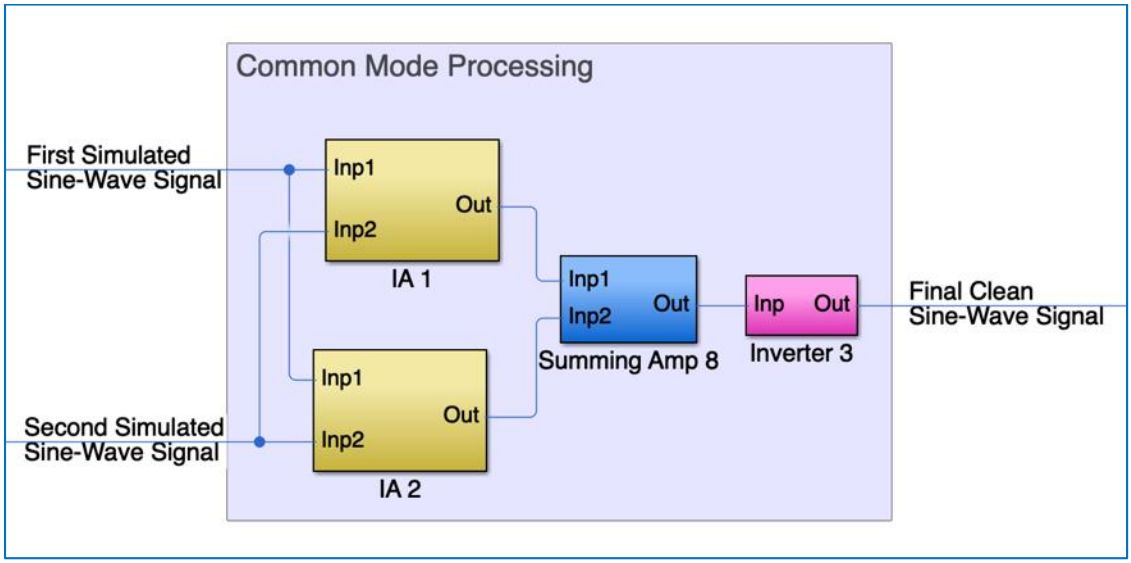

Fig. 4-22 Common-mode Rejection Simulation Block Diagram.

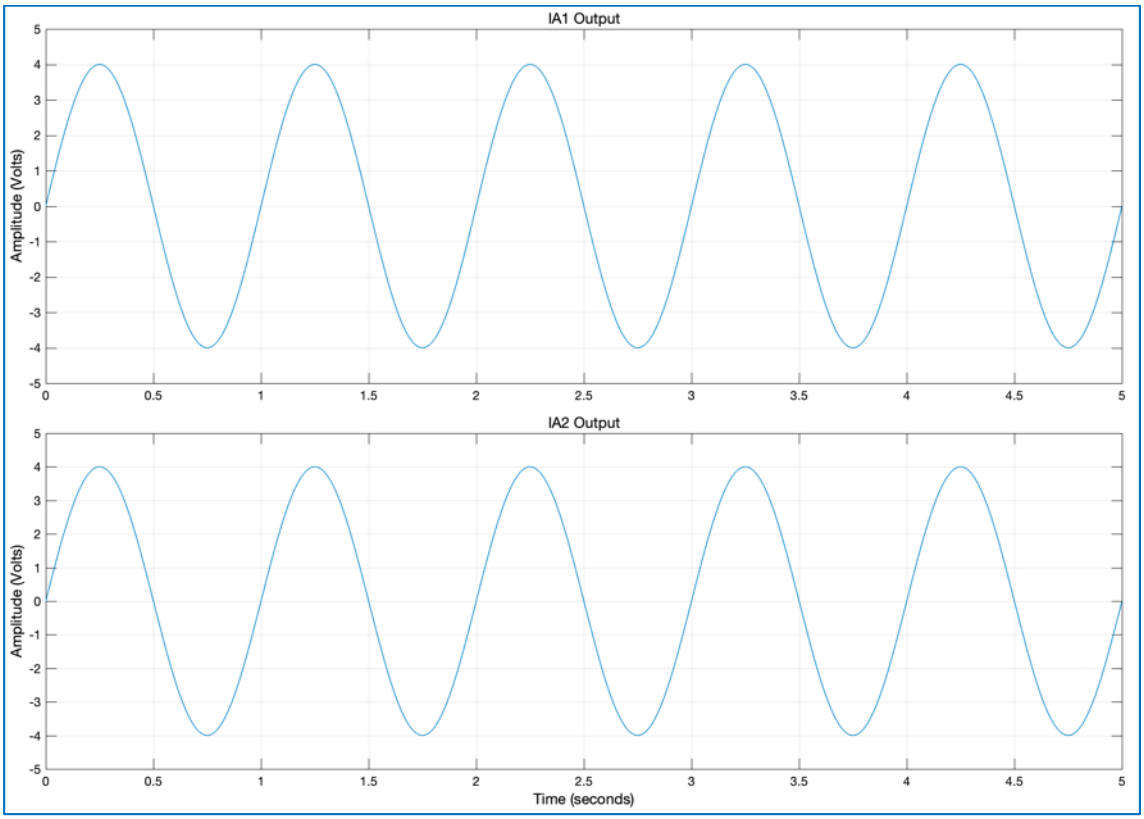

Fig. 4-23 Outputs from IA-1 and IA-2

The output of both IAs was then fed to the summing amplifier, which produced the final clean sinewave. This was eight times greater than the original signal's amplitude due to the amplification from each of the IAs.

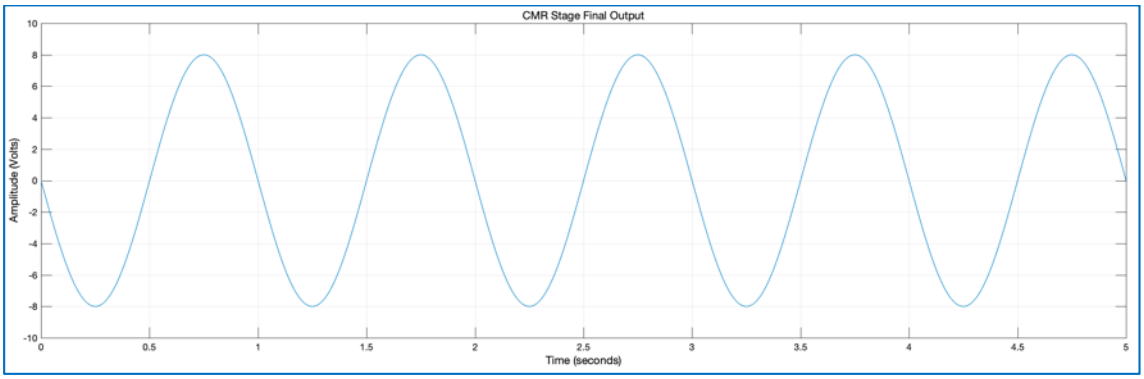

Fig. 4-24 CMR Stage Final Output

Fig. 4-25 shows the original differential sinewave signals along with the distorted version of the signal. Additionally, it shows the final clean signal compared to the other source and distorted signals.

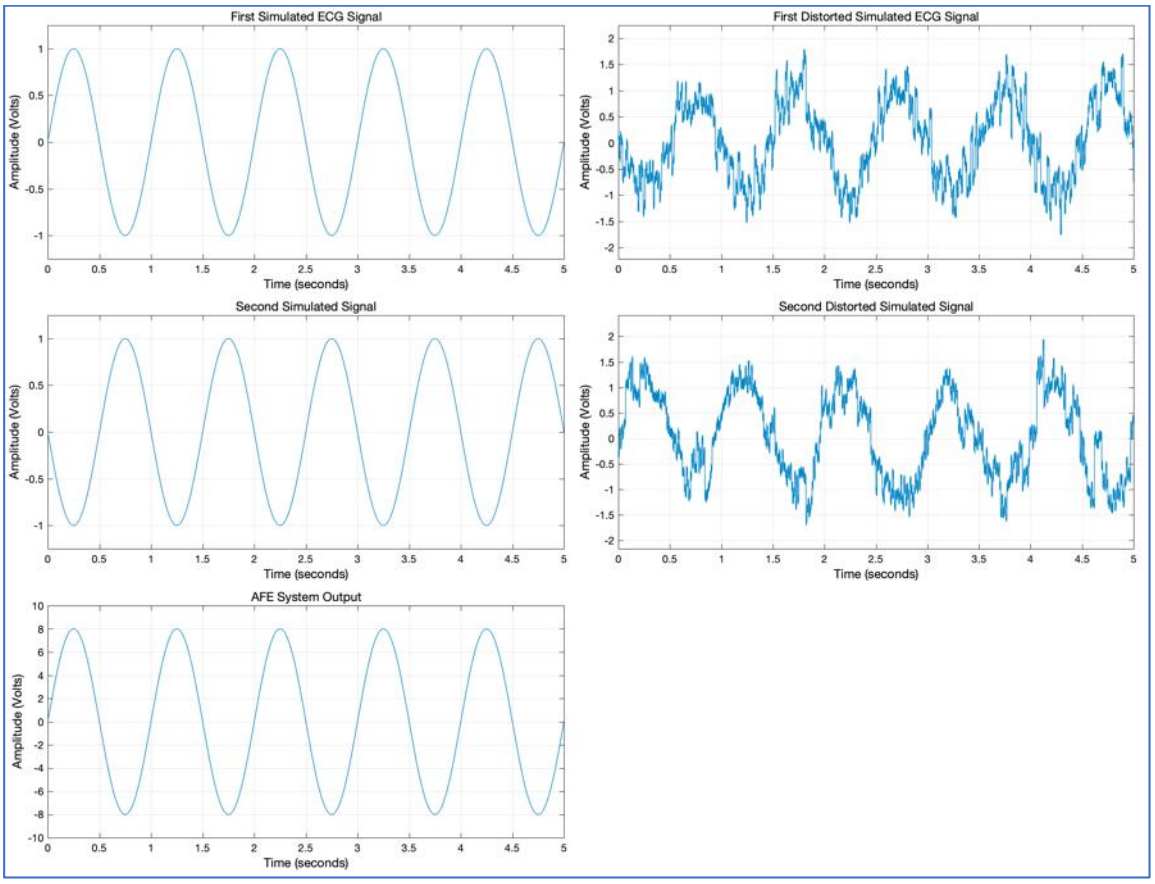

Fig. 4-25 First Simulated ECG Signal (top-left), First Distorted ECG Signal (top-right), Second Simulated ECG Signal (middle-left), Second Distorted ECG Signal (middle-right), and Final Output After Signal processing (bottom-left)

Fig. 4-26 shows the harmonic distortion spectrum of the original sinewave signal compared to the distorted and final output sinewave signals. The harmonic spectrum the amount of noise that was added to the source signal to become noisy. Also, it shows that the spectrum of the original input signal was close to the final output signal spectrum.

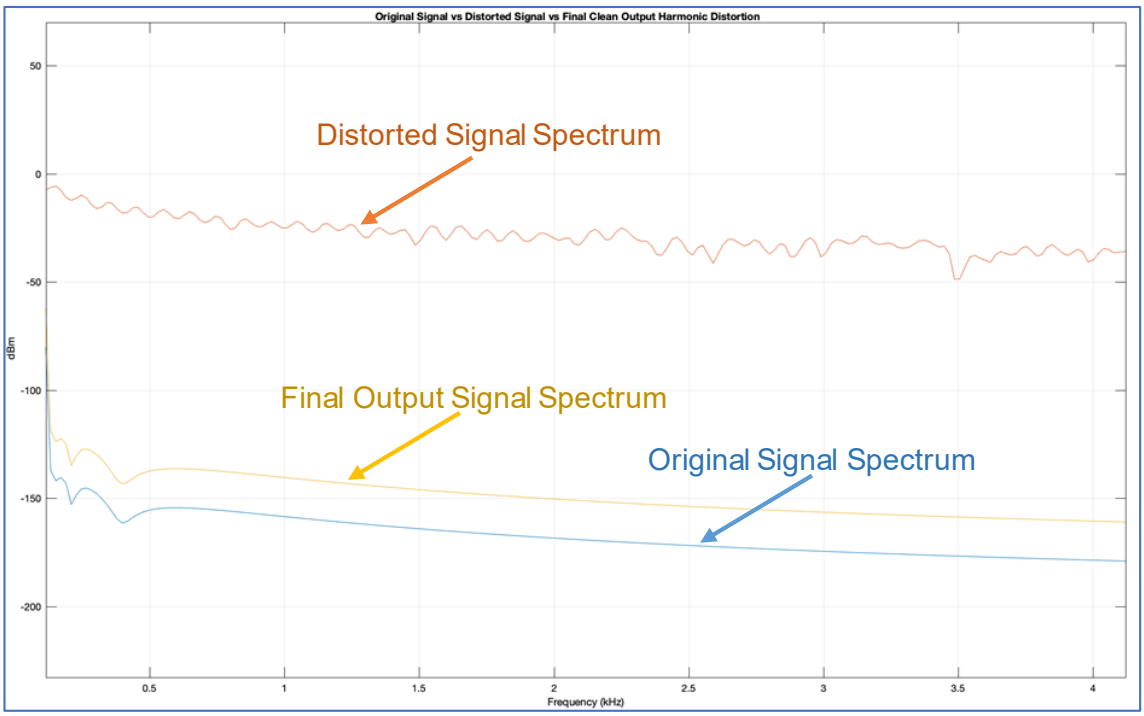

Fig. 4-26 Distortion Harmonics of the Original Signal, Distorted Signal and Final Output Sinewave Signals

As presented in Table 4-4, after processing the distorted signal in the AFE system, the THD decreased from 76.21% to 29.89%. The percentage of this decrease was 61%. In addition, the SNR was also increased by 3.49 dB (from -2.98 dB to 0.51 dB).

Table 4-4 Harmonic Distortion Spectrum measures of Distorted signal Compared to the Output Signal

	Clean Source Signal	Combined Noisy Signal	AFE Clean Output	Improvement
THD	29.68%	76.21%	29.89%	61% (decreased)
SNR	0.52 dB	-2.98 dB	0.51 dB	3.49 dB (increased)

Table 4-5 shows a comparison between the original generated clean signal and the AFE output signal. The THD and SNR of the output signal was 99.5% and 98% like the THD and SNR of the original signal, respectively. This result was better than other methods, such as (Zhang and Wei, 2020), when comparing the clean source signal with the output signal. The output signal was clean from most of the added noise during this simulation process.

Table 4-5 Harmonic Distortion Spectrum measures of Original Signal and Output Signal

	Clean Source Signal	AFE Clean Output	Improvement	Output Signal Similarity with Source Signal
THD	29.68%	30.16%	0.5% (increased)	99.5%
SNR	0.52	0.51	0.01 dB (decreased)	98%

The AFE system removed most of the added noise (including motion artefact, Power Supply Harmonic (50Hz), Power Line Interference (40kHz) and White noise), with an average correlation coefficient of 0.995 which was better than the other reported methods such as (Berwal et al., 2019) that achieved an average of 0.9337. The correlation between the original and output signals was displayed in Fig. 4-27. The linear correlation efficiency equation for both signals is y=8x, which meant that the output signal was eight times the original signal. The gradient of the line was 8, and the 'y' intercept was 3.49^{-16} which was rounded to zero.

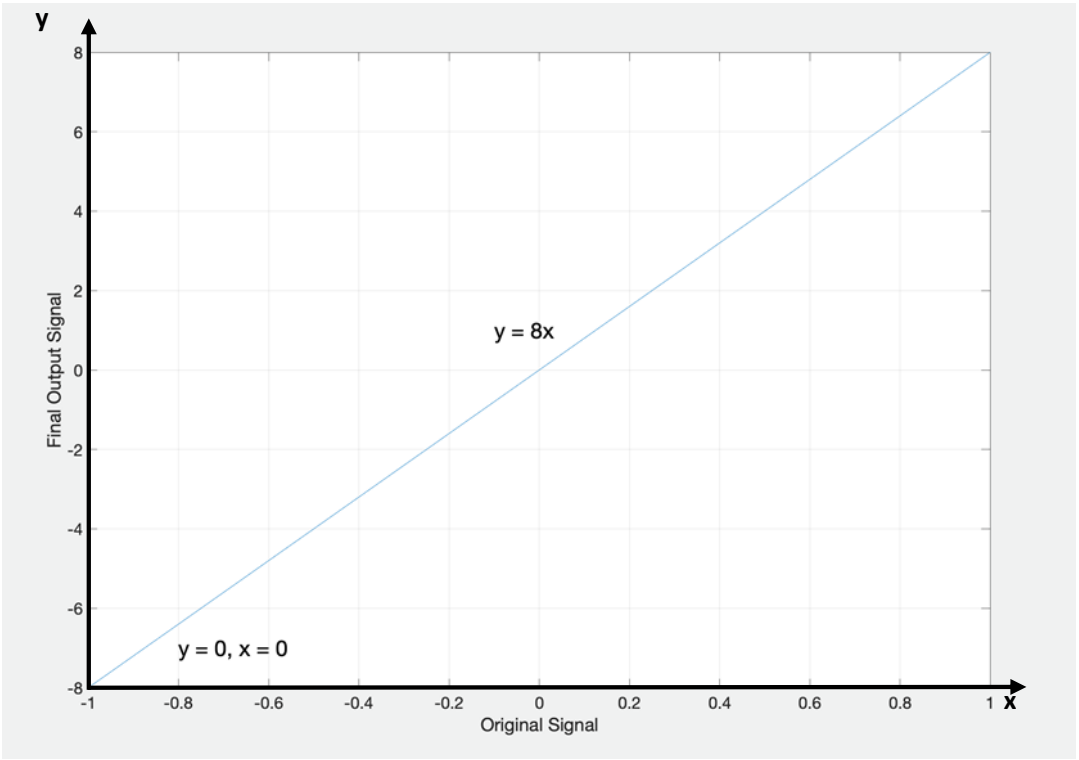

Fig. 4-27 Correlation Between Original Signal and Output Signal

4.6 Summary

The system design was developed in this chapter by introducing a double strain gauge solution. The system can deal with multi-dimensional (X and Y plane) motion artefacts that could affect the ECG biopotentials. Additionally, the motion artefact reduction for each ECG signal source was designed to be done separately before the removal of the common-mode signals to achieve the best results.

The system was simulated using MATLAB Simulink tools to prove that the design is working as expected. The resultant signals of each stage were explained in Fig. 4-25, showing that the intended functionality of the new design achieved the objectives.

The next chapter will explain how the system was built and tested using discrete components. It will also discuss the challenges that occurred during the implementation process and how these were addressed.

4.7 References

[1] AKTAKKA, E. E., WOO, J. K. & NAJAFI, K. On-chip characterization of scale-factor of a MEMS gyroscope via a micro calibration platform. 2017 IEEE International Symposium on Inertial Sensors and Systems (INERTIAL), 27-30 March 2017 2017. 1-4.

[2] BELGURZI, S., ELSHAFIEY, I. & NOUH, A. Artifacts removal from ECG signal using an ANFIS technique. Cybernetics and Computational Intelligence (CyberneticsCom), 2017 IEEE International Conference on, 2017. IEEE, 147-152.

[3] BERWAL, D., V, C. R., DEWAN, S., J, C. V. & BAGHINI, M. S. 2019. Motion Artifact Removal in Ambulatory ECG Signal for Heart Rate Variability Analysis. *IEEE Sensors Journal,* 19**,** 12432-12442.

[4] DOOL, B. J. V. D. & HUIJSING, J. K. 1993. Indirect current feedback instrumentation amplifier with a common-mode input range that includes the negative roll. *IEEE Journal of Solid-State Circuits,* 28**,** 743-749.

[5] KISHIMOTO, Y., KUTSUNA, Y. & OGURI, K. Detecting motion artifact ECG noise during sleeping by means of a tri-axis accelerometer. Engineering in Medicine and Biology Society, 2007. EMBS 2007. 29th Annual International Conference of the IEEE, 2007. IEEE, 2669-2672.

[6] NAGEL, J. H. 2000. Biopotential amplifiers. *Bronzino JD: Biomedical engineering hand book, 2nd edition, Springer-Verlag New York***,** 70.1-70.14.

[7] NEUMAN, M. R. 1998. Biopotential amplifiers. *Medical instrumentation: application and design***,** 316-318.

[8] PATTERSON, J. A. & YANG, G.-Z. 2011. Ratiometric artifact reduction in low power reflective photoplethysmography. *IEEE transactions on biomedical circuits and systems,* 5**,** 330-338.

[9] SATHIYABAMA, G., VINUDEVI, G., R, A. & INDHUPRIYA, P. 2015. A Survey on Instrumentation Amplifiers used for Biomedical Application. *International Journal of Advanced Research in Electrical, Electronics and Instrumentation Engineering,* 4**,** 1224-1231.

[10] SHAIK, B. S. & CHAKKA, V. K. Joint reduction of baseline wander, PLI and its harmonics in ECG signal using Ramanujan Periodic Transform. India Conference (INDICON), 2016 IEEE Annual, 2016. IEEE, 1-5.

[11] SHAIK, B. S., CHAKKA, V. K., GOLI, S. & REDDY, A. S. Removal of narrowband interference (PLI in ECG signal) using Ramanujan periodic transform (RPT). Signal Processing and Communication (ICSC), 2016 International Conference on, 2016. IEEE, 233-237.

[12] SINGH, B., SINGH, P. & BUDHIRAJA, S. Various Approaches to Minimise Noises in ECG Signal: A Survey. 2015 Fifth International Conference on Advanced Computing & Communication Technologies, 21-22 Feb. 2015 2015. 131-137.

[13] SOLIS-BUSTOS, S. & SILVA-MARTINEZ, J. Design considerations for biomedical signal interfaces. Proceedings of the Third International Workshop on Design of Mixed-Mode Integrated Circuits and Applications (Cat. No.99EX303), 1999 1999. 187-191.

[14] ŞTEFĂNESCU, D. M. Strain gauges and Wheatstone bridges — Basic instrumentation and new applications for electrical measurement of non-electrical quantities. Eighth International Multi-Conference on Systems, Signals & Devices, 22-25 March 2011 2011. 1-5.

[15] ZHANG, H., ZHANG, S., JIN, Q., LIU, X., LI, Q., YANG, J. & ZHAO, J. Motion artifact suppression in ambulatory ECG with feed forward combined adaptive filter. Computing in Cardiology Conference (CinC), 2016, 2016. IEEE, 1-4.

[16] ZHANG, M. & WEI, G. 2020. An integrated EMD adaptive threshold denoising method for reduction of noise in ECG. *PLOS ONE,* 15**,** e0235330.

CHAPTER 5

SYSTEM HARDWARE IMPLEMENTATION & TESTING

5.1 Introduction

After simulating the system and proving the quality of the results using MATLAB Simulink tools, the system needs to be tested and built using discrete components. This stage is critical to the project lifecycle as it will question the system functionality using real components that are expected to have different behaviour from the simulation environment. MATLAB signals are perfect signals, and results are always close to real. However, the physical components of the system may behave differently at one stage or another, which makes this test essentially important to the project.

Building the system in the lab is the final step in proving the methodology and proposal of this research. Testing such a system could be done in different ways, such as using real electrodes and trying to embed the strain gauges on top as proposed. Alternatively, mocking the test signals and producing a near-real scenario could be considered. The first approach is the ideal solution. However, it is not feasible at this stage of the research. Also, it is much more important to try to prove the proposed functionality using a much cheaper and faster method. Moreover, the size of the strain gauges and the electrodes need to be reconsidered to allow the fabrication of the strain gauges, which is not possible at this time.

Hence, the test methodology that was used in this section suggested the use of lab generated signals that lead to the same final results. This did not affect the design of the solution, its functionality or its expected final results.

The test was divided into two stages. The first stage was to generate all the required signals and prepare them for the next stage. The generated signals included the heartbeat signal, Motion Artefact (MA), and Common-mode (CM). The second stage was the signal processing stage, where all artefacts and noise would be minimised, and the final clean signal was gained.

5.2 Discrete Components Prototyping

The system was built and tested using discrete components to prove its capabilities in solving the research hypothesis. The process started with a plan to build each component on small individual breadboards as a block so that each block of the system could be tested and verified on their own. These blocks represented the mixer, IA, inverter, summing amplifier and a Wheatstone bridge.

Each block was tested on its own, and its functioning state was proved before starting to put all blocks together. This helped in detecting any faulty opamps or incorrect wiring easily before complete construction. The individual blocks can be seen in Fig. 8-1 of Appendix A of the thesis.

When everything was connected together, more wires were required to connect each component with the others and connect the power sources to each individual block. Additionally, more components, such as summing amplifiers and inverters, were required to prepare the test signal before starting to use it for testing. Fig. 5-1 shows the resultant complete system built from the individual components.

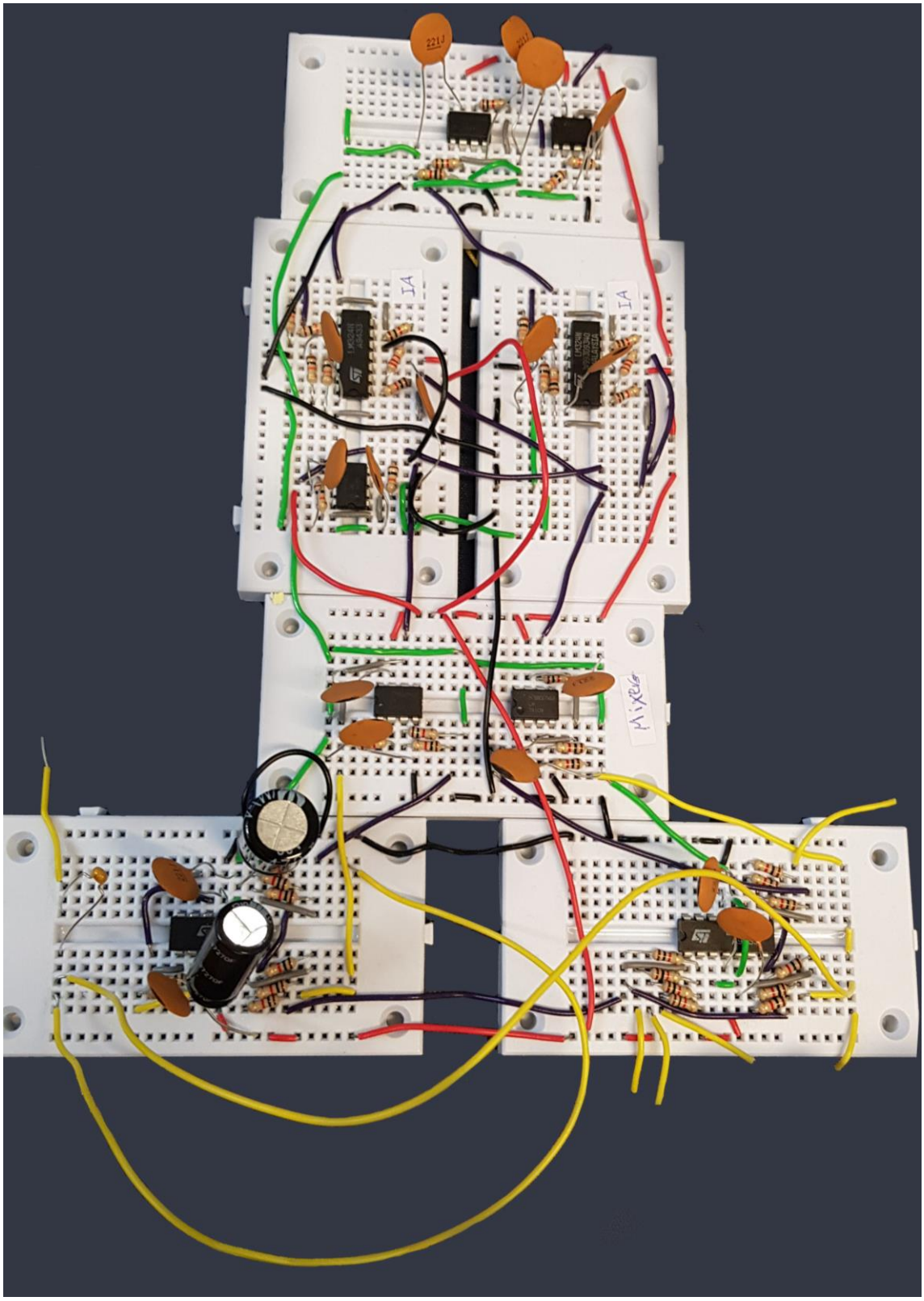

Fig. 5-1 System Built from Individual Blocks

As can be seen from the final complete system, more wires were required. Also, the signal was fluctuating and showing a non-stable, smooth flow. Therefore, capacitors

were used during testing to smooth the voltage flow between opamps of the individual blocks.

As the testing process was going on, the need for a neater design increased. Thus, open-source software, that helps in simulating the build process was used. Fritzing is a hardware initiative that facilitates the accessibility of the electronic components to anyone (Fritzing.org, 2019). It helped to reduce circuit build time in the lab as it was already implemented and checked using the software tools. More importantly, the wiring could always cause a mess when running the wires from one place to another far away; fortunately, the wiring was studied and planned well while using the simulation tool. This guaranteed much less waste during the building process. A clean build that was easy to understand and neater design that helped in spotting errors enabling them to be fixed quickly during the testing phase.

Some components were also replaced to ensure the final system was neat and tidy. In the initial design, summing amplifiers were mostly built using LM324 quad opamps to make the most use of the limited space available. However, they were replaced with the single opamp LM741 integrated circuit which made it easier to route the wires from one block to another. Additionally, IAs were initially built using LM324 quad opamps, but they were replaced with the AD623 IA to save space and granulate the final design. Fig. 5-2 shows the prototype of the system using Fritzing tools.

Wire colours were all coded to make it easier to deal with the design and help in following the voltage and signal routing effortlessly. Table 5-1 shows the wire code of the prototype.

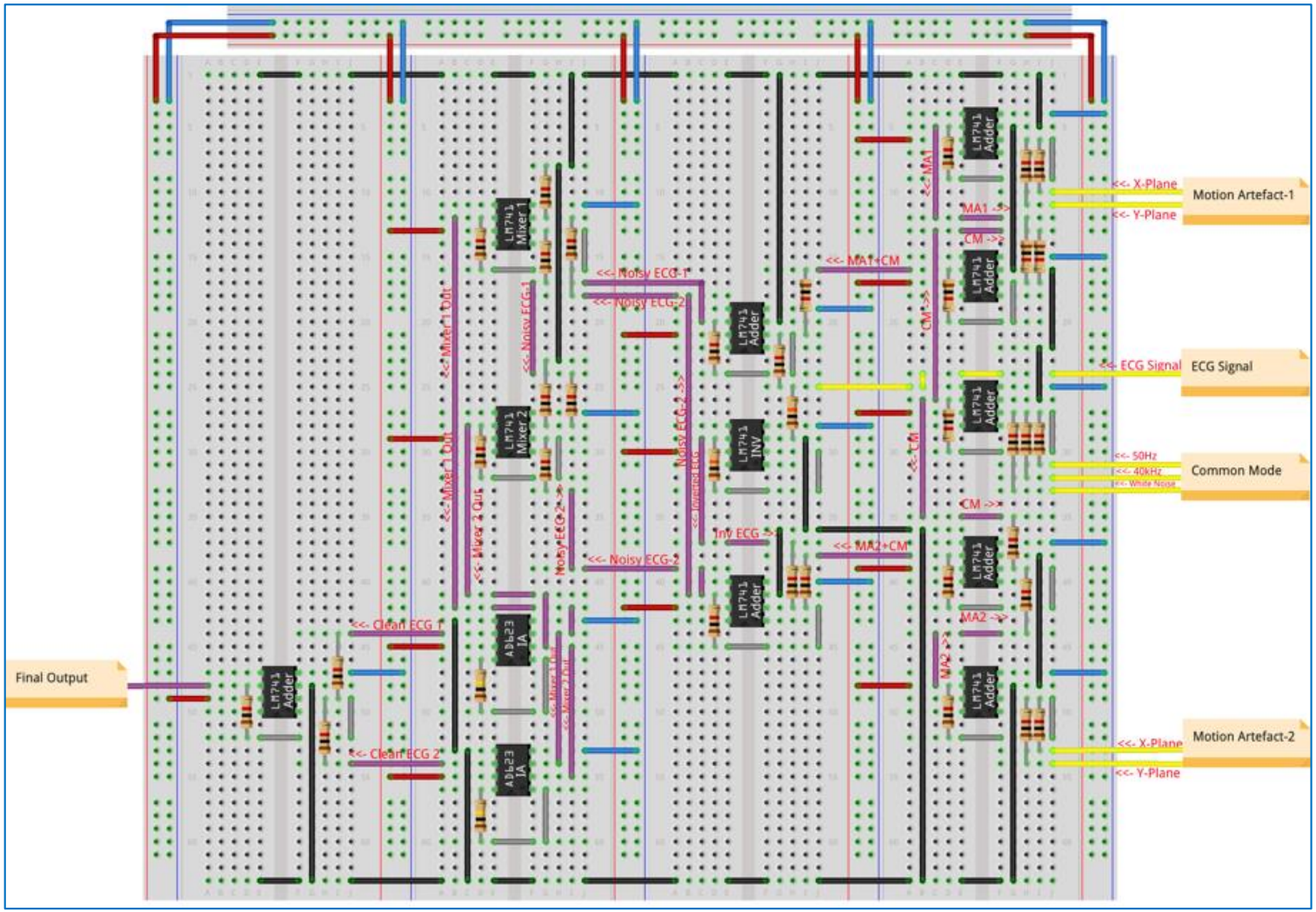

Fig. 5-2 System Prototype Built in Fritzing

Table 5-1 System Prototype Wires Colour Code

V(+)	V(-)
Input	Output
Ground	Inter-Connections

Due to the neat prototype that is produced using Fritzing tools, building the real version became much easier. Wire lengths and their routes were all defined, and it was simply a matter of putting things together. However, some incorrect wire routing and wrong connection mistakes were spotted during the build process, and changes were made on both designs to fix them. As can be seen from Fig. 5-2 when the prototype was firstly designed, the V(-) was prototyped using blue wires and the outputs of each component used purple wires. However, the blue wires were not available at the time, and the wire colours were changed and swapped to different colours. Table 5-2 explains the final colour codes that were used to produce the system design in the lab. Fig. 5-3 shows the final build of the prototype in the lab which was then used to obtain the results

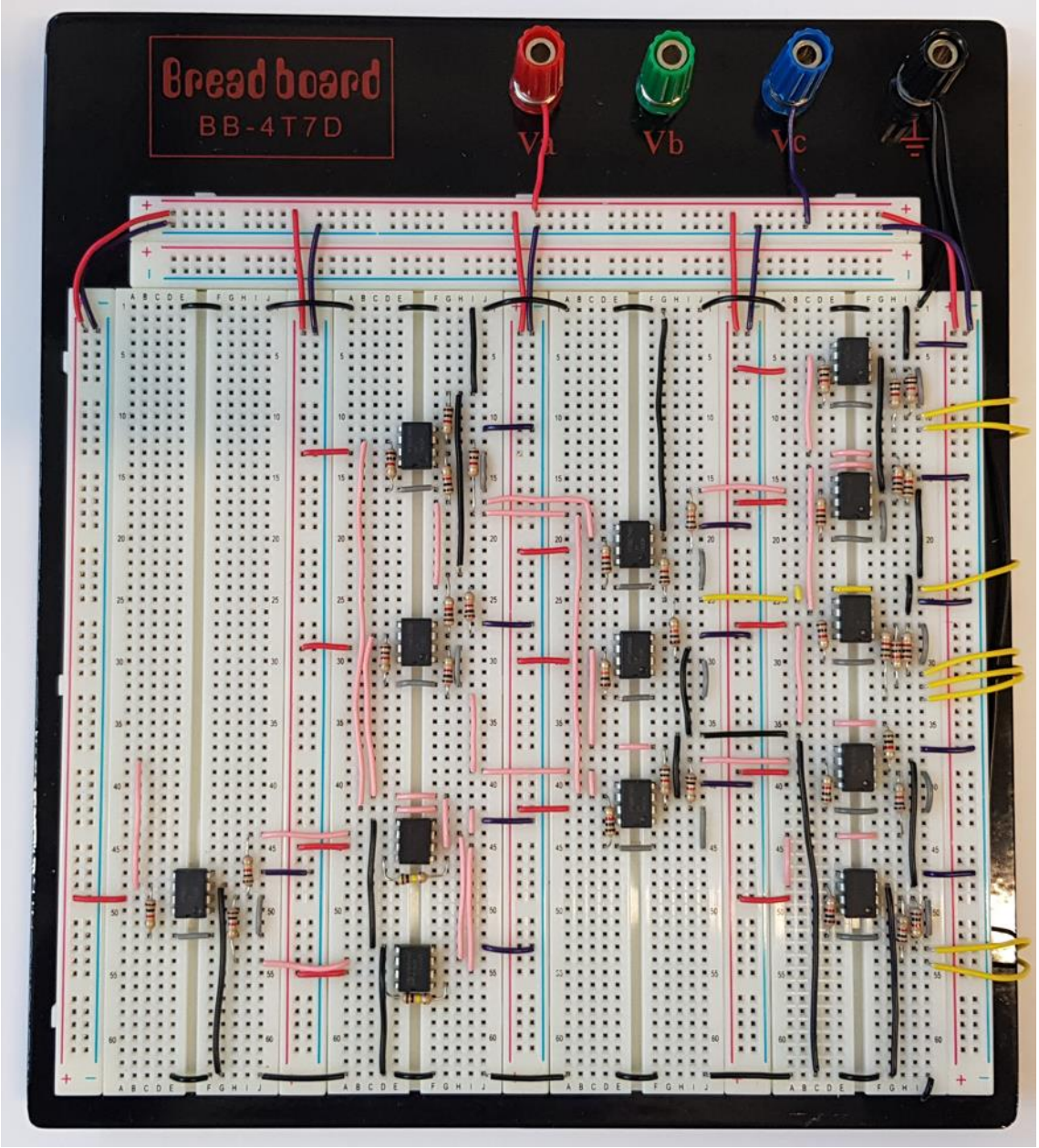

Fig. 5-3 System Prototype Built in Lab

Table 5-2 System Prototype Final Wires Colour Code

V(+)	V(-)
Input	Output
Ground	Inter-Connections

5.3 Prototype Components

The system build process included the use of LM741 opamps, LM324 quad opamps, AD623 IAs, 1kOhm resistors, 10kOhm resistors, and 100kOhm resistors. As mentioned earlier, some new components were used in this stage that was not needed in Simulink since it overcomes the issues related to these components. For example, the voltage follower was used to maintain any signal loss during the addition process of the voltages in the testing signal preparation stage. In this section, each of the roles of the used components was identified and explained.

5.3.1 Voltage Follower

In the discrete components implementation, a summing amplifier is used to combine a generated noise signal with a generated ECG signal and then fed the resultant signal to the differential amplifiers. However, this process could cause a signal loss due to the signal loading in the signal summation process. In order to avoid this signal loss, a voltage follower was used. Voltage follower is a circuit that consists of an opamp whose output voltage follows the input voltage. It does not introduce any amplification to the input signal, and it has a voltage gain of 1 (Bishop, 2001).

5.3.2 AD623 Instrumentation Amplifier

Instrumentation amplifiers (IAs) are a very important part of the system since the ECG biopotentials and all the related sources of noise are very small signals, and it is so difficult to maintain such signals without amplifying them. In the previous section, all IA circuits were built from scratch using op-amps and resistances. However, the AD623 IA was used in this stage to minimise the number of errors and sources of noise. The AD623 is an integrated, single- or dual-supply instrumentation amplifier that delivers rail-to-rail output swing using supply voltages from 3 V to 12 V (Analog Devices Inc., 2018). It also allows single gain set resistor programming, which gives the user the required flexibility to build different variations of the circuits. The gain of the AD623 is configurable by using

an external resistor to earn a maximum gain of 1000. However, it could be used without any external resistors, and the resultant unity gain will be a gain of 1 (Analog Devices Inc., 2018). The AD623 has a constant CMRR that is up to 200Hz, which means that all line noise harmonics will be easily rejected. Fig. 5-4 shows the functional block diagram of the AD623 IA.

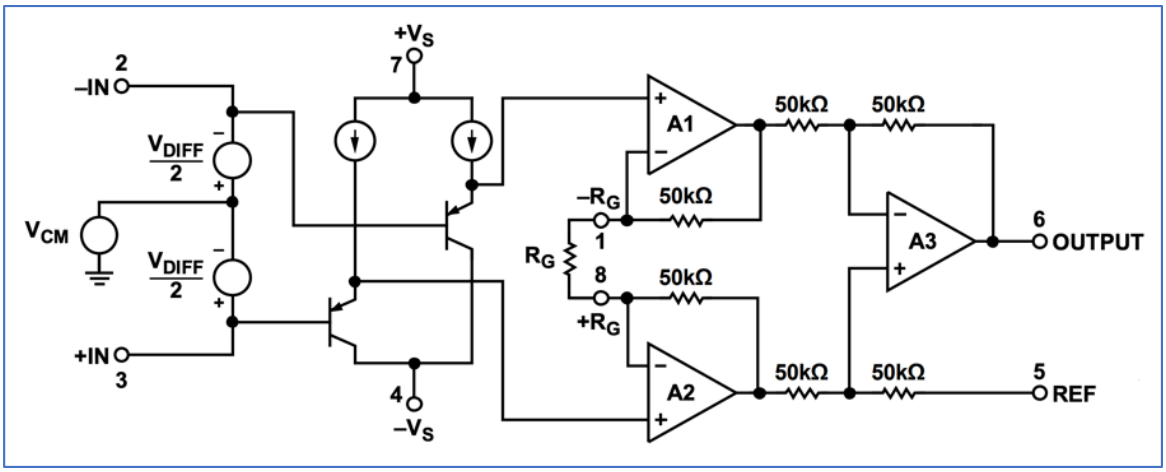

Fig. 5-4 AD623 Functional Block Diagram (Analog Devices Inc., 2018)

5.3.3 Strain Gauge Sensors

Strain gauges are voltage sensors that detect any strain that was introduced to the gauge. The gauge is normally connected to a Wheatstone bridge which is a balanced bridge as it was discussed in the strain gauges section of the design method and simulation in chapter 4. When a strain is detected on the strain gauge, the bridge becomes unbalanced, producing a voltage that represents the strain. Strain gauges are directional sensors, and their strain represents the amount of the applied strain and the direction that the gauge is installed in (Bowman, 1992). To capture multi-dimensional strains/noise, two strain gauges were installed on a 90° angle. Strain voltage outputs are typically small (~1mV) values and, therefore, the output of the Wheatstone bridge was connected to an AD623 IA to amplify the detected signal and feed it into the mixer where it would be processed. The AD623 was configured to have a gain of 2 by connecting a 100kΩ resistor in the R_g position of the circuit. Fig. 5-5 shows the Wheatstone bridge

and the IA circuits. The Wheatstone bridge consisted of three 100Ω resistors to match the resistance of the strain gauges that were used in the testing phase and produce a balanced bridge.

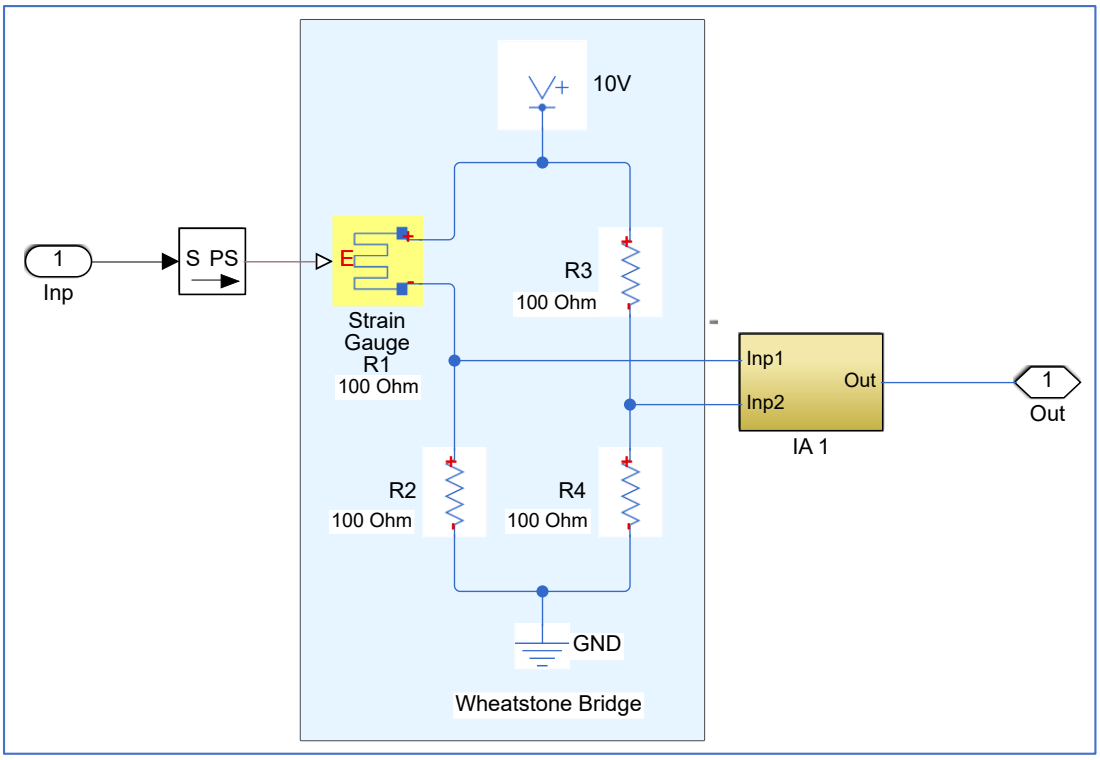

Fig. 5-5 Wheatstone Bridge and IA circuit

To test the functionality of the AFE system, the Wheatstone bridge circuitry was replaced with a random noise source that represented the output of the bridge. This proved that the AFE could handle any kind of noise that was fed to its differential amplifier. As a result, the noise was processed and subtracted from the original signal. This gave a noise-free signal as the output.

5.4 Test Signals Generation Stage

A heartbeat (ECG) signal was represented by a sinewave signal at this stage to make it easier to spot the errors. Additionally, the MA was represented by a square wave signal.

5.4.1 Heartbeat Signals Generation

In order to represent the ECG biopotentials as a sinewave signal, a function generator was used to generate a 1Hz (1V) sinewave signal. This step was similar to the MATLAB simulated signal, which made it possible to compare both results and confirm the correctness of this approach. The sinewave signal is simple, plus it facilitated the testing procedure and helped in gaining more precise results. Fig. 5-6 shows the resultant sinewave signal that was used to implement this test.

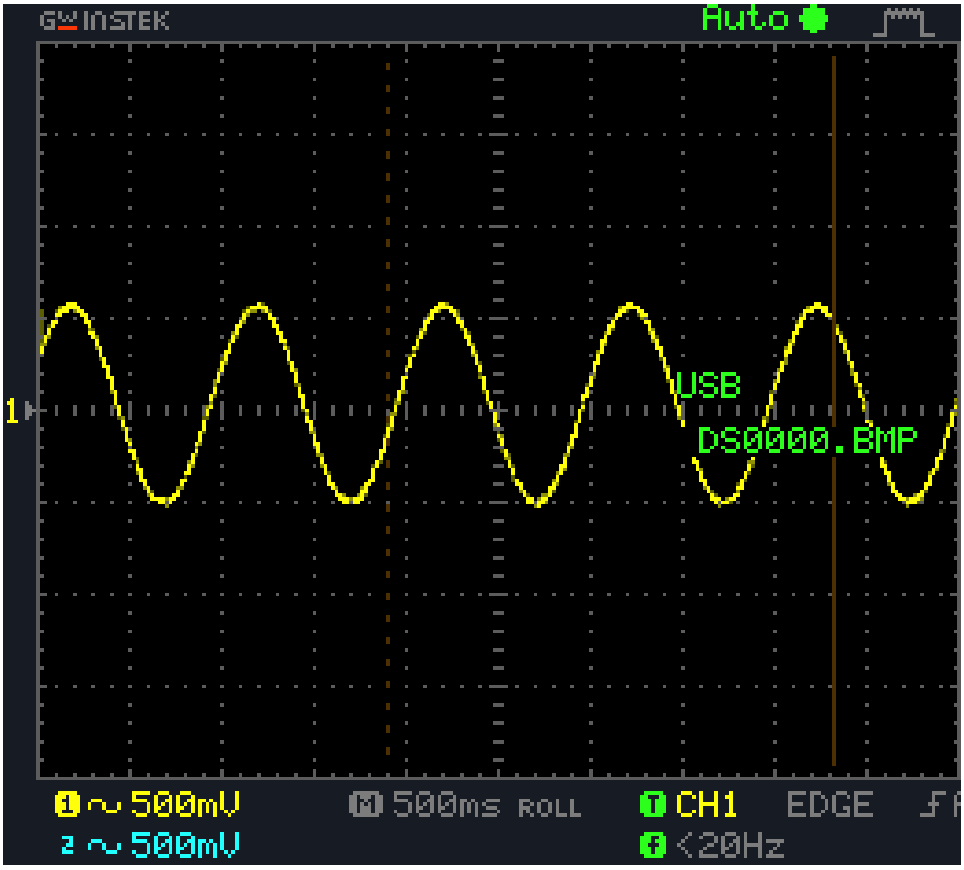

Fig. 5-6 Lab Generated Sinewave Signal

5.4.2 Noise Signals Generation

Noise signals were all generated in the lab using various generator configurations. Motion artefact, power supply harmonics (50hz) and the common-mode interference (40kHz) noise signals were generated, and all added together using summing amplifiers.

The resultant total noise signal was then fed into another summing amplifier to combine the noise with the sinewave signal to produce a noisy ECG signal.

1. Common-Mode Signals Generation

As for the heart biopotential, power supply harmonics (50Hz) and the common-mode interference (40kHz) noise signals were generated in the lab. Both signals were then added together to represent a single common-mode signal that is ready to be added to the motion artefact generated signal. Fig. 5-7 and Fig. 5-8 show the generated common-mode interference signal (40kHz) and the power supply harmonics (50Hz) respectively.

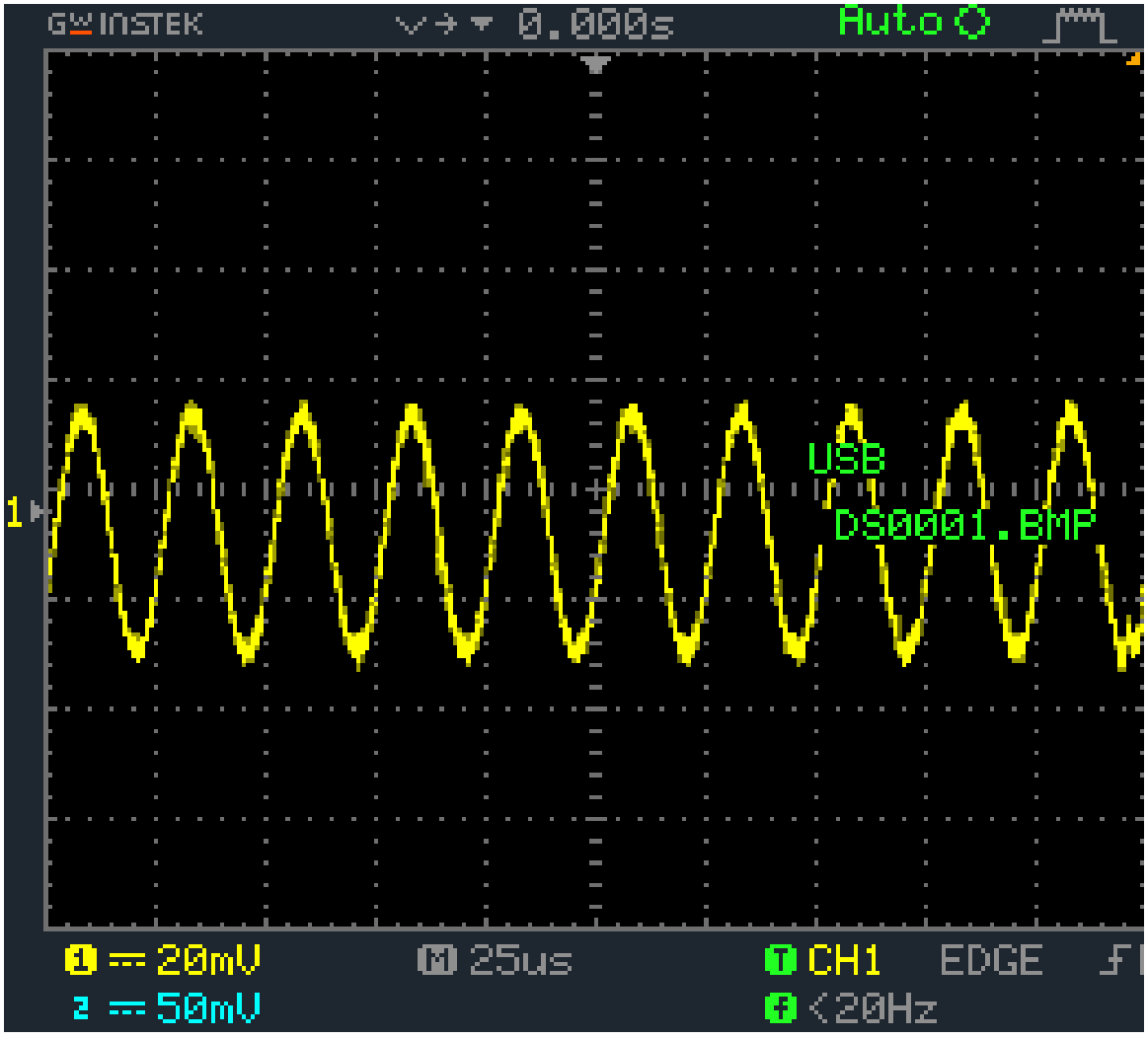

Fig. 5-7 Lab Generated Common-mode Interference (40kHz)

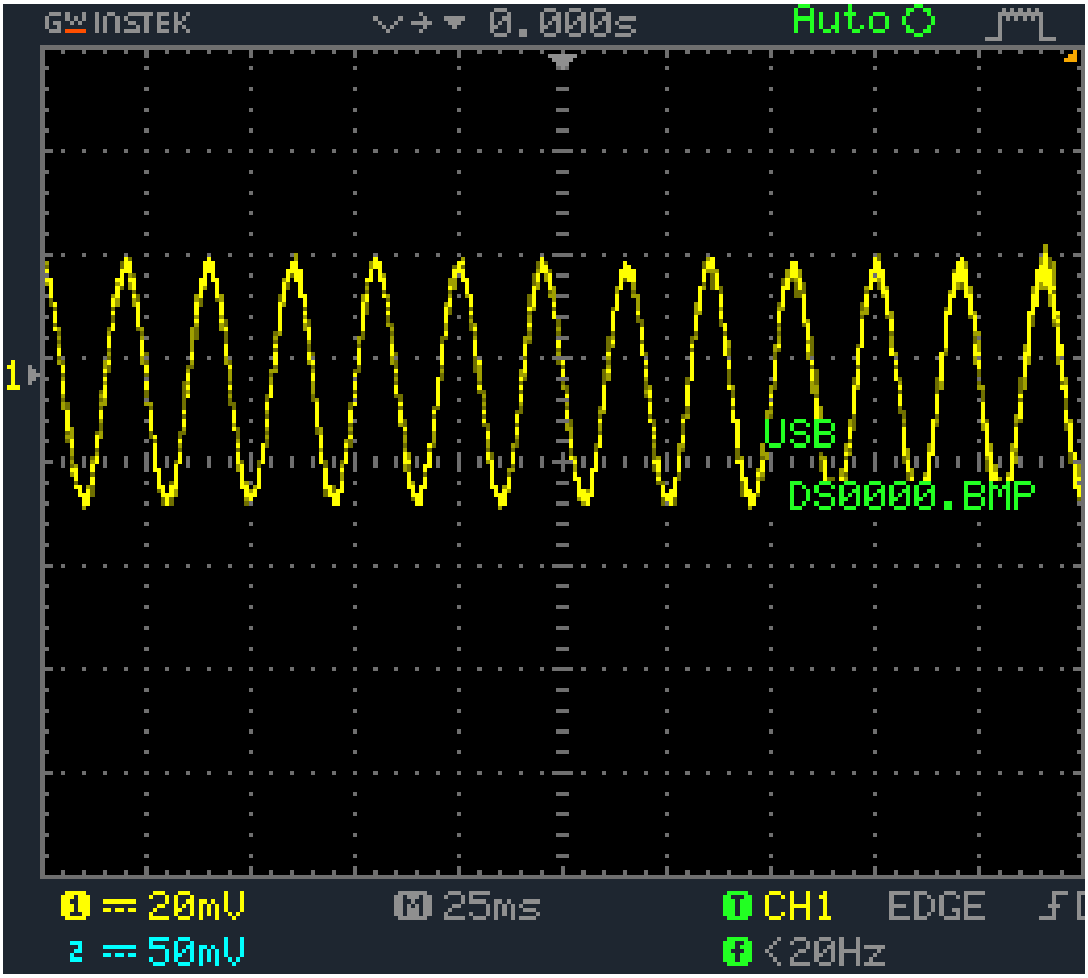

Fig. 5-8 Lab Generated Power Supply Harmonics (50Hz)

The total signal of both noise sources was now ready to be added to the MA noise in the next step. Then it was ready to be combined with the generated sinewave that represented the ECG signal.

2. Motion Artefact Signal Generation

The motion artefacts noise was represented as a square-wave signal of 20kHz and 50mV. The resultant signal was then combined with the generated common-mode noise signal that was prepared in the previous stage. A motion artefact could be in any shape and any form due to its random and unexpected occurrence (Kishimoto *et al.*, 2007, Liu, 2011, Nagai *et al.*, 2017). Therefore, an un-even square-wave signal was the right choice to examine and validate the functionality of the system. The generated motion artefact signal is shown in Fig. 5-9.

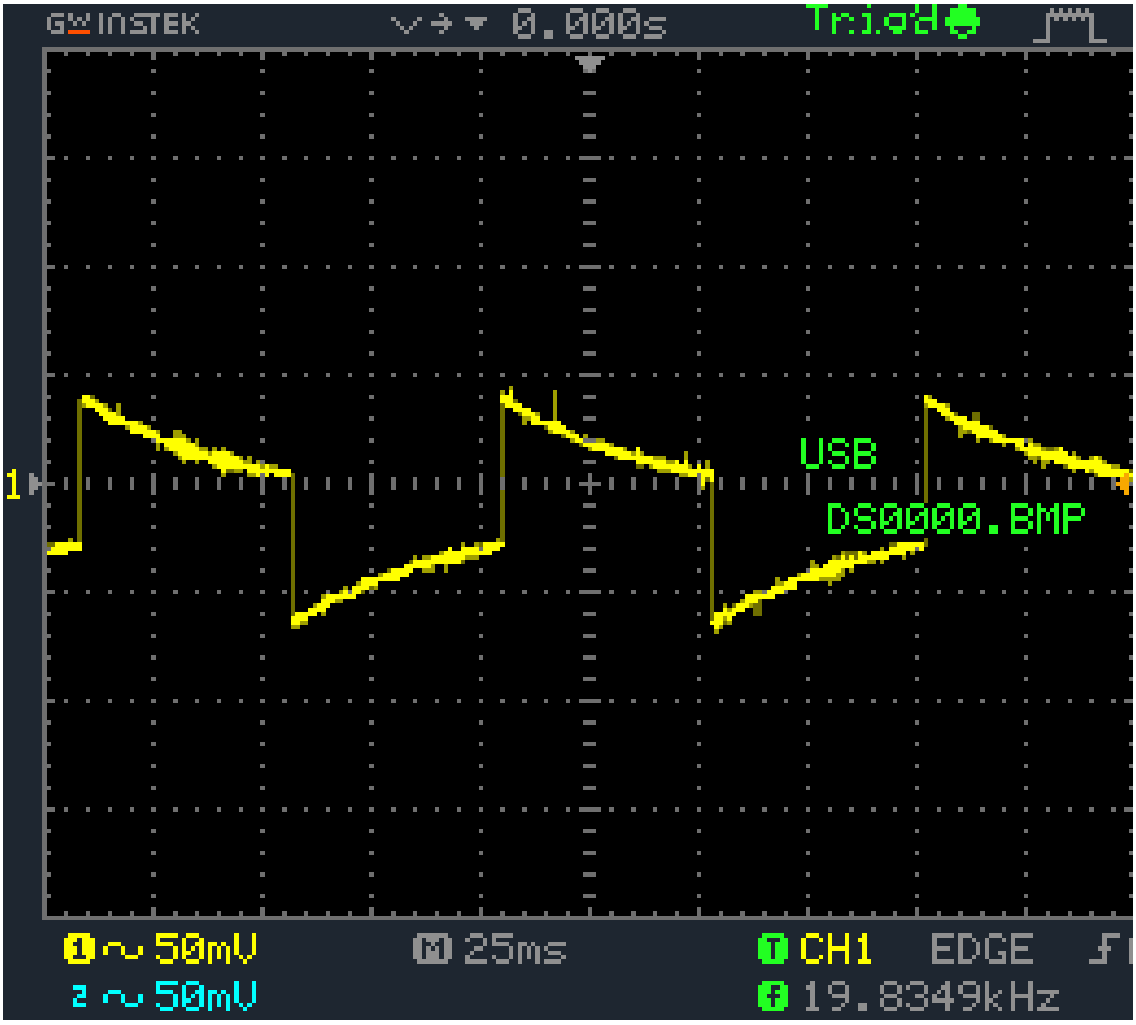

Fig. 5-9 Lab Generated Motion Artefact Noise

3. Combined Noise Signal

As stated earlier, noise sources need to be combined to represent a single source of noise as happens in real-life scenarios. Therefore, summing amplifiers were the key component to combine and construct the final total noise source. The final combined noise was about 36kHz and 20mV. Fig. 5-10 shows the resultant combined noise signal.

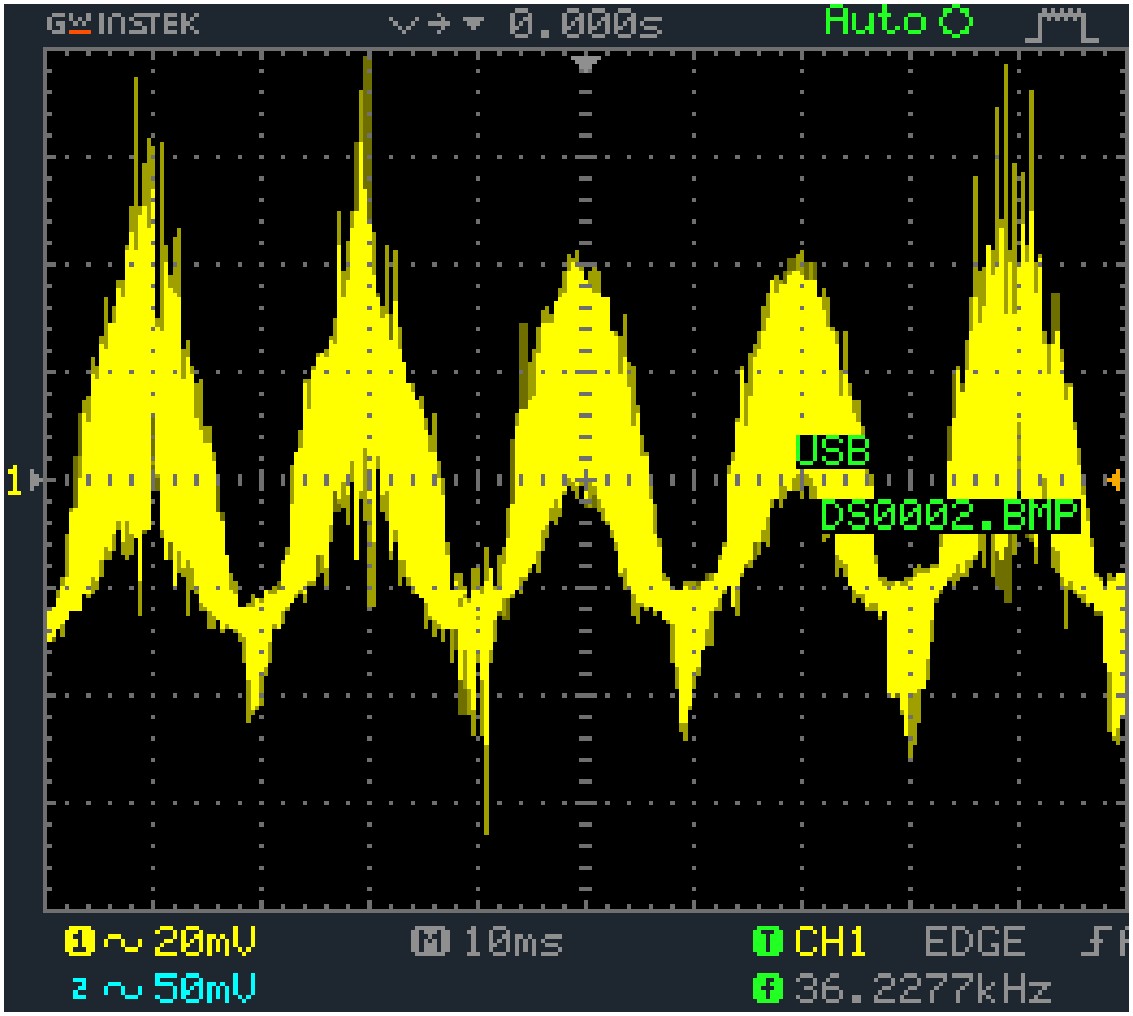

Fig. 5-10 Combined Lab Generated Noise Signals

5.4.3 Signal Generation Final Output

The noise sources and the generated sinewave signal were all added together to produce a final noisy signal that was used to examine the AFE system and validate its functionality. Fig. 5-11 shows the original ECG signal as well as the resultant noise signal of this stage. It is clear that the noisy signal held a lot of noise, which made the test more practical and put the AFE system under a real test procedure.

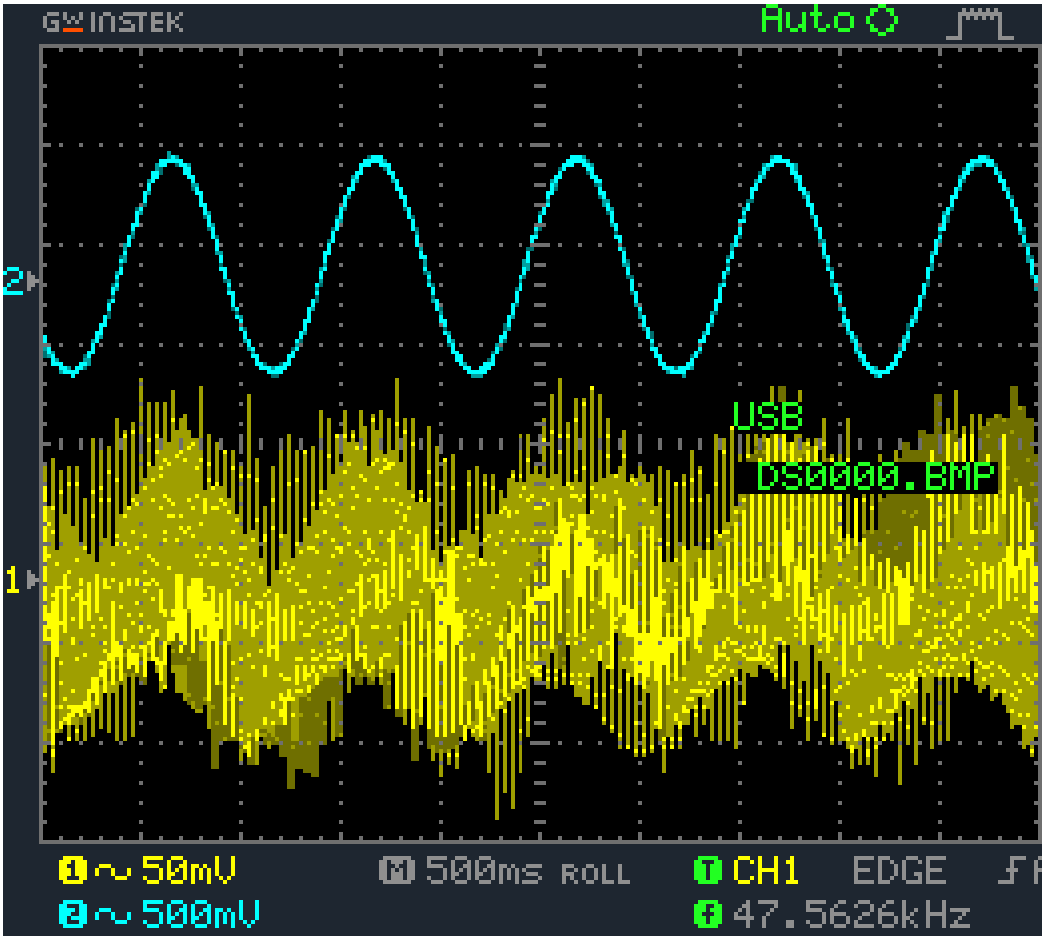

Fig. 5-11 Generated Sinewave (2) and The Noisy Sinewave (1)

Table 5-3 shows the harmonic distortion spectrum measurements of the original clean signal compared to the distorted signal (clean signal plus added noise). The THD of the clean signal increased from 38.82% to 80.63% in the new distorted signal. The percentage of this increase was 108%, which illustrated the amount of noise that was added to the source signal. In addition, SNR of the original signal was 0.86 dB and then became -3.73 dB in the distorted signal with a decrease of 4.59 dB.

Table 5-3 Lab - Harmonic Distortion Spectrum measures of original signal and Distorted Signal

	Clean Source Signal (A)	Combined Noisy Signal (B)	Decrease
THD	38.82%	80.63%	108% (increased)
SNR	0.86 dB	-3.73 dB	4.59 dB (decreased)

5.5 Signal Processing Stage

By this stage of the test, noise signals were combined to represent a single source of noise and then added to the generated sinewave signal to gain a noisy signal that was used as the input of the AFE system. Also, the MA signal is the second input of the AFE as it represented the signal that was captured by the strain gauge.

5.5.1 Motion Artefact Minimisation

The first processing stage was to minimise the motion artefact from the noisy sinewave. A fundamental benefit of having the strain gauges connected to the system was to capture any electrode movements and feed them directly to the system. At the same time, the desired signal was being captured. This provided a reference to what motion artefacts were and gave the system the ability to remove those noise signals of the input signal, in order to produce the desired signal.

The noisy sinewave signal and the captured motion artefacts were fed into a differential amplifier to extract the noise of the desired signal and remove it. Fig. 5-12 and Fig. 5-13 show the originally generated sinewave signal compared to the resultant signal at this stage.

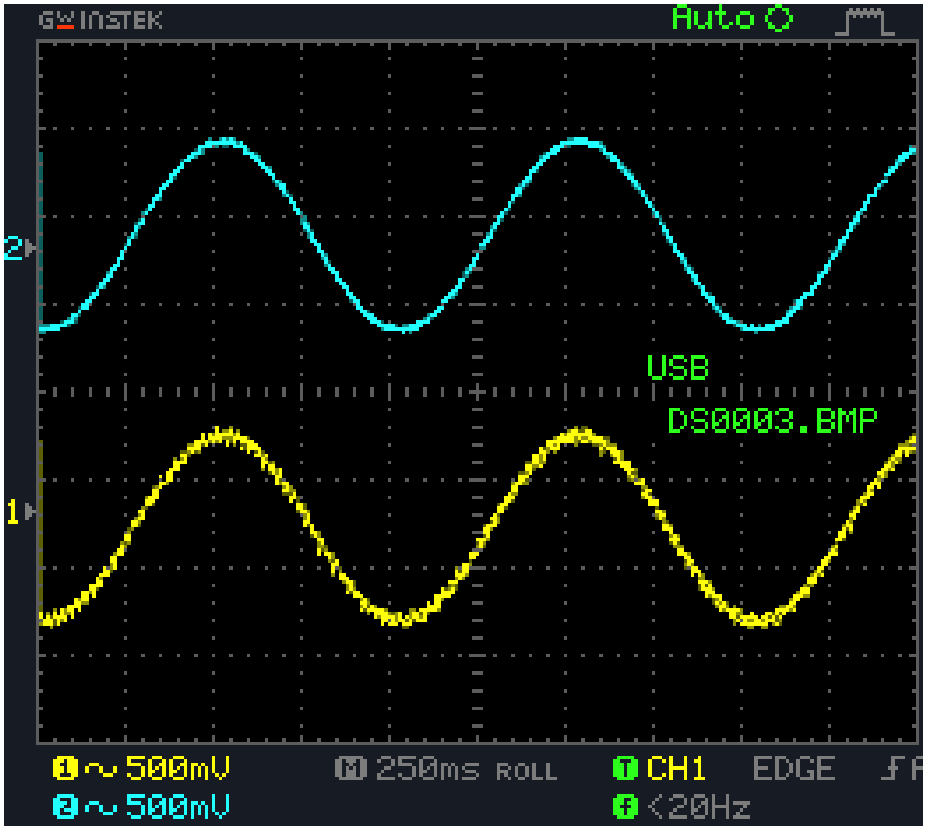

Fig. 5-12 Generated Sinewave (2) Compared to the result of the motion artefact minimisation stage (1)

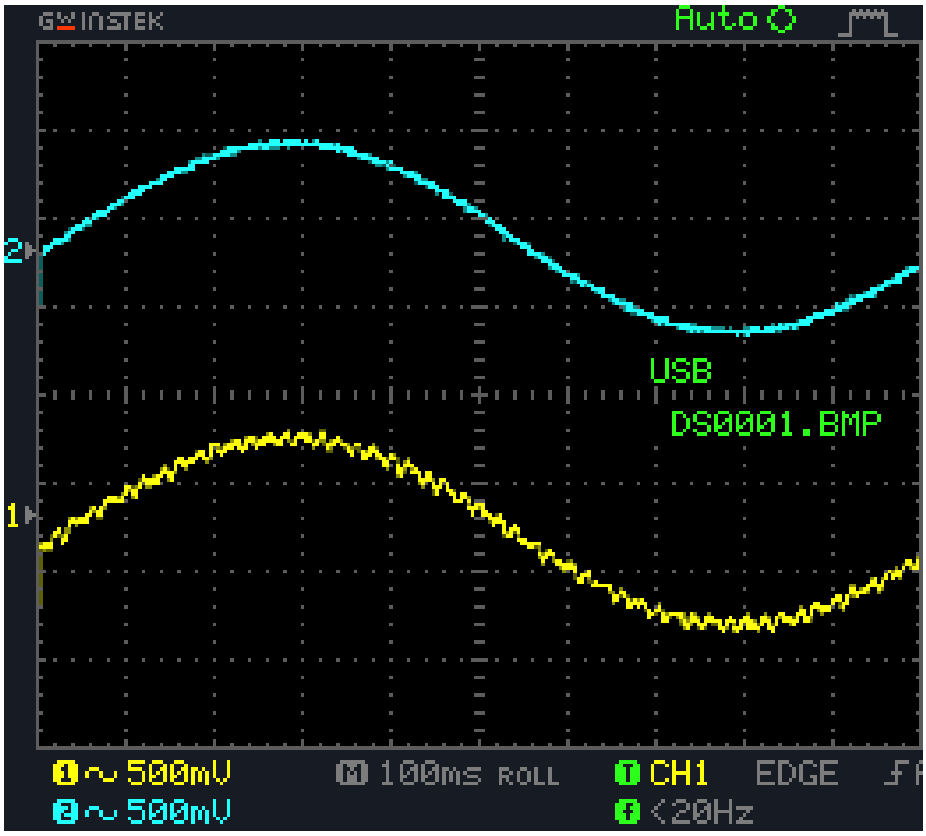

Fig. 5-13 Generated Sinewave (2) Compared to the result of the motion artefact minimisation stage (1)

The result was a signal that contained common-mode noise only, which confirmed the results found in the MATLAB motion artefacts minimisation simulation.

5.5.2 Common-mode Signal Processing

As explained earlier, the process of removing the common-mode signal was done by using the AD326 conventional IAs. A conventional instrumentation amplifier is an appropriate component to deal with the common-mode signals, as they are limited by the common-mode rejection ratio (CMRR) of the amplifier. Each IA was configured to have a gain of 2. Hence, the output signal of each IA is a sinewave that was four times the originally generated signal's amplitude. Fig. 5-14 shows the output from one of the IAs.

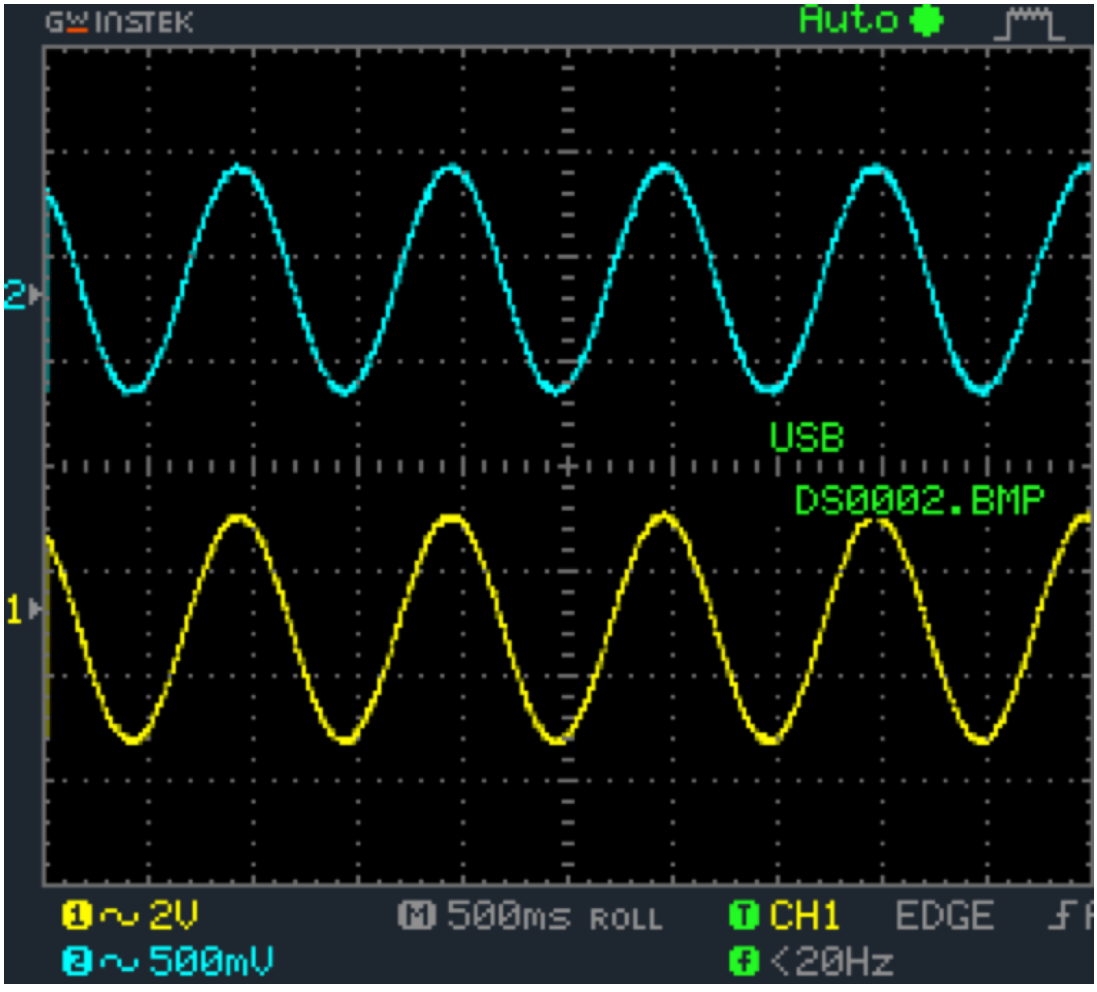

Fig. 5-14 CMR stage IA output

Finally, the output from both IAs was added together to gain one final clean signal, as shown in Fig. 5-15.

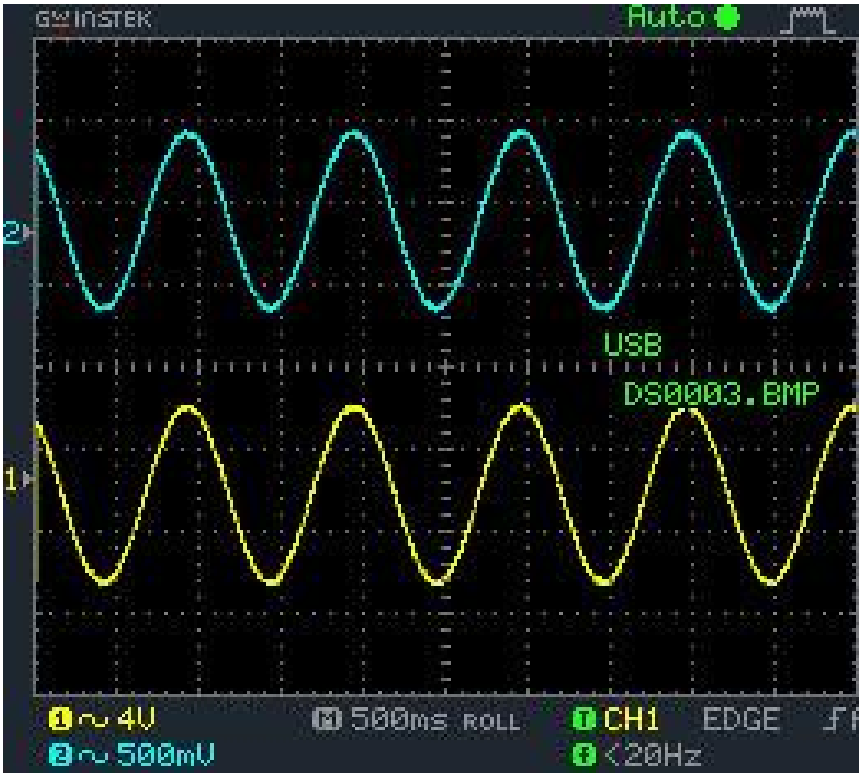

Fig. 5-15 Final Mixer Output Oscillator

5.5.3 Signal Processing Stage Results

As can be seen in Table 5-4, after processing the distorted signal in the AFE system, the THD decreased from 80.63% to 39.99%. The percentage of this decrease was 50.4%. In addition, the SNR was also increased by 4.57 dB (increasing from -3.73 dB to 0.84 dB).

Table 5-4 Lab - Harmonic Distortion Spectrum measures of Distorted signal Compared to the Output Signal

	Clean Source Signal	Combined Noisy Signal (A)	AFE Clean Output (B)	Improvement
THD	38.82%	80.63%	39.99%	50.4% (decreased)
SNR	0.86 dB	-3.73 dB	0.84 dB	4.57 dB (increased)

Table 5-5 exhibits a comparison between the original generated clean signal and the AFE output signal. The THD and SNR of the output signal was 98.8% and 97.8% like the THD and SNR of the original signal, respectively. This result is better than other methods, such as (Zhang and Wei, 2020), when comparing the clean source signal with the output signal. The output signal was clean from most of the added noise during this simulation process.

Table 5-5 Lab - Harmonic Distortion Spectrum measures of Original Signal and Output Signal

	Clean Source Signal	AFE Clean Output	Improvement	Output Signal Similarity with Source Signal
THD	38.82%	39.99%	1.2% (increased)	98.8%
SNR	0.86 dB	0.84 dB	0.02 dB (decreased)	97.8%

The AFE system removed most of the added noise, with an average correlation coefficient of 0.974 which is better than the other reported methods such as (Berwal et al., 2019) that has achieved an average of 0.9337.

5.6 Test Rig Measurement

Previous tests were all testing the Analog Frontend (AFE) by feeding it with direct lab generated signals. All signals, heartbeat (ECG), motion artefacts and common-mode, were all mixed before being fed to the system. As shown in the results of the earlier test, the system responded actively well and cleaned the motion artefacts and common-mode signals.

Testing the system with strain gauges needed more than feeding the system with the motion artefact signal. Also, varying the resistance of the strain gauges was not helpful and gave unrealistic results. In reality, testing the strain gauges required straining and flexing of the gauges. Therefore, a newly developed idea, to use a loudspeaker with a plastic rod and covered with a plastic sheet, was used.

5.6.1 Speaker Prototype design

The test rig was firstly prototyped using computer software called “3D Paint” to have a high-level representation of the expected output. 3D Paint is a product of Microsoft Corporation application that can be downloaded and installed on Microsoft Windows machines and used to draw 3D models that can be manipulated from all angles.

As can be seen in Fig. 5-16, the prototype showed how the speaker would be covered with a plastic sheet that represented the skin. In the middle of the upper view of the sheet, a magnetic sheet was placed with an ECG electrode on top. The ECG signal, represented by a sinewave, was injected underneath the electrode using a layer of foil.

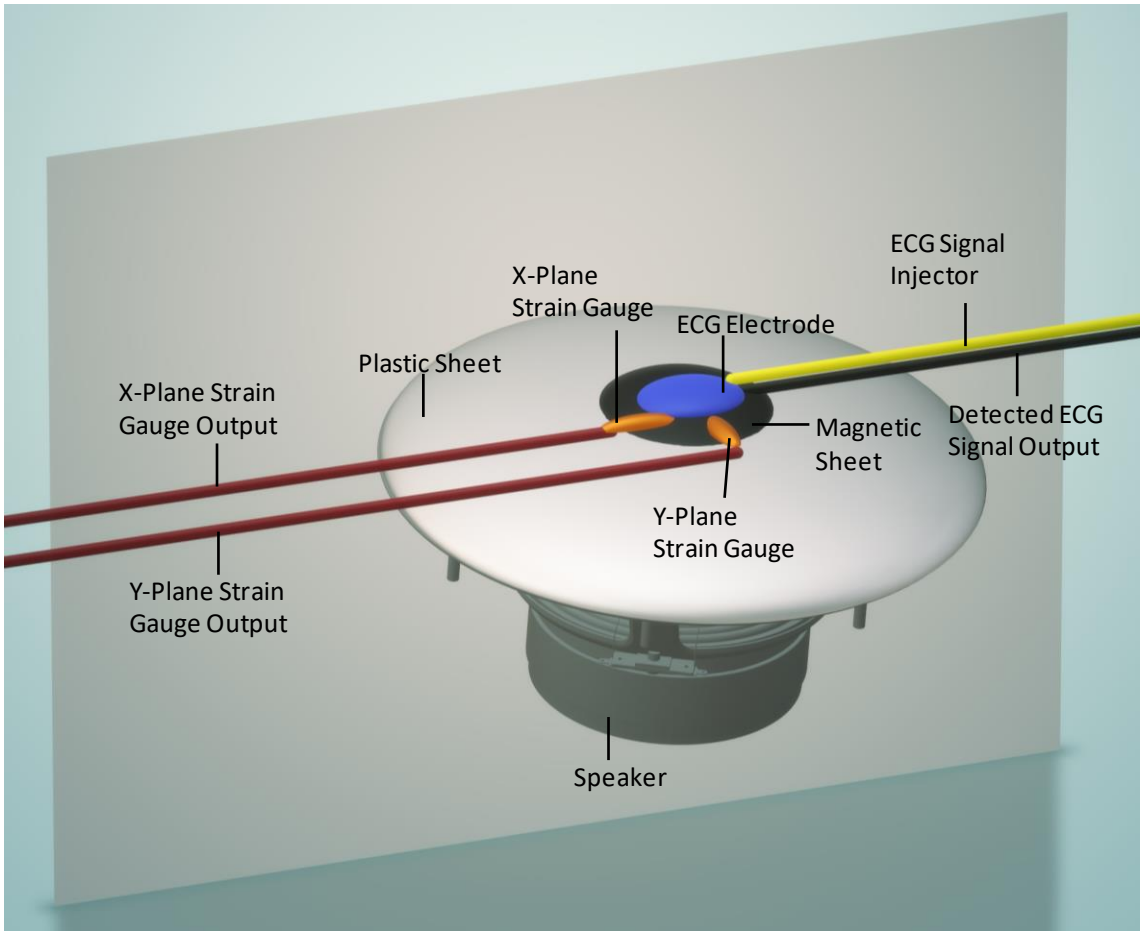

Fig. 5-16 Speaker Prototype Design (top view)

The X-Plane and Y-Plane strain gauges were connected to the magnetic layer and the plastic sheet, to detect any motion of the electrode surface. At the same time, the electrode captured the injected sinewave signal along with any motion or flexing in the strain gauges. Fig. 5-17 showed a side view of the speaker prototype test rig.

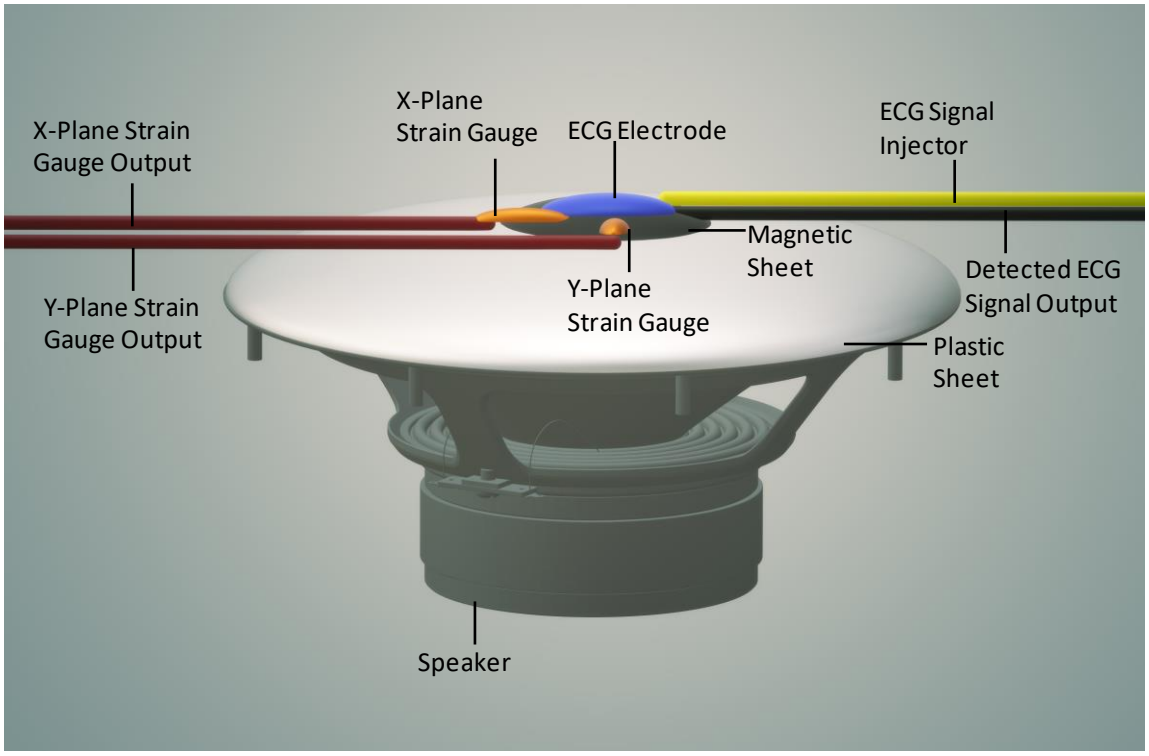

Fig. 5-17 Speaker Prototype Design (side view-a)

To simulate the motion artefacts and cause the strain gauges to flex, an audio track was played on the speaker, causing the plastic rod to move up and down, as shown in Fig. 5-18.

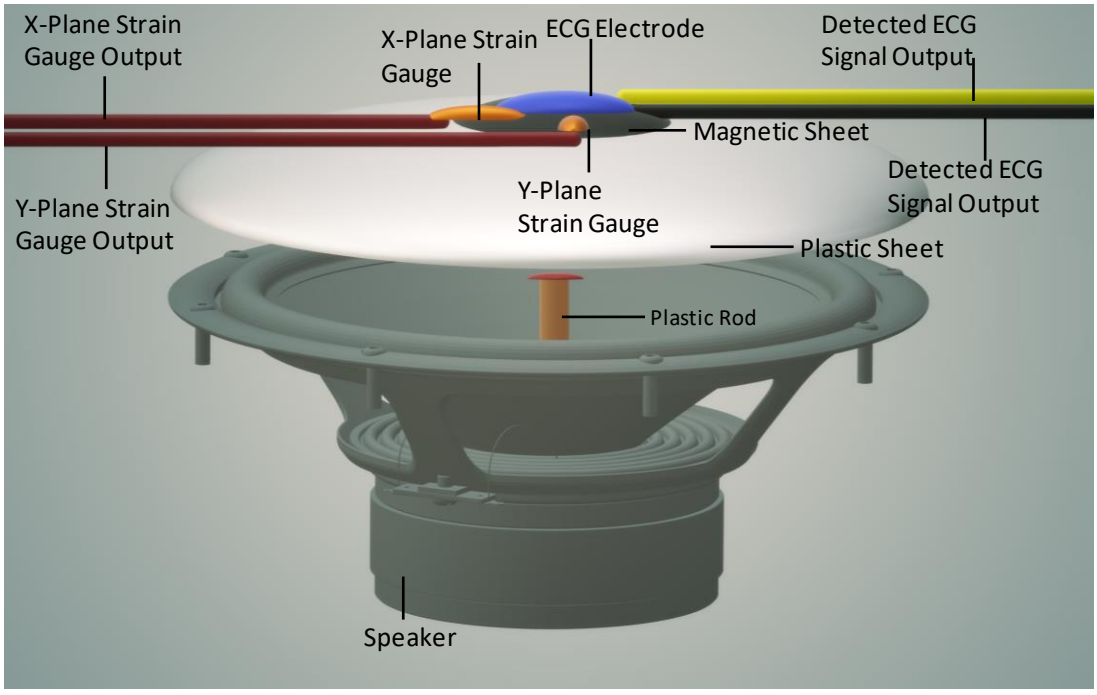

Fig. 5-18 Speaker Prototype Design (side view-b)

5.6.2 Speaker Prototype Implementation

To build this test rig, an 8 Ohm speaker with a size of 5" and a closed-back magnet was used. It takes a peak power of 40W and a frequency of 600-7500Hz. Also, XLBLEU ECG electrode was used to detect the injected sinewave signal. As shown in Fig. 5-19 and Fig. 5-20, the speaker was connected to a flexible plastic sheet which represented the skin, and it was connected with a plastic rod that was very stiff. As the cone moved up and down, the pseudo-skin moved up and down as well. The strain gauges were then attached to this sheet via the magnetic layer, and the produced strain was detected.

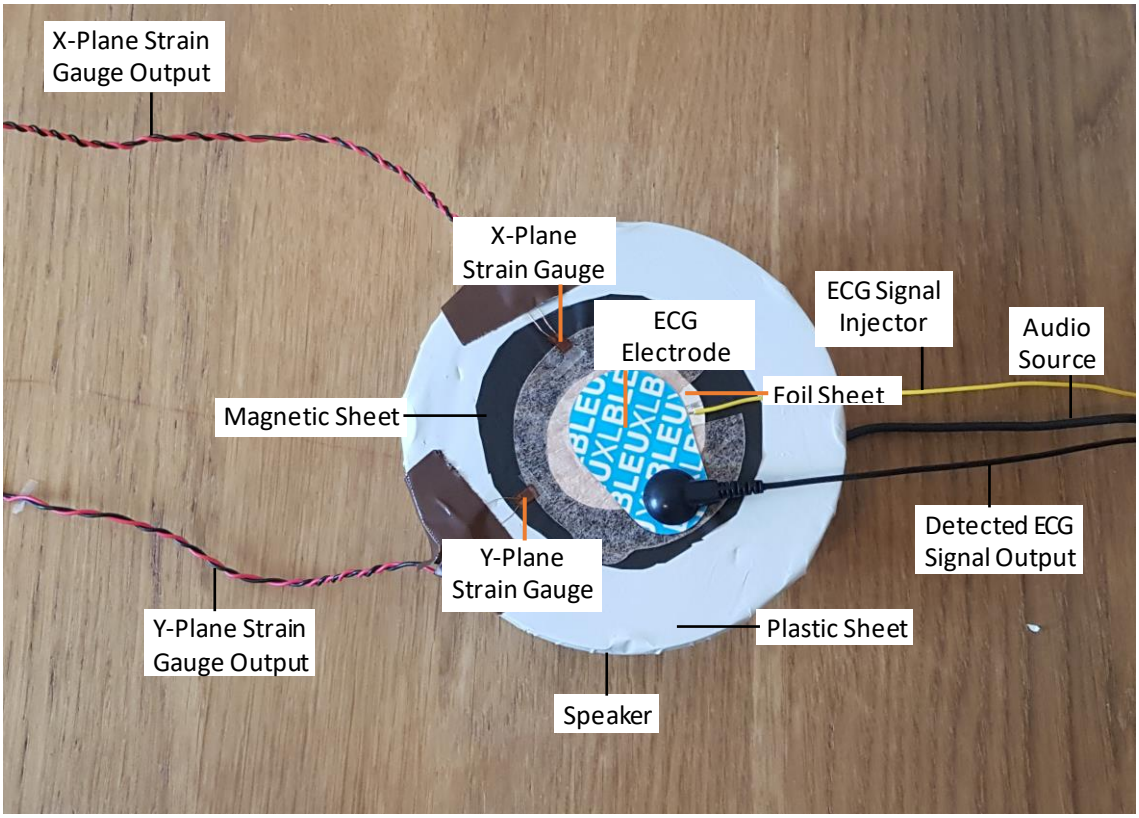

Fig. 5-19 Test Rig (top view)

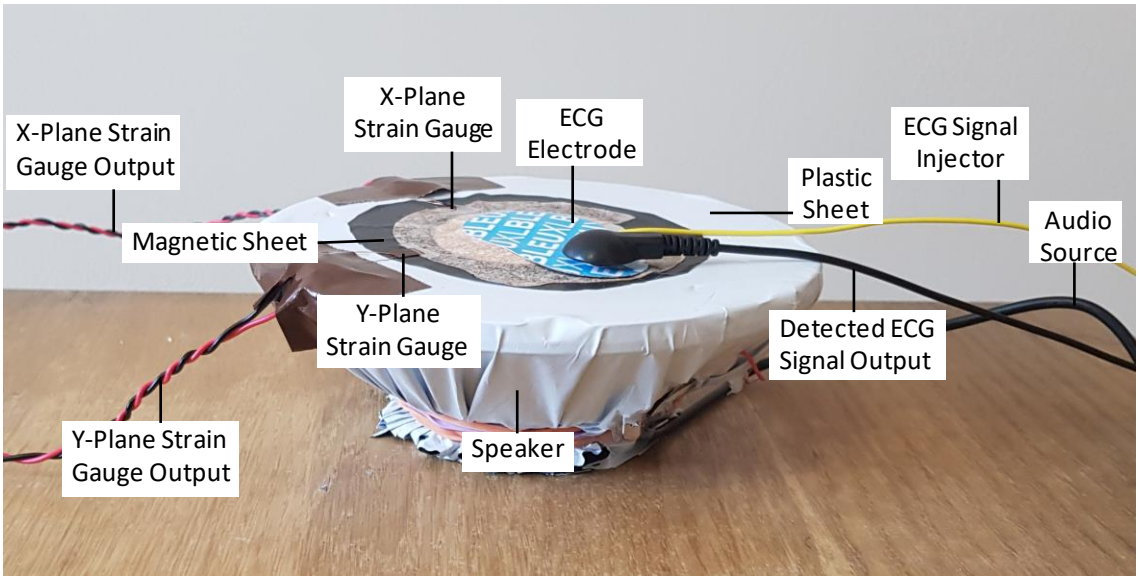

Fig. 5-20 Test Rig (side view)

5.6.3 Test Rig Output Signal and The Final Signal Processing

1. Test Rig Output

To accurately simulate the chest's up and down movements, an audio source was fed into the loudspeaker. The audio track was synced to the heartbeat (sinewave) signal to coincide with the beating of the heart to simulate chest movement due to heartbeat. As shown in Fig. 5-21, the MA was overlapping with the sinewave signal when the plastic rod moved the pseudo skin up and down.

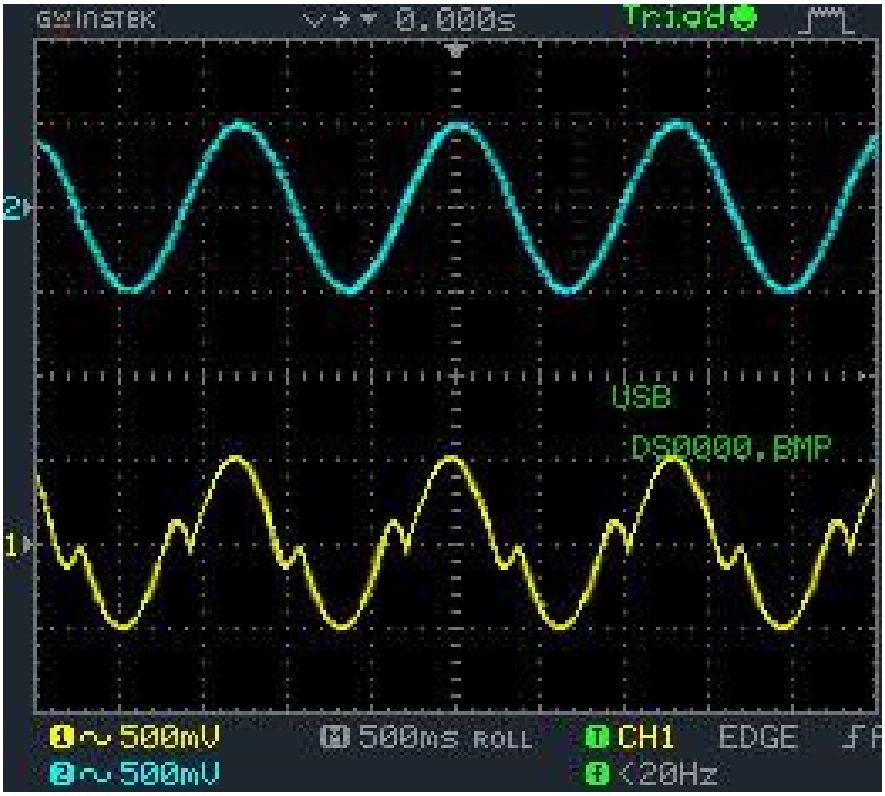

Fig. 5-21 Signal [1] Test Rig output signal before processing, Signal [2] Original injected signal

2. Final Output After Signal Processing

The detected signal was then fed into the Analog Frontend (AFE) to minimise the attached motion artefact (MA). The AFE interacted with the input signal and was able to minimise the MA and produce a final clean signal, as shown in Fig. 5-22. The final output signal was eight times greater than the original source signal.

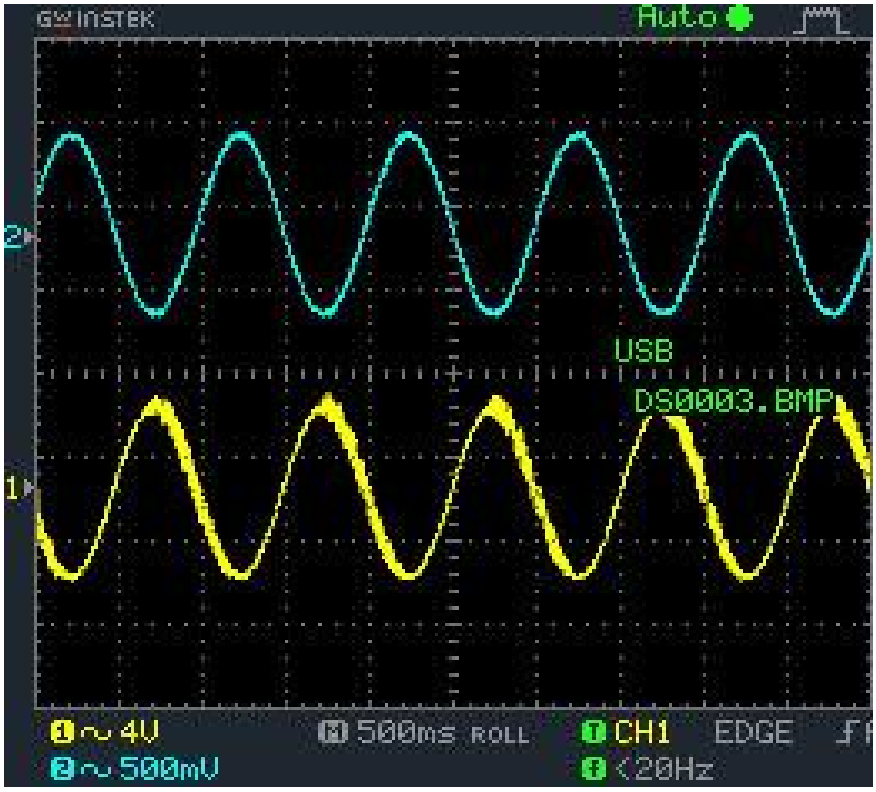

Fig. 5-22 Signal [1] Final signal after processing, Signal [2] Original injected signal

Table 5-6 shows the harmonic distortion spectrum measurements of the original clean signal compared to the distorted signal (clean signal plus added noise). The THD of the clean signal increased from 54.20% to 129.27% in the new distorted signal. The percentage of this increase was 139%, which illustrates the amount of noise that was added to the source signal. In addition, SNR of the original signal was 0.86 dB then became -4.26 dB in the distorted signal with a decrease of 5.12 dB.

Table 5-6 Test Rig - Harmonic Distortion Spectrum measures of original signal and Distorted Signal

	Clean Source Signal	Combined Noisy Signal	Decrease
THD	54.20%	129.27%	139% (increased)
SNR	0.86 dB	-4.26 dB	5.12 dB (decreased)

As can be seen in Table 5-7, after processing the distorted signal in the AFE system, the THD decreased from 129.27% to 57.74%. The percentage of this decrease was 55.3%. In addition, the SNR was also increased by 5.07 dB (from -4.26 dB to 0.91 dB).

Table 5-7 Test Rig - Harmonic Distortion Spectrum measures of Distorted signal Compared to the Output Signal

	Clean Source Signal	Combined Noisy Signal	AFE Clean Output	Improvement
THD	54.20%	129.27%	57.74%	55.3% (decreased)
SNR	0.86 dB	-4.26 dB	0.81 dB	5.07 dB (increased)

Table 5-8 shows a comparison between the original generated clean signal and the AFE output signal. The THD and SNR of the output signal was 96.5% and 94.2% like the THD and SNR of the original signal, respectively. This meant that the output signal was cleaned from most of the added noise during this simulation process.

Table 5-8 Test Rig - Harmonic Distortion Spectrum measures of Original Signal and Output Signal

	Clean Source Signal	AFE Clean Output	Improvement	Output Signal Similarity with Source Signal
THD	54.20%	57.74%	-3.5% (increased)	96.5%
SNR	0.86 dB	0.81 dB	0.05 dB (decreased)	94.2%

The AFE system removed most of the added noise, with an average correlation coefficient of 0.957 which was better than the other reported methods, such as (Berwal et al., 2019), that had achieved an average of 0.9337.

5.7 Summary

Planning the build of the electronic system was very important to any system testing process. A system is much easier to test when it is well built, enabling issues to be effortlessly spotted. The final test results relied on the correct wiring of each of the used components, and any connection mismatches would cause the resultant signal to drop.

Using open-source tools is very beneficial in saving time and minimises the waste during the build process. Fritzing was capable of providing a satisfying design and helped in seeing the final design before manufacturing begins. Also, it could be used to design the system schematic and produce the Printed Circuit Boards (PCBs).

This section showed how good planning for the final design could save time and effort. Additionally, it made the final design as neat as possible to avoid wires overlapping and detect missing or wrong connections. Moreover, the used components of the final design were explained, their role was identified, and the reason behind their use was elaborated.

In this section, the test of the AFE system was completed over two main stages. The first stage started with the preparation and generation of the test signal. This included the generation of a representation of a heartbeat signal (ECG), Motion Artefact (MA) signal, and Common-mode (CM) signal. The resultant test signal and the MA were used as an input to the AFE system to start the signal processing stage.

The second stage of the test was the signal processing stage, and it was examining the system using two methods. In the first method, the system was directly fed with the generated signal from the signal generation stage. The AFE system itself was divided into two steps, MA minimisation and CM minimisation. The output of the MA minimisation step was showing a successfully minimised MA, and it only had CM noise that was dealt with, in the next step. The CM minimisation final output showed a clean signal that was eight times the original signal's amplitude.

The second method of the signal processing stage was using a test rig to detect the Motion Artefact (MA) noise from strain gauges and fed that back to the AFE system. The test rig consisted of a loudspeaker that was covered by a plastic sheet that was representing the skin. A sinewave signal represented the ECG signal, and it was detected by sticking an ECG electrode on the plastic sheet. The sinewave signal was injected to the electrode via a layer of foil that was placed underneath the electrode. MA was caused by having a plastic rod under the plastic sheet that moved the sheet up and down when the loudspeaker was turned on. Both outputs, the detected and distorted ECG signal and the MA, were fed back to the AFE system to run them through the same steps as before. The AFE system successfully interacted with the signal and was able to minimise the MA and clean the CM signal, producing the final clean output.

With the system hardware explained, the research conclusions and future work will be discussed in the next chapter.

5.8 References

[1] ANALOG DEVICES INC. 2018. *AD623 Single and Dual-Supply, Rail-to-Rail, Low Cost Instrumentation Amplifier* [Online]. Analog.com: Analog Devices Inc. Available: https://www.analog.com/media/en/technical-documentation/data-sheets/ad623.pdf [Accessed Feb, 22 2020].

[2] BERWAL, D., V, C. R., DEWAN, S., J, C. V. & BAGHINI, M. S. 2019. Motion Artifact Removal in Ambulatory ECG Signal for Heart Rate Variability Analysis. *IEEE Sensors Journal,* 19**,** 12432-12442.

[3] BISHOP, O. 2001. Understand Electronics. *In:* BISHOP, O. (ed.) *Understand Electronics (Second Edition).* Oxford: Newnes.

[4] BOWMAN, B. R. 1992. Strain gauge for medical applications. Google Patents.

[5] FRITZING.ORG. 2019. *Fritzing* [Online]. Fritzing.org: Fritzing.org. Available: https://fritzing.org/home/ [Accessed 01/03 2020].

[6] KISHIMOTO, Y., KUTSUNA, Y. & OGURI, K. Detecting motion artifact ECG noise during sleeping by means of a tri-axis accelerometer. Engineering in Medicine and Biology Society, 2007. EMBS 2007. 29th Annual International Conference of the IEEE, 2007. IEEE, 2669-2672.

[7] LIU, S.-H. 2011. Motion artifact reduction in electrocardiogram using adaptive filter. *J. Med. Biol. Eng,* 31**,** 67-72.

[8] NAGAI, S., ANZAI, D. & WANG, J. Motion artifact removal for wearable ECG using stationary wavelet multi-resolution analysis. Electromagnetic Compatibility (EMC-Beijing), 2017 IEEE 5th International Symposium on, 2017. IEEE, 1-5.

[9] ZHANG, M. & WEI, G. 2020. An integrated EMD adaptive threshold denoising method for reduction of noise in ECG. *PLOS ONE,* 15**,** e0235330.

CHAPTER 6

CONCLUSIONS AND FUTURE WORK

6.1 Conclusions

This thesis has presented the design, build and evaluation of a novel artefact reduction technique. The design of the system included the use of sensors to detect any vertical or horizontal movement of the electrode, which then fed this information back to the system for the removal of any movement artefact. In this thesis, two strain gauges, separated by 90° were fitted onto the electrode to detect any X and Y plane movements, with regards to the patient's chest. The output of these was then fed back into the novel Analog Frontend (AFE) system for signal processing and artefact removal.

The research started by looking at the causes of the artefacts and their effect to the biomedical systems. Additionally, the current field of study and the different techniques that are used to minimise artefacts, were discussed. Also, a detailed investigation of the various causes of artefacts, such as the movement of the electrodes while they are attached to the patient, mains electrical noise, and electromagnetic interference, was presented. The information gathered from this study enabled understanding of the extent and nature of the problem, which was then used to develop the means to tackle it. It also included a revision of the strain gauges design and usage in the medical instrumentations as well as the different types of amplifiers and electrodes that are widely used for biopotential capturing.

As can be seen from the thesis, the design and implementation of the system were done over multiple iterations and levels. Each of these stages was giving a better understanding of the way the system should be built and which components were needed for every stage of the design. The first stage of the design was started in MATLAB Simulink tools to build and simulate the core idea of the Analog Frontend (AFE). During this stage, lots of changes were made to adjust and improve the original idea. These changes included the use of two strain gauges to improve the results and get closer to the real-life scenario. Also, the use of 3D gyroscopes was omitted due to the

bad results during the simulation. Also, using MATLAB's signal generators was so flexible, which helped in identifying the nature of the test signal that would be used in the lab after building the system. This identification of the test signals helped in comparing the results from the simulation and the hardware implementation stages.

On the other hand, the system components were identified and divided into sub-systems in this stage. This helped in tracing the output of each sub-system separately and identifying any design faults such as missing connections or electric loading points. These subsystems were combined together to represent two main blocks, which were the test signal preparation block and the signal processing block. The test signal preparation block was able to prepare a noisy sinewave signal that is ready for the processing stage. The noisy signal had a total harmonic distortion (THD) of 76.23% and its signal to noise ratio (SNR) was -2.98 dB. The processing stage started by the motion artefacts minimisation and it was able to remove the motion that was detected by the strain gauges and produced a signal that has only common mode noise. Then, the common mode rejection stage cleaned the signal from the remaining common mode signal and draw a clean final output. The results from this simulation stage showed a promising design that eliminated the majority of both motion artefacts and common-mode signal, while an average correlation coefficient of 0.995 was achieved. Also, the system output had a 98% SNR similarity with the clean source signal.

After defining the final specifications of the AFE system in the simulation stage, the system hardware implementation started. Building the system into electronic components was not simulated at the beginning, and the components were directly built into small breadboards to represent each sub-system. However, the design got busier during tests with all the wiring that was not planned properly beforehand. Results from the initial attempt were as expected, as the system was cleaning most of the noise but left some noise that was not avoidable due to the extra components that were added during the testing stage. Tracing the faults in the implementation was challenging and

took longer than expected. Therefore, wire planning was needed to avoid having a messy design and to effortlessly spot any issues. Therefore, an open-source tool called Fritzing was very beneficial in saving and minimising the time during the build process. Fritzing provided a satisfying design and helped in seeing the final design before manufacturing would begin. Also, it can be used to design the system schematic and produce the Printed Circuit Boards (PCBs). The design on Fritzing was very clear and had zero-overlapping wires which made it easy to trace the connections and check each sub-system output.

The practical test stage of the system was done over two steps, the test signal generation and the signal processing stage. The first step was to prepare and generate the heartbeat signal (represented as a sinewave), motion artefacts (MA), and the common-mode signals (CM). All signals were added using the summation amplifier sub-systems to produce the final distorted ECG signal. The resultant noisy signal had a total harmonic distortion (THD) of 80.63% and its signal to noise ratio (SNR) was -3.73 dB. The resultant distorted signal and the generated MA signals were fed to the AFE system to start the signal processing step. The first stage of the signal processing was for MA minimisation from the distorted signal. The output of this stage had a minimised MA, and it only had CM in the resultant signal. The remaining CM in the output of the previous stage was cleaned in the second stage of the signal processing step. The results of this test showed a clean signal sinewave signal that was eight times greater than the original signal's amplitude, with an average correlation coefficient of 0.974. Additionally, the final output had a 97.8% SNR similarity with the clean source signal.

To improve the test results of the system, a novel idea, of using a loudspeaker covered by a plastic sheet to represent the skin, was developed. This test rig used a plastic rod under the pseudo-skin to cause the plastic sheet to move up and down whenever there was movement caused by the loudspeaker. Also, a sinewave signal was injected to an ECG electrode that was fitted on top of the plastic sheet. Also, the strain gauges were

fitted onto the electrode and were separated by 90° to allow vertical and horizontal motion detection. The detected noisy signal had a total harmonic distortion (THD) of 129.27% and its signal to noise ratio (SNR) was -4.26 dB. This method simulated the random motion artefacts by having different levels of sounds that caused the sheet to vibrate. The resultant signal of this test was a clean signal with minimal distortion and an average correlation coefficient of 0.957. In addition, the final output had a 94.2% SNR similarity with the clean source signal.

In conclusion, the thesis aims and objectives that were defined at the beginning of the thesis were met. Particularly, designing a system that was capable of minimising motion artefacts using strain gauges. The use of strain gauges in the system and the way the test rig was designed provided an original contribution to the field of motion artefacts reduction.

6.2 Future Work

As it was seen in the analysis of the thesis outcomes, the Analog Frontend (AFE) was all designed and built in the lab using electrical components and showed promising results. However, such a solution has the opportunity to be taken to a more advanced level by getting the system fabricated into an integrated chip (IC). This will need the use of some Nano Technology research work to be done and might include some redesign work to get the system to work as expected. The system could be fully integrated with the electrode to work on cleaning the heartbeat biopotentials and outputs a final clean signal to the connected wires. This option means that the system needs to be fabricated in a way that allows it to be safely disposed along with the single-use electrodes. However, it is important to note that this option might not be the best option when it comes to cost-effectiveness. Therefore, a better cost-effective solution would include designing and building the system as a pluggable attachment that can be attached to the ECG electrode and works as an intermediate layer between the electrode and the connected wires. This design means that the system would not need to be disposed of with every single use.

Another opportunity for future work is to transmit the cleaned signal wirelessly to the ECG recording machine. This could be achieved by integrating the AFE system with an Analog wireless IC that transmits the final clean signal to a remote receiver that can be plugged into the ECG recorder (Lu and Ki, 2017, Manganaro and Leenaerts, 2013). This wireless feature would improve the system portability and open the door for further research work. For example, the research could be conducted to identify and implement a solution to protect the transmitted signal against any packets dropping during the signal transmission process. This would open the door for some digital processing techniques that will allow the use of computer hashing algorithms to confirm the validity and integrity of the transmitted signal (Xiao *et al.*, 2007).

Opening the digital processing world would allow the exploration of the use of a Raspberry Pi (Watkiss, 2020, Waller, 2020), and some other Field Programmable Gate Arrays (FPGA) (Rafiquzzaman and McNinch, 2019, Chu, 2011, Wain *et al.*, 2006, Amano, 2018) to allow more signal processing opportunities. A Raspberry Pi could be effectively used as the final signal receiver, which would introduce more options into the way that signal is handled. The received signal could be transferred into computer software that is capable of storing the signal into a local or remote database. The stored data can then be retrieved at any moment to be rechecked or compared with previous ECG readings of the same patient. The computer software would have some features that give statistical reports to the medical teams about the health of the person and if their heart health state was improved or declined. The software would anonymously give more stats about the regional heart health status of a specific region depending on the recorded data of the patient of the area in question (Divyabharathi *et al.*, 2019, Tara and Sarkar, 2017, Lee *et al.*, 2015). This would help researchers in studying the different lifestyles of the people of the area that shows higher heart diseases and help these people in improving their lifestyle and avoid the causes of the disease.

Finally, another opportunity for other future work is the use of the AFE system in improving the captured signal of ambulatory wearable systems. The AFE system would need to be integrated into the wearable system to process the detected signal and minimise the motion artefacts.

The outcomes and conclusions that were reached after spending the time researching the different motion artefacts minimisations researches lead me to believe the potential this field has in furthering detection and MA minimisation systems. I hope these research findings will provide a foundation for further research opportunities and improvements of the MA minimisation techniques. Thereby making biomedical signals interpretation safer and giving a better medical diagnostic to the patients' health condition.

6.3 References

[1] AMANO, H. 2018. *Principles and Structures of FPGAs*, Springer Singapore.

[2] CHU, P. P. 2011. *FPGA prototyping by VHDL examples: Xilinx Spartan-3 version*, John Wiley & Sons.

[3] DIVYABHARATHI, O., SUNDAR, A., MUKHERJEE, C. & DEEPIKA, S. Analysis of Human Physiological Parameters Using Real-Time HRV Estimation from Acquired ECG Signals. 2019 International Conference on Data Science and Communication (IconDSC), 1-2 March 2019 2019. 1-4.

[4] LEE, R., HSIAO, C., CHEN, C. & LIN, R. Heart Rate Monitoring Systems in Groups for Assessment of Cardiorespiratory Fitness Analysis. 2015 IEEE International Conference on Systems, Man, and Cybernetics, 9-12 Oct. 2015 2015. 1145-1150.

[5] LU, Y. & KI, W. H. 2017. *CMOS Integrated Circuit Design for Wireless Power Transfer*, Springer Singapore.

[6] MANGANARO, G. & LEENAERTS, D. 2013. Advances in Analog and RF IC Design for Wireless Communication Systems. *Advances in Analog and RF IC Design for Wireless Communication Systems.* Oxford: Academic Press.

[7] RAFIQUZZAMAN, M. & MCNINCH, S. A. 2019. *Digital Logic: With an Introduction to Verilog and FPGA-Based Design*, Wiley.

[8] TARA, K. & SARKAR, A. K. Real-time monitoring of heart conditions via electrocardiogram processing at different lifestyle situations. 2017 4th International Conference on Advances in Electrical Engineering (ICAEE), 28-30 Sept. 2017 2017. 546-550.

[9] WAIN, R., BUSH, I., GUEST, M., DEEGAN, M., KOZIN, I. & KITCHEN, C. 2006. An overview of FPGAs and FPGA programming-Initial experiences at Daresbury. Technical report, CCLRC Daresbury Laboratory, Cheshire, UK. http://epubs. cclrc. ac. uk/bitstream/1167/DL-TR-2006-010. pdf.

[10] WALLER, J. S. 2020. *Raspberry Pi 3 Model B For Beginners: Explore What Raspberry Pi 3 Model B Can Do*, Jeffrey S. Waller.

[11] WATKISS, S. 2020. *Learn Electronics with Raspberry Pi: Physical Computing with Circuits, Sensors, Outputs, and Projects*, Apress.

[12] XIAO, Y., SHEN, X. & DU, D. Z. 2007. *Wireless Network Security*, Springer US.

CHAPTER 7

REFERENCES

7.1 List of References

[1] AKTAKKA, E. E., WOO, J. K. & NAJAFI, K. On-chip characterization of scale-factor of a MEMS gyroscope via a micro calibration platform. 2017 IEEE International Symposium on Inertial Sensors and Systems (INERTIAL), 27-30 March 2017 2017. 1-4.

[2] ALBULBUL, A. 2016. Evaluating major electrode types for idle biological signal measurements for modern medical technology. *Bioengineering,* 3**,** 20.

[3] ALKHIDIR, T., SLUZEK, A. & YAPICI, M. K. Simple method for adaptive filtering of motion artifacts in E-textile wearable ECG sensors. Engineering in Medicine and Biology Society (EMBC), 2015 37th Annual International Conference of the IEEE, 2015. IEEE, 3807-3810.

[4] AMANO, H. 2018. *Principles and Structures of FPGAs*, Springer Singapore.

[5] ANALOG DEVICES INC. 2018. *AD623 Single and Dual-Supply, Rail-to-Rail, Low Cost Instrumentation Amplifier* [Online]. Analog.com: Analog Devices Inc. Available: https://www.analog.com/media/en/technical-documentation/data-sheets/ad623.pdf [Accessed Feb, 22 2020].

[6] BELGURZI, S., ELSHAFIEY, I. & NOUH, A. Artifacts removal from ECG signal using an ANFIS technique. Cybernetics and Computational Intelligence (CyberneticsCom), 2017 IEEE International Conference on, 2017. IEEE, 147-152.

[7] BERWAL, D., V, C. R., DEWAN, S., J, C. V. & BAGHINI, M. S. 2019. Motion Artifact Removal in Ambulatory ECG Signal for Heart Rate Variability Analysis. *IEEE Sensors Journal,* 19**,** 12432-12442.

[8] BISHOP, O. 2001. Understand Electronics. *In:* BISHOP, O. (ed.) *Understand Electronics (Second Edition).* Oxford: Newnes.

[9] BOWMAN, B. R. 1992. Strain gauge for medical applications. Google Patents.

[10] BUSONO, P. Algorithm for respiration estimation from 12-lead ECG machine. Information, Communication Technology and System (ICTS), 2014 International Conference on, 2014. IEEE, 43-46.

[11] CHANDRAKAR, C. & KOWAR, M. 2012. Denoising ECG signals using adaptive filter algorithm. *International Journal of Soft Computing and Engineering (IJSCE),* 2**,** 120-123.

[12] CHEVALIER, R. 2011. Understanding the Benefits of Strain Gauge Technology in OEM Medical Devices and Equipment. *Electronic Component News* [Online], 2018. Available: https://www.hbm.com/en/3517/understanding-the-benefits-of-strain-gauge-technology-in-oem-medical-devices-and-equipment/#:~:text=The%20relatively%20low%2Dcost%20design,and%20minimally%20invasive%20device%20designs.

[13] CHU, P. P. 2011. *FPGA prototyping by VHDL examples: Xilinx Spartan-3 version*, John Wiley & Sons.

[14] DESHPANDE, S. & RAJANKAR, S. 2013. Removing Artifacts from the ECG By using Independent component analysis. *International Journal for Research in Science & Advanced Technologies,* 5**,** 182-184.

[15] DIVYABHARATHI, O., SUNDAR, A., MUKHERJEE, C. & DEEPIKA, S. Analysis of Human Physiological Parameters Using Real-Time HRV Estimation from Acquired ECG Signals. 2019 International Conference on Data Science and Communication (IconDSC), 1-2 March 2019 2019. 1-4.

[16] DJERMANOVA, N. J., MARINOV, M. B. & GANEV, B. T. 2015. Alternating Current-Driven Strain-gage Bridge Amplifier System for Brushless Motors Torque Measurement. *ANNUAL JOURNAL OF ELECTRONICS***,** 159-162.

[17] DONGHUI, Z. Wavelet Approach for ECG Baseline Wander Correction and Noise Reduction. 2005 IEEE Engineering in Medicine and Biology 27th Annual Conference, 2005 2005. 1212-1215.

[18] DOOL, B. J. V. D. & HUIJSING, J. K. 1993. Indirect current feedback instrumentation amplifier with a common-mode input range that includes the negative roll. *IEEE Journal of Solid-State Circuits,* 28**,** 743-749.

[19] DUMITRU, C. & GAVAT, I. Voice-dial by statistical recognition of continuous speech. Signals, Circuits and Systems, 2003. SCS 2003. International Symposium on, 2003. IEEE, 157-160.

[20] FIEDLER, P., HAUEISEN, J., JANNEK, D., GRIEBEL, S., ZENTNER, L., VAZ, F. & FONSECA, C. 2014. Comparison of three types of dry electrodes for electroencephalography. *Acta Imeko,* 3**,** 33-37.

[21] FRANCO, S. 1989. Current-feedback amplifiers benefit high-speed designs. *EDN,* 34**,** 161.

[22] FRITZING.ORG. 2019. *Fritzing* [Online]. Fritzing.org: Fritzing.org. Available: https://fritzing.org/home/ [Accessed 01/03 2020].

[23] GARG, G., GUPTA, S., SINGH, V., GUPTA, J. R. P. & MITTAL, A. P. Identification of optimal wavelet-based algorithm for removal of power line interferences in ECG signals. India International Conference on Power Electronics 2010 (IICPE2010), 28-30 Jan. 2011 2011. 1-5.

[24] GAUTAM, A., LEE, Y. D. & CHUNG, W. Y. ECG Signal De-noising with Signal Averaging and Filtering Algorithm. 2008 Third International Conference on Convergence and Hybrid Information Technology, 11-13 Nov. 2008 2008. 409-415.

[25] HADDAD, S. A. P. & SERDIJN, W. A. 2009. *Ultra low-power biomedical signal processing: an analog wavelet filter approach for pacemakers*, Springer Science & Business Media.

[26] HAMPTON, J. 2008. The ECG made easy, Churchill Livingstone. Elsevier.

[27] HASAN, M. N. & LEE, K.-S. 2015. A wide linear output range biopotential amplifier for physiological measurement frontend. *IEEE Transactions on Instrumentation and Measurement,* 64**,** 120-131.

[28] HONEYWELL 2019. 1- and 2-Axis Magnetic Sensors. *In:* INC, H. I. (ed.). Honeywell.com.

[29] IMTIAZ, S. A., MARDELL, J., SAREMI–YARAHMADI, S. & RODRIGUEZ–VILLEGAS, E. 2016. ECG artefact identification and removal in mHealth systems for continuous patient monitoring. *Healthcare technology letters,* 3**,** 171-176.

[30] JENKAL, W., LATIF, R., TOUMANARI, A. & CHARRI, O. E. B. Efficient method Of QRS complex extraction using a multilevel algorithm and an adaptive thresholding technique. 2015 Third World Conference on Complex Systems (WCCS), 23-25 Nov. 2015 2015. 1-5.

[31] KANNAN, N. & KUNDU, D. 2016. Statistical Signal Processing. *Wiley StatsRef: Statistics Reference Online*.

[32] KASHIRI, N., MALZAHN, J. & TSAGARAKIS, N. G. 2017. On the Sensor Design of Torque Controlled Actuators: A Comparison Study of Strain Gauge and Encoder-Based Principles. *IEEE Robotics and Automation Letters,* 2**,** 1186-1194.

[33] KASTURIWALE, H. P. 2012. Analysis & Interpretation of Biomedical Signals using component extraction techniques. *Analysis,* 7**,** 8.

[34] KASTURIWALE, H. P. & INGOLE, P. 2012. Component extraction of complex biomedical signals and performance analysis. *Int. J. Comput. Sci. Inf. Technol,* 3**,** 3544-3547.

[35] KESTER, W. 2009. Understand SINAD, ENOB, SNR, THD, THD + N, and SFDR so You Don't Get Lost in the Noise Floor.

[36] KISHIMOTO, Y., KUTSUNA, Y. & OGURI, K. Detecting motion artifact ECG noise during sleeping by means of a tri-axis accelerometer. Engineering in Medicine and Biology Society, 2007. EMBS 2007. 29th Annual International Conference of the IEEE, 2007. IEEE, 2669-2672.

[37] KONG, W., VANDERBURG, C. R., GUNSHIN, H., ROGERS, J. T. & HUANG, X. 2008. A review of independent component analysis application to microarray gene expression data. *BioTechniques,* 45**,** 501-520.

[38] KWAK, Y. H., KIM, J. & KIM, K. 2018. Sleep monitoring sensor using flexible metal strain gauge. *Japanese Journal of Applied Physics,* 57**,** 05GD03.

[39] LANATA, A., GUIDI, A., BARAGLI, P., VALENZA, G. & SCILINGO, E. P. 2015. A Novel Algorithm for Movement Artifact Removal in ECG Signals Acquired from Wearable Systems Applied to Horses. *PloS one,* 10**,** e0140783.

[40] LEE, R., HSIAO, C., CHEN, C. & LIN, R. Heart Rate Monitoring Systems in Groups for Assessment of Cardiorespiratory Fitness Analysis. 2015 IEEE International Conference on Systems, Man, and Cybernetics, 9-12 Oct. 2015 2015. 1145-1150.

[41] LEE, W.-C., YANG, Y.-S. O., KE, T.-C., WEI, C.-S. & LEE, H.-C. Adaptive reduction of motion artifact in a portable ECG system. Sensors, 2010 IEEE, 2010. IEEE, 704-707.

[42] LIU, C.-X. & CHOI, J.-W. An embedded PDMS nanocomposite strain sensor toward biomedical applications. Engineering in Medicine and Biology Society, 2009. EMBC 2009. Annual International Conference of the IEEE, 2009. IEEE, 6391-6394.

[43] LIU, S.-H. 2011. Motion artifact reduction in electrocardiogram using adaptive filter. *J. Med. Biol. Eng,* 31**,** 67-72.

[44] LU, Y. & KI, W. H. 2017. *CMOS Integrated Circuit Design for Wireless Power Transfer*, Springer Singapore.

[45] MA, C. T., MAK, P. I., VAI, M. I., MAK, P. U., PUN, S. H., FENG, W. & MARTINS, R. P. A 90nm CMOS bio-potential signal readout front-end with improved powerline interference rejection. 2009 IEEE International Symposium on Circuits and Systems, 24-27 May 2009 2009. 665-668.

[46] MA, S., CHEN, C., ZHANG, Y. & REN, J. A low power programmable band-pass filter with novel pseudo-resistor for portable biopotential acquisition system. 2012 IEEE Asia Pacific Conference on Circuits and Systems, 2-5 Dec. 2012 2012. 232-235.

[47] MAJUMDER, S., MONDAL, T. & DEEN, M. J. 2017. Wearable sensors for remote health monitoring. *Sensors,* 17**,** 130.

[48] MANGANARO, G. & LEENAERTS, D. 2013. Advances in Analog and RF IC Design for Wireless Communication Systems. *Advances in Analog and RF IC Design for Wireless Communication Systems.* Oxford: Academic Press.

[49] MARTINSEN, O. G. & GRIMNES, S. 2011. *Bioimpedance and bioelectricity basics*, Academic press.

[50] MICRO-MEASUREMENTS. 2016. *Precision Strain Gages and Sensors Databook* [Online]. docs.micro-measurements.com: Micro-Measurements.com. Available: https://docs.micro-measurements.com/?id=4079 [Accessed 02/05/2020].

[51] MITHUN, P., PANDEY, P. C., SEBASTIAN, T., MISHRA, P. & PANDEY, V. K. A wavelet based technique for suppression of EMG noise and motion artifact in ambulatory ECG. 2011 Annual International Conference of the IEEE Engineering in Medicine and Biology Society, Aug. 30 2011-Sept. 3 2011 2011. 7087-7090.

[52] MNEIMNEH, M. A., YAZ, E. E., JOHNSON, M. T. & POVINELLI, R. J. An adaptive kalman filter for removing baseline wandering in ECG signals. 2006 Computers in Cardiology, 17-20 Sept. 2006 2006. 253-256.

[53] NAGAI, S., ANZAI, D. & WANG, J. Motion artifact removal for wearable ECG using stationary wavelet multi-resolution analysis. Electromagnetic Compatibility (EMC-Beijing), 2017 IEEE 5th International Symposium on, 2017. IEEE, 1-5.

[54] NAGEL, J. H. 2000. Biopotential amplifiers. *Bronzino JD: Biomedical engineering hand book, 2nd edition, Springer-Verlag New York***,** 70.1-70.14.

[55] NEUMAN, M. R. 1998. Biopotential amplifiers. *Medical instrumentation: application and design***,** 316-318.

[56] PATTERSON, J. A. & YANG, G.-Z. 2011. Ratiometric artifact reduction in low power reflective photoplethysmography. *IEEE transactions on biomedical circuits and systems,* 5**,** 330-338.

[57] PRIYA, K. D., RAO, G. S. & RAO, P. S. V. S. 2016. Comparative Analysis of Wavelet Thresholding Techniques with Wavelet-wiener Filter on ECG Signal. *Procedia Computer Science,* 87**,** 178-183.

[58] RAFIQUZZAMAN, M. & MCNINCH, S. A. 2019. *Digital Logic: With an Introduction to Verilog and FPGA-Based Design*, Wiley.

[59] RAGHEB, T. & GEDDES, L. 1991. The polarization impedance of common electrode metals operated at low current density. *Annals of biomedical engineering,* 19**,** 151-163.

[60] ROMERO, I., GENG, D. & BERSET, T. Adaptive filtering in ECG denoising: A comparative study. 2012 Computing in Cardiology, 9-12 Sept. 2012 2012. 45-48.

[61] RUTLEDGE, D. N. & JOUAN-RIMBAUD BOUVERESSE, D. 2013. Independent Components Analysis with the JADE algorithm. *TrAC Trends in Analytical Chemistry,* 50**,** 22-32.

[62] SATHIYABAMA, G., VINUDEVI, G., R, A. & INDHUPRIYA, P. 2015. A Survey on Instrumentation Amplifiers used for Biomedical Application. *International Journal of Advanced Research in Electrical, Electronics and Instrumentation Engineering,* 4**,** 1224-1231.

[63] SCHMIDT, R. N., LISY, F. J., SKEBE, G. G. & PRINCE, T. S. 2004. Dry physiological recording electrode. Google Patents.

[64] SHAIK, B. S. & CHAKKA, V. K. Joint reduction of baseline wander, PLI and its harmonics in ECG signal using Ramanujan Periodic Transform. India Conference (INDICON), 2016 IEEE Annual, 2016. IEEE, 1-5.

[65] SHAIK, B. S., CHAKKA, V. K., GOLI, S. & REDDY, A. S. Removal of narrowband interference (PLI in ECG signal) using Ramanujan periodic transform (RPT). Signal Processing and Communication (ICSC), 2016 International Conference on, 2016. IEEE, 233-237.

[66] SINGH, B., SINGH, P. & BUDHIRAJA, S. Various Approaches to Minimise Noises in ECG Signal: A Survey. 2015 Fifth International Conference on

Advanced Computing & Communication Technologies, 21-22 Feb. 2015 2015. 131-137.

[67] SOLIS-BUSTOS, S. & SILVA-MARTINEZ, J. Design considerations for biomedical signal interfaces. Proceedings of the Third International Workshop on Design of Mixed-Mode Integrated Circuits and Applications (Cat. No.99EX303), 1999 1999. 187-191.

[68] SPINELLI, E. M., MARTÍNEZ, N., MAYOSKY, M. A. & PALLÀS-ARENY, R. 2004. A novel fully differential biopotential amplifier with DC suppression. *IEEE transactions on biomedical engineering,* 51**,** 1444-1448.

[69] ŞTEFĂNESCU, D. M. Strain gauges and Wheatstone bridges — Basic instrumentation and new applications for electrical measurement of non-electrical quantities. Eighth International Multi-Conference on Systems, Signals & Devices, 22-25 March 2011 2011. 1-5.

[70] STELAND, A. 2012. *Financial Statistics and Mathematical Finance: Methods, Models and Applications*.

[71] STORK, M. Modeling and simulation of some biomedical signals. Measurement, 2017 11th International Conference on, 2017. IEEE, 221-224.

[72] STOUT, D. F. & KAUFMAN, M. 1976. Handbook of operational amplifier circuit design.

[73] TARA, K. & SARKAR, A. K. Real-time monitoring of heart conditions via electrocardiogram processing at different lifestyle situations. 2017 4th International Conference on Advances in Electrical Engineering (ICAEE), 28-30 Sept. 2017 2017. 546-550.

[74] THAKOR, N. V. & ZHU, Y.-S. 1991. Applications of adaptive filtering to ECG analysis: noise cancellation and arrhythmia detection. *IEEE transactions on biomedical engineering,* 38**,** 785-794.

[75] TONG, D., BARTELS, K. & HONEYAGER, K. Adaptive reduction of motion artifact in the electrocardiogram. Engineering in Medicine and Biology, 2002. 24th

Annual Conference and the Annual Fall Meeting of the Biomedical Engineering Society EMBS/BMES Conference, 2002. Proceedings of the Second Joint, 2002. IEEE, 1403-1404.

[76] VAN, D. E. & VAN DE PLASSCHE, R. J. 1975. A WIDE-BAND MONOLITHIC INSTRUMENTATION AMPLIFIER.

[77] WAIN, R., BUSH, I., GUEST, M., DEEGAN, M., KOZIN, I. & KITCHEN, C. 2006. An overview of FPGAs and FPGA programming-Initial experiences at Daresbury. Technical report, CCLRC Daresbury Laboratory, Cheshire, UK. http://epubs. cclrc. ac. uk/bitstream/1167/DL-TR-2006-010. pdf.

[78] WALLER, J. S. 2020. *Raspberry Pi 3 Model B For Beginners: Explore What Raspberry Pi 3 Model B Can Do*, Jeffrey S. Waller.

[79] WANG, Z., WONG, C. M., DA CRUZ, J. N., WAN, F., MAK, P.-I., MAK, P. U. & VAI, M. I. Muscle and electrode motion artifacts reduction in ECG using adaptive Fourier decomposition. Systems, Man and Cybernetics (SMC), 2014 IEEE International Conference on, 2014. IEEE, 1456-1461.

[80] WATKISS, S. 2020. *Learn Electronics with Raspberry Pi: Physical Computing with Circuits, Sensors, Outputs, and Projects*, Apress.

[81] WEBSTER, J. 2009. *Medical instrumentation: application and design*, John Wiley & Sons.

[82] WEI, Z., XU, W., LINLIN, G. & ZHUO, Z. Noise Reduction in ECG Signal Based on Adaptive Wavelet Transform. 2005 IEEE Engineering in Medicine and Biology 27th Annual Conference, 17-18 Jan. 2006 2005. 2699-2702.

[83] WU, Y. & RANGAYYAN, R. M. An Algorithm for Evaluating the Performance of Adaptive Filters for the Removal of Artifacts in ECG Signals. 2007 Canadian Conference on Electrical and Computer Engineering, 22-26 April 2007 2007. 864-867.

[84] XIAO, Y., SHEN, X. & DU, D. Z. 2007. *Wireless Network Security*, Springer US.

[85] YAZICIOGLU, R. F., VAN HOOF, C. & PUERS, R. 2008. *Biopotential readout circuits for portable acquisition systems*, Springer Science & Business Media.

[86] YAZıCıOĞLU, R. F., VAN HOOF, C. & PUERS, R. 2009. Introduction to Biopotential Acquisition. *Biopotential Readout Circuits for Portable Acquisition Systems.* Dordrecht: Springer Netherlands.

[87] YOON, H., KIM, H., KWON, S. & PARK, K. An automated motion artifact removal algorithm in electrocardiogram based on independent component analysis. Proceedings of the 5th International Conference on eHealth, Telemedicine, and Social Medicine (eTELEMED'2013), 2013. 15-20.

[88] ZHANG, H., ZHANG, S., JIN, Q., LIU, X., LI, Q., YANG, J. & ZHAO, J. Motion artifact suppression in ambulatory ECG with feed forward combined adaptive filter. Computing in Cardiology Conference (CinC), 2016, 2016. IEEE, 1-4.

[89] ZHANG, M. & WEI, G. 2020. An integrated EMD adaptive threshold denoising method for reduction of noise in ECG. *PLOS ONE,* 15**,** e0235330.

CHAPTER 8

APPENDICIES

8.1 Appendix A: System Discrete Components Individual Boards

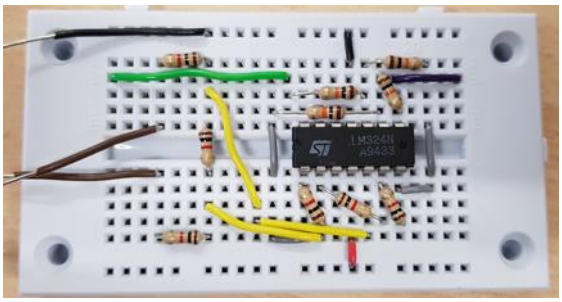

(a)

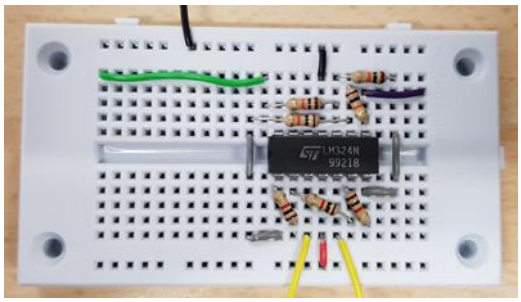

(b)

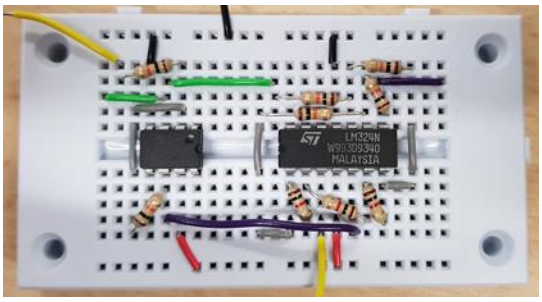

(c)

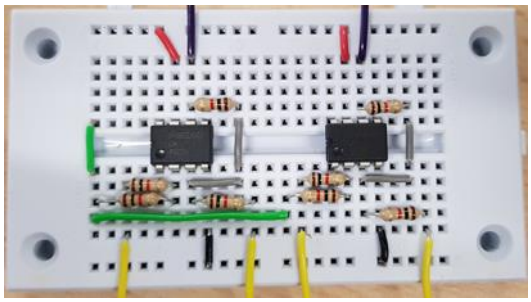

(d)

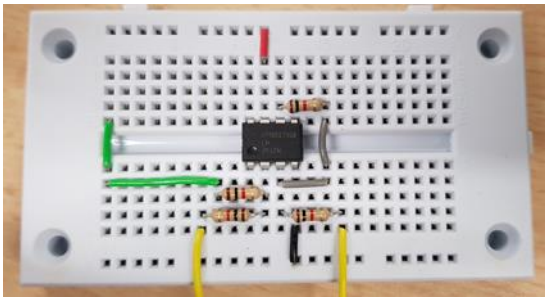

(e)

Fig. 8-1 System Individual Blocks: (a) Wheatstone Bridge and IA, (b) Instrumentation Amplifier (IA), (c) IA and an Inverter, (d) Differential amplifiers, (e) Summing Amplifier

CHAPTER 9

PUBLISHED WORK

Published Work

1. S Zourob, K Hayatleh, S Barker, R Nagulapalli ,N Yassine, R Ramsbottom, J Lidgey, 'Increasing Signal to Noise Ratio and Minimizing Artefacts in Biomedical Instrumentation Systems' Accepted for publication in the Journal of Analog Integrated Circuits and Signal Processing, Feb 2018, DOI: 10.1007/s10470-018-1150-4.